SCATTERING AND ABSORPTION BY

ACOUSTIC RESONATORS

by

KARL UNO INGARD

E.E., Chalmers Inst. of Techn.
Gothenburg, Sweden.
(1944)

Techn. Licentiate. Chalmers
Inst. of Techn.
(1948)

SUBMITTED IN PARTIAL FULFILLMENT OF THE
REQUIREMENTS FOR THE DEGREE OF
DOCTOR OF PHILOSOPHY

at the

MASSACHUSETTS INSTITUTE OF TECHNOLOGY
(1950)

Signature of Author .....
Department of Physics, May 12, 1950.

Certified by .....
Thesis Supervisor

.....
Chairman, Department Committee on Graduate Students

ABSTRACT FOR

"SCATTERING AND ABSORPTION

BY ACOUSTIC RESONATORS"

by

UNO INGARD

Abstract.

The study of acoustic (Helmholtz) resonator performed in this work consists of three sections: I. On the transmission of sound through apertures. II. The acoustic resonator in free field. III. Resonators in walls.

In the first section, devoted to transmission of sound through apertures, the emphasize is put on a study of non-linear effects. It is shown that the transmission of sound through an aperture is in general associated with steady circulations and jet effects (at higher levels) which cause additional dissipation and influence the acoustic conductivity of the aperture. Studies of these effects have been made by the use of smoke particles introduced in the apertur region, and it is found that there exist at least four characteristic types of circulations as the particle velocity in the aperture is increased. "Phase diagrams" have been made up, showing at what frequencies and particle velocities these different types of circulations occur, and photographs of the various flow patterns characteristic for the different regions in the phase diagrams have been taken.

A turbulence criterion for sound through an aperture is presented, showing that onset of turbulence is velocity determined in some cases and displacement determined in others.

It is shown that the non-linear properties of the acoustic resistance of an aperture is closely connected with the circulation effects. Quantitative check in one of the circulation regions and a good qualitative overall agreement indicates that the non-linearity of the aperture resistance is caused by the circulation effects. The reactance of the aperture is independent of sound level until turbulence is obtained, where the reactance starts to decrease.

In addition to these studies the "linear" impedance of apertures is also discussed. The reactances of different apertures in partitions in tubes are determined, and an analysis of the excentric circular aperture in a cylindrical tube and the interaction between two apertures is made. It is shown that the reactance of a circular aperture in a circular cylindrical tube has a minimum when the aperture is located approximately half way between the axis and the wall of the tube.

In the second section an analysis of the spherical resonator in free field is given. The particle velocity in the hole of the resonator is then assumed uniform and the field inside and outside the cavity are fitted together at the boundary of the sphere. The viscous dissipation on the surfaces of the sphere is calculated , and an analysis of characteristic properties is made, in which the dimensions of the resonator yielding maximum values of absorption, Q-value and reverbera-

tion time are determined.

Conditions for turbulence are then discussed and finally measurements of the near field of the resonator is shown to be in good agreement with calculations. Some notes of resonators in free field are also presented.

In the third section a brief discussion of the single resonator in a wall is first taken up with special attention to the design for maximum absorption. The remaining part of this section is mainly devoted to an experimental investigation of the angular dependence of the normal impedance and absorption coefficient of the special kind of resonator arrays in walls represented by perforated facings. A new method of measurement is then applied in which the pressure and phase of the sound in steady state are measured at a point in the absorptive surface and compared with pressure and phase measured at the same point in space at the surface of a perfectly reflecting material. From these data are determined the phase and magnitude of both the incident and the reflected waves, and this information in turn yields both the complex impedance and the free wave absorption coefficient for the particular angle of incidence involved. Tests have been made with an 8 ft sq sample of material mounted in an anechoic chamber and rotated about a vertical axis in the presence of a fixed horizontal beam of approximately plane waves. The pressure magnitude and phase were

recorded graphically, continously as a function of angle as the sample was rotated. The necessary transformations of data have been reduced to chart form.

Measurements have thus been made on perforated facings the normal impedance of which is matched to ρc at resonance by use of a proper flow resistance put over the surface. The angular dependence of the resonance frequency, characteristic for perforated facings without partitions has been checked nicely and the measured impedance and absorption coefficients for facings both with and without partitions are found to be in good agreement with theory.

In an appendix the use of a resonator as an acoustic Q-meter is discussed to be used for measuring the acoustic impedance of thin layers of material or for determining the complex compressibility of porous material.

Acknowledgement.

The author wishes to express his sincere thanks to Professor R.H. Bolt for all advise and steady encouragement given during the course of this study. Professor P.M. Morse has been particularly kind in giving his suggestions and making available some of his unpublished material on the subject of resonators. The author wishes also to thank Professor L.L. Beranek for inspiring discussions and Mr. S.Labate for his collaboration in the measurements involved.

Finally the author wants to express his thanks to the Physics Department at M.I.T. for the award of a fellowship sponsored by the Acoustical Materials Association, which made the completion of this work possible.

Table of content.

III. Resonators in walls.

§ 1. A single resonator in a wall.

Application to architectural acoustics.

§ 2. Perforated facings.

§ 3. Measurement of the normal impedance and the absorption coefficient of perforated facings for sound of oblique incidence.

The surface pressure method.
Experimental arrangement.
Measurements on perforated facings
Perforated facings without partitions.
Perforated facings with partitions.

Appendix.

Measurement of small flow resistances by means of an acoustic Q-meter.

List of figures.

tion effects.

Figures 10-17. Phase diagram for circular apertures.

Figures 18-21. Steady circulations in the vicinity of an aperture. Figures 17 and 18 are characteristic of region 1, and figures 19 and 20 of region 2 in the phase diagrams. (See figures 10-17.)

Figure 22. Steady circulations and pulsations superposed. These effects are characteristic of region 3.

Figures 23-24. Jets caused by sound waves of amplitudes corresponding to those of region 4. The aperture diameter $d = 0.5$ cm and the frequency $\nu = 234$ cps.

Figure 25. Vortex rings from an aperture. Aperture diameter $d = 0.5$ cm and frequency $\nu = 234$ cps.

Figure 26. Acoustic jet.

Figure 27. Acoustic resistance of an aperture as a function of the average particle velocity U in the aperture at relatively low values of U.

Figures 28-37. The non-linear part of the resistance of an aperture expressed in terms of equivalent aperture thickness Δ_{NL} ξ = particle displacement in the aperture. t = thickness of the aperture. U = particle velocity.

Figure 38. Assumed velocity distribution in the vortex ring.

Figure 39. Torsion balance for measuring the stagnation force of a jet.

Figure 40. The non-linear part of the acoustic resistance of an aperture obtained from impedance (R_{NL}) and from measurements of the kinetic energy of jets (R_K).

Figures 41-45. By turbulence caused decrease Δ_{NL} of the mass end correction of an aperture plotted as a function of ξ/t and U.

Figure 46. Pressure distribution around the aperture of an undampened resonator terminating a tube.

Figure 47. Pressure distribution around the aperture of a dampened resonator terminating a tube. The input impedance is matched to ρc at resonance. (100% absorption)

Figure 48. Spherical resonator in free field.

Figure 49. Mass end correction for the aperture in a spherical resonator.

Figure 50. Frequency chart for a spherical resonator.

Figures 51-55. Design charts for a spherical resonator.

Figure 56. Measured and calculated Q-values of a spherical resonator as a function of hole diameter.

Figure 57. Measurement of the pressure distribution around a spherical resonator.

Figure 58. Measured and calculated pressure distributions around a spherical resonator.

Figure 59. Index of refraction $n = n_1 - i n_2$ for a lattice of acoustic resonators in air. The lattice period is much smaller than a wave length.

Figure 60. The normal reactance of a perforated facing without partitions plotted as a function of $\gamma = \omega/\omega_o$ with the angle of incidence φ as parameter.

Figure 61. Vector diagram of pressures considered in the surface pressure method.

Figure 62. Schematic illustration of the surface pressure method.

Figure 63. Absorption chart.

Figure 64. Impedance chart.

Figure 65. Electronic equipment used in the surface pressure measurements.

Figure 66. Arrangement representing a perforated facing without partitions.

Figure 67. Finished test panel with a perforated facing.

Figure 68. Examples of hard wall pressures P_1 as a function of angle of incidence φ.

Figure 69. Arrangement representing a perforated facing with partitions.

Figure 70. The normal impedance of a perforated facing.

Figure 71. Measured values of P_1/P_2 and Ψ as a function of angle incidence for a perforated facing without partitions.

Figure 72. Experimental and theoretical curves of the absorbtion coefficient as a function of angle of incidence for a perforated facing without partitions.

Figure 73. Calculated curves of α_{stat} for perforated facings with and without partitions. The experimental results are indicated by circles and cross marks.

Figure 74. The calculated and measured normal reactance of a perforated facing without partitions.

Figure 75. Measured resistance of a perforated facing without partitions as a function of angle of incidence.

Figure 76. Measured values of P_1/P_2 and Ψ as a function of angle of incidence for a perforated facing with partitions.

Figure 77. Experimental and theoretical curves of the absorption coefficient as a function of angle of incidence for a perforated facing with partitions.

Figure 78. Measured normal impedance of a perforated facing with partitions as a function of angle of incidence.

Introduction.

The analysis of an acoustic cavity resonator (Helmholtz type) can in many respects be considered completed by the classical work by Helmholtz and Rayleigh. However, a more detailed analysis has been suggested repeatedly in recent years by reported discrepances found in measurements on resonators and apertures, and the application of acoustic resonators in architectural acoustics has brought up new problems of general interest which require consideration.

Measured resonance frequencies of acoustic resonators have consistently been found to be higher than the calculated and measurements on the dampening of resonators and the acoustic resistance of apertures have given results varying within a large range of values and in most cases in serious disagreement with calculations.

Reported non-linear behaviour of resonators may in part explain some of these discrepances concerning dampening. The mechanism of this non-linearity has not been understood, however, and is in itself an interesting problem, which is considered in some detail in the first section of the studies presented here. This section deals also with the other problems mentioned briefly above connected with the aperture of

a resonator, but the major part consists of an investigation of the second (or higher) order effects in the aperture region and their effect upon the acoustic impedance. Since these problems are characteristic not only for resonators but associated with the propagation of sound through apertures in general, we have in the first section for convenience considered the effect of apertures in partitions in tubes.

In many applications in architectural acoustics there is a great need for absorption of relatively low frequencies where usual acoustic materials are no longer applicable. The use of acoustic resonators in such a case is a well-known possibility and it is of both theoretical and practical interest to investigate the conditions under which a resonator can serve the purpose as a sound absorber. It is this question which has suggested the analysis of the resonator in free field, presented in the second section of this study. The optimum dimensions for maximum absorption have been determined and the result has been brought into a form suitable for practical applications. With minor changes introduced, the design criteria obtained are valid also for a resonator in a wall, which is discussed in the third section.

A criterion for the onset of turbulence is also given based on the results found in section I and calculations of the near field of the resonator are verified by measurements.

The third section starts with a brief discussion of the single resonator in a wall employing the analysis of the resonator in free field. The most common application of resonators in walls is a somewhat extreme one, namely the perforated facing, which can be considered built up of an array of small resonators. The facings are then always combined with a porous material so that the viscous resistance of the facing itself can be neglected besides the resistance of the porous material. In the idealized case when the individual resonators are separated by partition walls, the surface has a normal impedance independent of angle of incidence. If the partitions are removed the normal impedance is going to be strongly dependent of angle of incidence and the statistical average of the absorption coefficient of the surface changes considerably. This problem is taken up in the third section were an experimental study of the angular dependence of the normal impedance and absorption coefficient of perforated facings with and without partitions is presented, yielding results in good agreement with theory.

I. On the transmission of sound through apertures.

1. The reactance of apertures in partitions in tubes.

When a constriction is introduced in a tube which carries a constant flow of an incompressible fluid, an increase in the total kinetic energy is obtained, at least as long as the flow is laminar and no jets are formed. This is analogous to the increase of the electrical losses caused by a constriction on a conductor. At sufficiently low frequencies the situation is analogous for sound waves, and we get a mass reactance due to the increase in the "kinetic mass" caused by the constriction. An approximate value of this mass can then be obtained directly by use of well-known results of corresponding problems in electrostatics or for stationary electric currents [1]. In the two dimensional cases the possibility of transforming boundaries by conformal mapping is then helpful.

A solution of the problem of sound transmission through tubes with constrictions or discontinuities, presented by Miles [5] [6], was not given until similar problems had been solved for electromagnetic waves in tubes [2], [3]. The variational method, due to Schwinger [4], which then was applied by Miles makes use of the fact that the velocity in the aperture distributes itself in such a way as to give maximum acoustic conductivity, a principle familiar in the

theory of steady flow of fluids or electric current. The coefficients in the expansion for the velocity in the aperture are then obtained by iteration, which, however, converges too slowly to be useful for practical purposes. The frequency was considered to be low enough to exclude propagation of higher order modes. An earlier paper [7] by the same author on the same subject seems to be in error. The boundary conditions at the discontinuity in the tube are incorrect and the resulting infinite set of linear equations which are supposed to give the coefficients in the expansion for the velocity are all identically zero.

The radiation of sound from a circular plane piston into a finite circular cylindrical tube with arbitrary (point reacting) terminal impedance has been studied in some detail [8]. No restriction on frequency is made, and the frequency dependence of the mass reactance of the piston is computed as a function of piston size. The results are then applied to apertures and resonators, assuming a uniform velocity distribution across the opening.

Recently a detailed study of the circular cylindrical case has been done by Nielsen [9], in which the assumption of a uniform velocity distribution is dropped. Instead of using one distribution a combination of two is chosen in such a way as to make the kinetic mass a minimum. In principle this is the same method as used in [6], the difference being

that instead of rigorously using an infinite number of "component distributions", a combination of only two physically reasonable distributions have been considered, thus making calculations practically possible. The reactance thus obtained for small circular apertures in a tube is about 8 - 10 % less than that obtained with the uniform velocity distribution. However, reactance measurements have been reported [10] in which a considerably smaller difference is obtained.

It is the purpose of the present section to list some additional results for apertures of interest in the study of resonators, and to report briefly some reactance measurements on apertures of various thicknesses intended to supplement the results for thin apertures given in [10] . In addition a discussion of the excentric aperture and the interaction between two apertures is taken up.

A consequence of the uniform velocity assumption.

Before starting our discussion of the reactance it is worth emphasizing a point of general interest. Let us consider a tube loaded with an aperture at $x = 0$ as shown in figure 1.

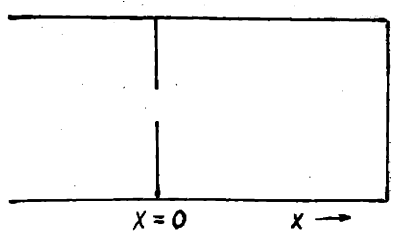

Figure 1.

We make the assumption that the velocity in the aperture is uniform and equal to U. The specific impedance of the aperture piston looking to the right consists of two parts, ζ and ζ_s, where ζ is the plane wave contribution and ζ_s is the mass reactance caused by the higher order modes to the right of the aperture. If the total average pressure over the right side of the aperture is $\bar{p}_2$ we have $\rho c(\zeta + \zeta_s) = \bar{p}_2/U$.

Using Morse's notation [11] the sound field to the left can be written $p_1 = 2p_+ e^{-\Psi} \sinh(ikx+\Psi) + p_{1s}$, where p_{1s} represents the higher order modes scattered to the left. From the boundary condition $\bar{p}_1 = \bar{p}_2$ at $x = 0$ we get

$$2P_+ e^{-\Psi} \sinh\Psi + p_{1s} = U \rho c(\zeta + \zeta_s) \qquad (1.1)$$

Since $p_{1s}/U = -\rho c \zeta_s$ this gives

$$U = \frac{2P_+ e^{-\Psi} \sinh\Psi}{(\zeta + 2\zeta_s)\rho c} = \frac{P_+ + P_-}{\rho c(\zeta + 2\zeta_s)} \qquad (I.2)$$

and the condition of continuity of flow yields

$$\tgh\Psi = (A_1/A_o)(\zeta + 2\zeta_s) \qquad (I.3)$$

A_1 = tube area and A_o = aperture area. This shows, as expected, that the effect of the aperture on the plane wave is to introduce in series with ζ an impedance $2\zeta_s = 2\bar{p}_{1s}/U$, which is the mass reactance of the aperture to be discussed.

The uniform velocity distribution assumed leads to a boundary condition $\overline{p_1(o)} = \overline{p_2(o)}$ rather than the correct one $p_1(o) = p_2(o)$ across the aperture. By $\overline{p}_1$ and $\overline{p}_2$ we then mean the average pressure over the aperture. The consequence of the uniform velocity distribution with regard to pressure distribution is then a discontinuity at the aperture

$$(p_1 - p_2)_{x=0} = 2(\overline{p_{s1}} - p_{s1})_{x=o} \qquad (I.4)$$

which is illustrated by an example in §4.

The reactance of circular and rectangular apertures.

We consider an aperture in a tube as indicated in figure 1 and neglect the thickness of the wall at the moment and consider only the mass reactance caused by the higher order modes on both sides of the aperture. The contribution from the two sides are different if there is a change in cross section of the tube in the plane of the aperture. If the specific mass reactance on one side of the aperture is $\varrho c \zeta_s = -i\omega m$, we introduce as a measure for $\underline{m}$ the mass end correction $\delta = m/\varrho$, where ϱ is the air density.

The expression for δ obtained in some cases of special interest in connection with resonators are listed in table 1. Of these the concentric circular aperture in a circular tube, obtained with $a = 0$ in (I.5), has been discussed in consider-

Table 1.

Aperture	Tube	Mass end correction on one side of the aperture.
Circular	Circular	

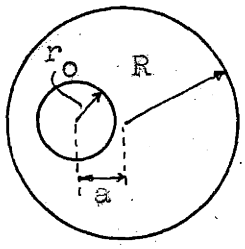

$$\delta = \sqrt{A_o}\frac{4}{\sqrt{\pi}}\frac{1}{\xi}\sum_{m=0}^{\infty}\sum_{n=1}^{\infty}\frac{J_1^2(q_{mn}\xi)J_m^2(q_{mn}a/R)}{q_{mn}^3(1-m^2/q_{mn}^2)J_m^2(q_m)}$$

$$\xi = r_o/R \qquad A_o = \pi r_o^2 \qquad \text{(I.5)}$$

Circular — Rectangular

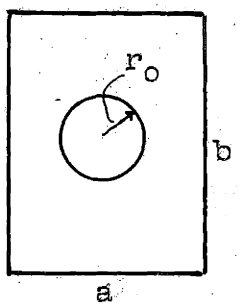

$$\delta = \sqrt{A_o}\frac{4}{\pi^{3/2}}(\xi\eta)^{-1/2}\sum_{m=0}^{\infty}\sum_{n=1}^{\infty}\nu_{mn}\frac{J_1^2(\pi\sqrt{m^2\xi^2+n^2\eta^2})}{\left[m^2b/a+n^2a/b\right]^{3/2}}$$

$$\nu_{on} = 1/2 \qquad \nu_{mn} = 1 \qquad \text{(I.6)}$$

$$A_o = \pi r_o^2 \qquad \xi = r_o/a \qquad \eta = r_o/b$$

Rectangular — Rectangular

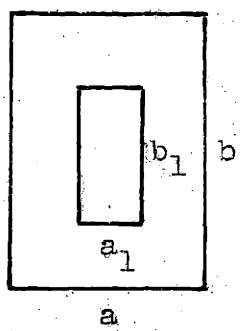

$$\delta = \sqrt{A_o}\frac{2}{\pi}\sum_{m}\sum_{n}\nu_{mn}\frac{G_{mn}}{\sqrt{\xi(b_1/a)m^2+\eta(a_1/b)n^2}}$$

$$G_{mn} = \left[\frac{\sin(\pi m\xi)}{\pi m\ \xi}\cdot\frac{\sin(\pi n\eta)}{\pi n\ \eta}\right]^2 \qquad \text{(I.7)}$$

$$\nu_{oo} = 0 \qquad \nu_{on} = \nu_{mo} = 1/2 \qquad \nu_{mn} = 1$$

$$\xi = a_1/a \qquad \eta = b_1/b \qquad A_o = 4a_1b_1$$

able detail before, as already mentioned. The results now listed are obtained in a similar way.

It has been assumed that the aperture is located sufficiently far away from the sound source and the termination of the tube so that attenuated waves are not affected by these boundaries. Or, in other words, we have assumed the frequency low enough so that the mass can be considered as a local quantity at the position of the aperture. When the frequency approaches the first cut-off frequency of the tube, the attenuation of higher order modes decreases and their "action distance" increases fast. The "mass" can then no longer be considered local and independent of frequency. The frequency dependence of m for the circular orifice in the circular cylindrical tube has been discussed in [8].

The end correction obtained from the expressions listed in table 1 in the three simplest cases, namely concentric aperture in a circular tube, a circular aperture in a square tube, and a square aperture in a square tube, is plotted in figure 2 as a function of ξ. (ξ is defined in table 1).

Since $\delta/\sqrt{\bar{A}_o}$ can be considered the same for these three cases and practically linearly dependent on ξ for small values of ξ, we may introduce an approximate expression for the end correction for these apertures. It follows from figure 2 that

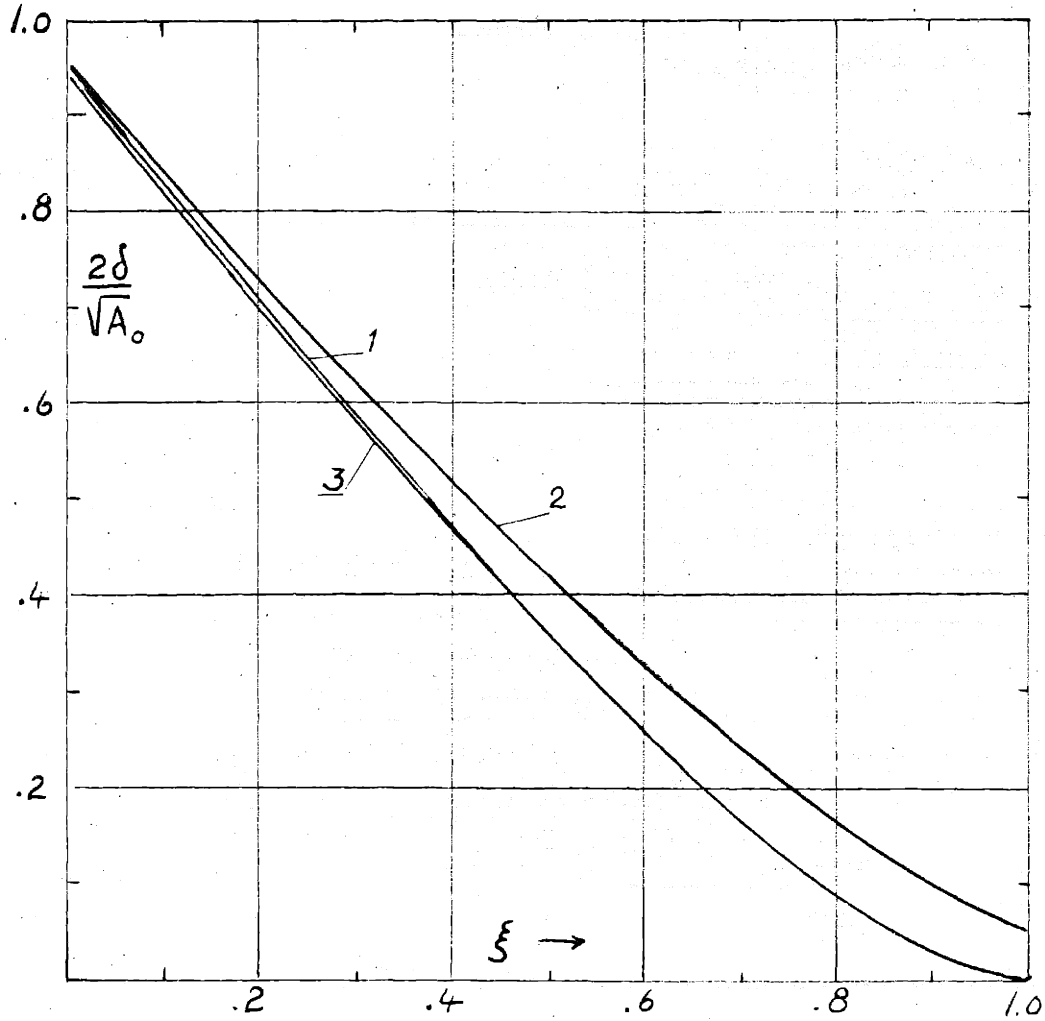

Figure 2

$$\delta = 0.48\sqrt{A_o}(1-1.25\xi) \quad (\xi < 0.4) \qquad (I.8)$$

is a good approximation for $\xi < 0.4$, the region of most interest concerning resonators. If this end correction is used when calculating the resonance frequency of a reasonator in a tube, we obtain an expression which is in very good agreement with measurements.

For a circular aperture in an infinite wall we know that $\delta_o/\sqrt{A_o}$ equals $(8/3)\pi^{-3/2} \simeq 0.48$ and we see that $\delta/\sqrt{A_o}$ for the circular aperture approaches this value when $\xi \to 0$. The corresponding value for the square aperture is somewhat smaller. When $\xi \to 1$ we have $\delta \to 0$ as expected, except for the circular aperture in a square tube. In that case there is a little "space" left for higher order modes even if the diameter of the aperture equals the side of the tube.

The end correction for a rectangular aperture in a square tube, obtained by setting $a = b$ in (I.7), is shown in figure 3. These curves are useful in connection with the design of resonators or facings with slits used to some extent in architectural acoustics.

Of special interest is the end correction for the excentric circular aperture given in (I.5). In the derivation of this expression the addition theorem for the Bessel functions

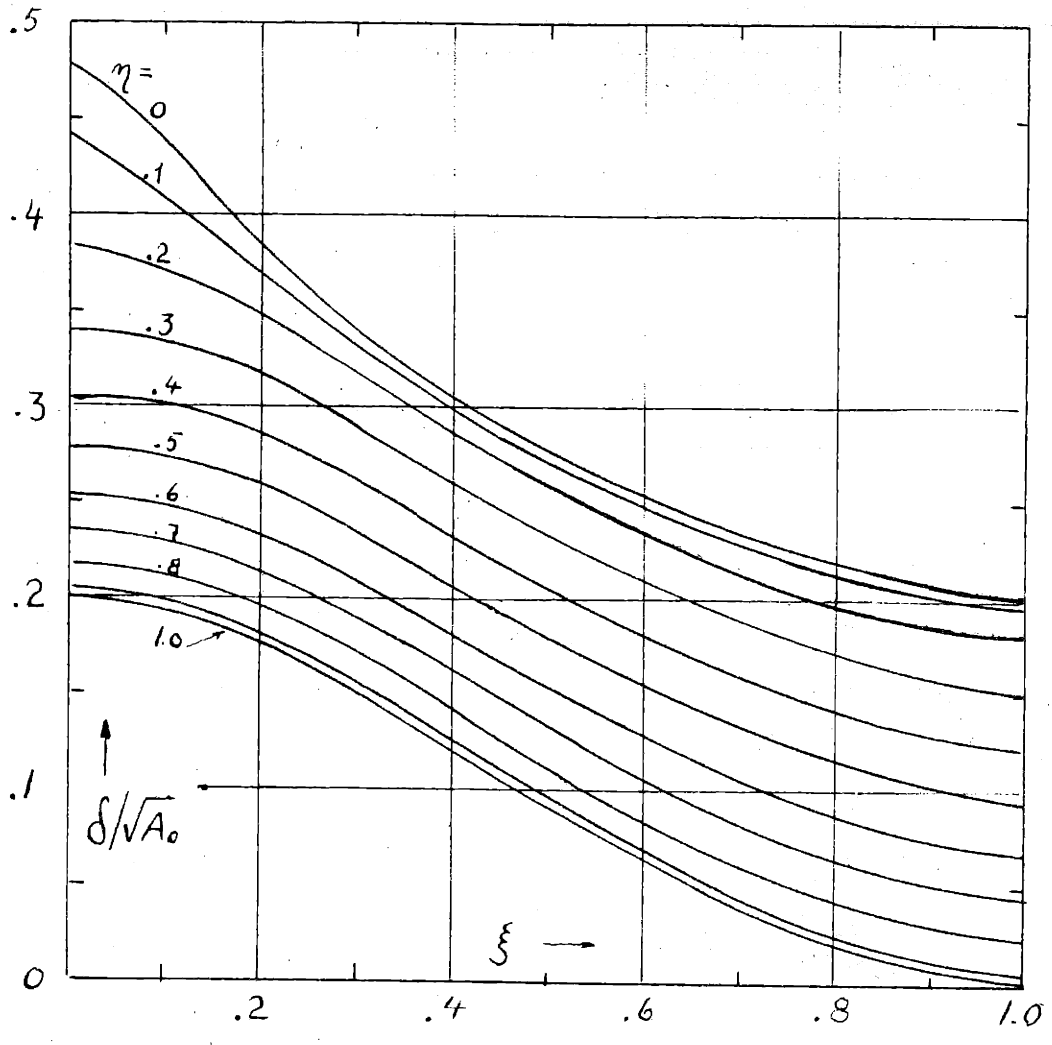

Figure 3

was used [12] when moving the origin of the coordinate system from the centrum of the tube to the centrum of the aperture. The calculations are somewhat lengthy and will not be given here. The end correction is computed as a function of $\underline{a}$, i.e. the distance between the aperture centrum and the tube axis, for a single value of $\xi = r_o/R$ ($\xi = 0.15$), and the result is shown in figure 4, where the curve is labelled $\delta_{11}/\sqrt{A_o}$. The interesting feature of this result is that the end correction is a minimum, or the conductivity of the aperture a maximum, when $\underline{a}$ is approximately equal to $0.5R$ that means, when the aperture is located half way between the axis and the wall of the tube. The curve indicates a maximum value of the end correction when $a = R$, but, since $r_o = 0.15R$ in this case it follows that a/R cannot be larger than 0.85 and the maximum end correction is therefore obtained for $a = 0$. The difference between the maximum and minimum value is considerable, and the resonance frequency of a resonator in a tube can be increased almost by 35 % merely by moving the aperture from $a = 0$ to $a = 0.5R$. We have then assumed that the thickness of the aperture is smaller than its radius so that the end correction is the major part of the kinetic mass.

Interaction between two circular apertures.

Let us consider two equal, thin circular apertures, each of area A_o, placed diametrically with their centra located a distance $\underline{a}$ from the axis of a circular tube, as shown in

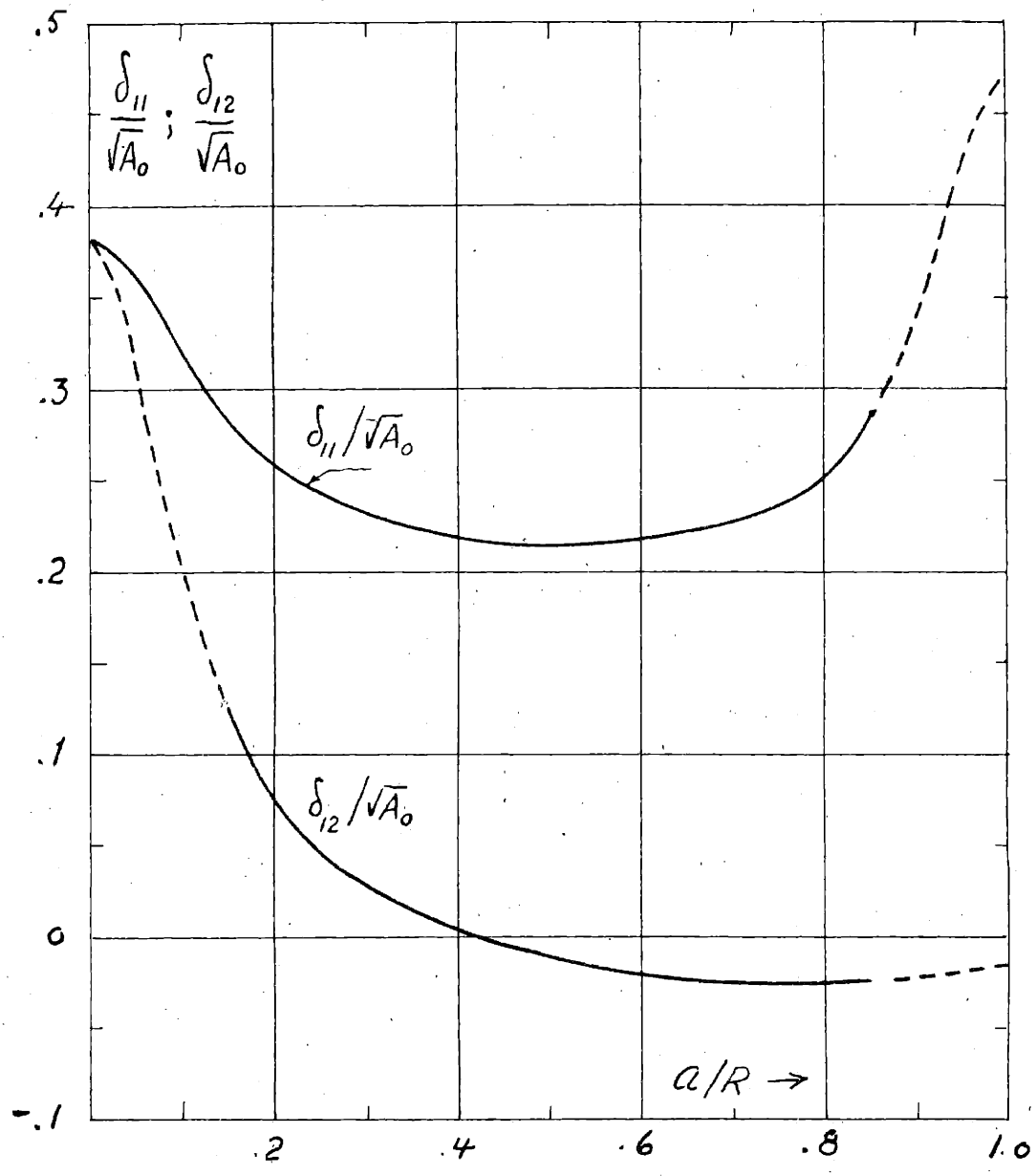
.5
.4
.3
.2
.1
0
-.1
$\frac{\delta_{11}}{\sqrt{A_0}}$; $\frac{\delta_{12}}{\sqrt{A_0}}$
$\delta_{11}/\sqrt{A_0}$
$\delta_{12}/\sqrt{A_0}$
a/R →
.2
.4
.6
.8
1.0

Figure 4

figure 5.

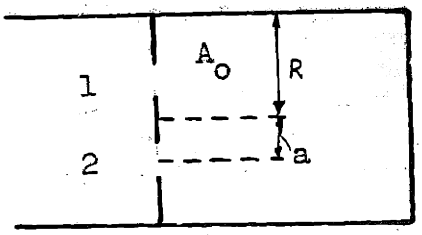

Figure 5

If interaction is disregarded each aperture can be considered as a single excentric one and its mass reactance is given by (I.5). When the two apertures approach each other it is expected that their total acoustic mass reactance should become almost equal to that of a single aperture with an area $2A_o$. However, this is found to be far from the case if the apertures are considered independent of each other, and a study of the interaction suggests itself.

We calculate then the pressure p_{12} caused by the first "aperture piston" at the surface of the second and determine the interaction impedance

$$Z_{12} = \frac{1}{U} \int_{A_2} p_{12} \, dA_2 \qquad (I.9)$$

where U, the particle velocity, is the same in both apertures due to symmetry. The results from the analysis of the excentric aperture can be applied when determining p_{12}, and by naking use of the addition theorem for the Bessel functions, the integral (I.9) can be evaluated. (The calculations are somewhat lengthy and will not be given here). It can then be shown that the end correction δ_{12} corresponding to Z_{12} is

$$\delta_{12} = \sqrt{A_o}\,\frac{4}{\sqrt{\pi}}\,\frac{R}{r_o}\sum_{m=o}\sum_{n=1}(-1)^m F_{mn} \qquad (I.10)$$

$$F_{mn} = \frac{J_1^2(b_{mn}r_o)\,J_m^2(b_{mn}a)}{(b_{mn}R)^3\left[1-m^2/(b_{mn}R)^2\right]J_m^2(b_{mn}R)}$$

The expression for δ_{12} is the same as that for δ_{11}

$$\delta_{11} = \sqrt{A_o}\,\frac{4}{\sqrt{\pi}}\,\frac{R}{r_o}\sum_{m=o}\sum_{n=1} F_{mn} \qquad (I.5)$$

except for a factor of $(-1)^m$.

The interaction end correction δ_{12} has been computed as a function of a/R for $r_o/R = 0.15$ and the result is shown in figure 4. The part of the curve outside the range. $0.15 < a < 0.85$ has of course no meaning in this case and is shown dashed.

Let us now compare the total mass reactance caused by these two apertures, each with an area A_o, with that of a single aperture with an area $2A_o$. The largest value of $\delta_{11}+\delta_{12}$ is 0.415 and is obtained when $a/R = 0.15$, i.e. when the two apertures just touch each other. The minimum value is 0.20 obtained when $a/R \simeq 0.60$. The corresponding total acoustic reactances caused by the two apertures is $\omega \rho\, 0.83/2\sqrt{A_o}$ and $\omega \rho\, 0.40/2\sqrt{A_o}$ respectively. The end correction for a single concentric aperture with an area $2A_o$, i.e. $\xi = \sqrt{2}\ 0.15$), is obtained from figure 2 and equals

$0.355\sqrt{2A_o}$. The corresponding total acoustic mass reactance $\rho c\chi/2A_o = \omega\rho\, 1.01/2\sqrt{A_o}$, exceeds the value for the two apertures by a factor varying between 1.2 and 2.5. In order to obtain maximum acoustic reactance of a given open area in a partition we must therefore concentrate the open area into a single concentric aperture. This is important to realize in the design of resonators and acoustic filters in tubes.

Measurements.

The discussion so far has been limited to thin apertures. The effect of thickness is naturally expected to cause an additional mass reactance $A_o\rho t\omega$. Besides, it is of course possible that the end correction may vary somewhat with thickness. In order to investigate this question a series of measurements were performed on a set of circular apertures with diameters ranging from 0.36 cm to 2.0 cm and thicknesses from 0.05 to 2.5 cm. The frequency range was 200 - 1000 cps.

The reactance measurements were made with the precision impedance tube at the Acoustics Laboratory [13] using the conventional standing wave method. The plate containing the aperture was placed at the end of the impedance tube and backed up with a tube section, terminated by a movable rigid piston. The length of this section was always chosen to be a quarter wave length so that the plane wave reactance of the

cavity behind the aperture is zero. That is $\zeta = 0$ in (I.3), and the measured impedance is just $2\zeta_s$, which is the reactance of the aperture.

Curves illustrating the measured specific reactances as a function of aperture thickness t are shown in figure 6. The reactance increases linearly with t and the slope should be $\varrho\omega$. The maximum deviation from this value is less than 2 % as can be seen in table 2.

Table 2.

Frequency ν cps	Aperture diameter $2r_o$ cm	Measured specific reactance per unit length of the aperture	Calculated acoustic reactance per unit length $\varrho\omega$
234	0.5	1.78	1.76
234	1.0	1.79	1.76
246	1.4	1.83	1.86
246	2.0	1.88	1.86

The residual part of the reactance at $t = 0$, shown in figure 6, represents the end correction. A special study of this part of the reactance was made by measurements on a group of very thin apertures, $t = 0.05$ cm, for which the end correction is the essential part of the mass. The results of these measurements are chown in figure 7 where the quantity x/r_o is plotted as a function of frequency, x

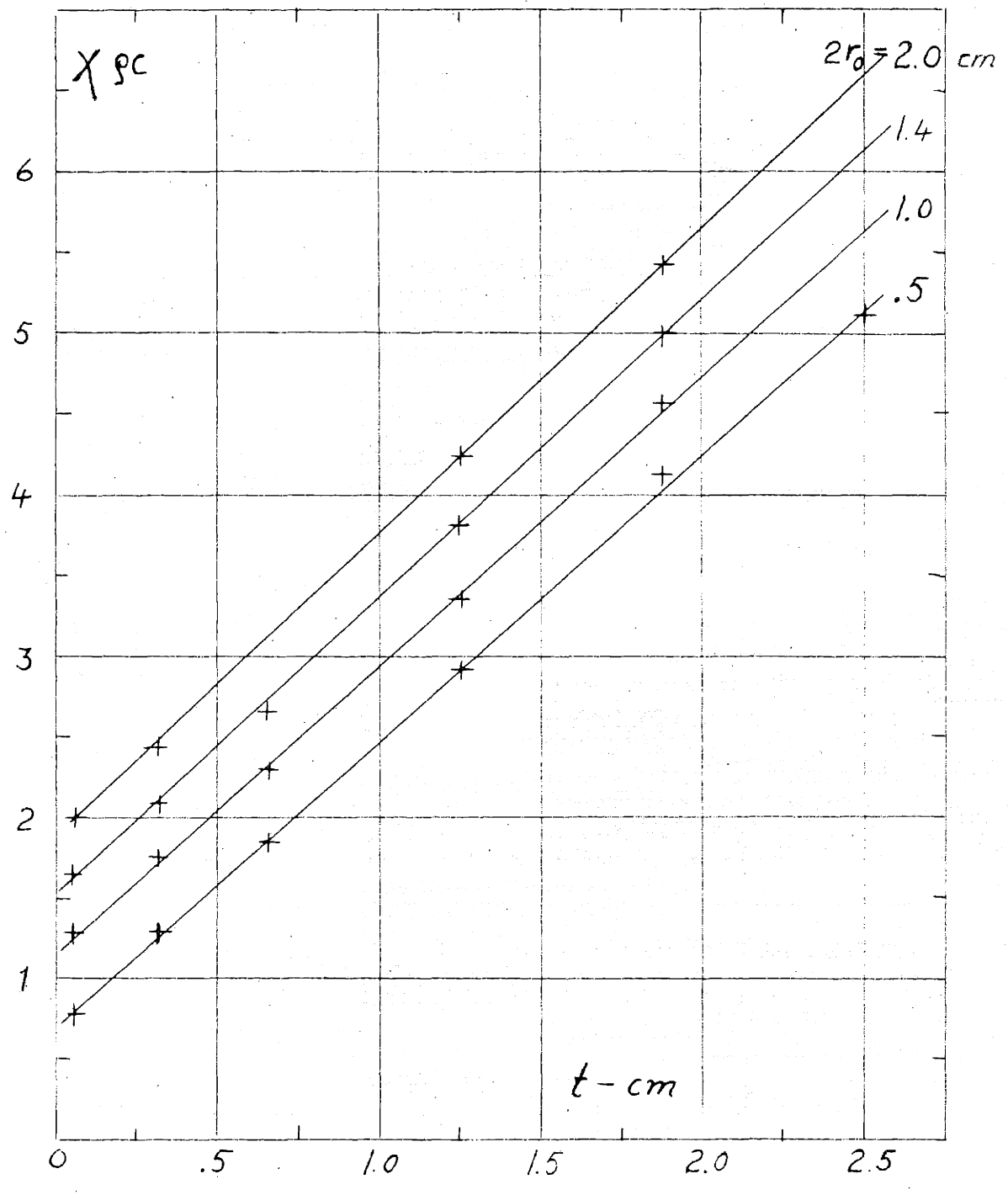

Figure 6

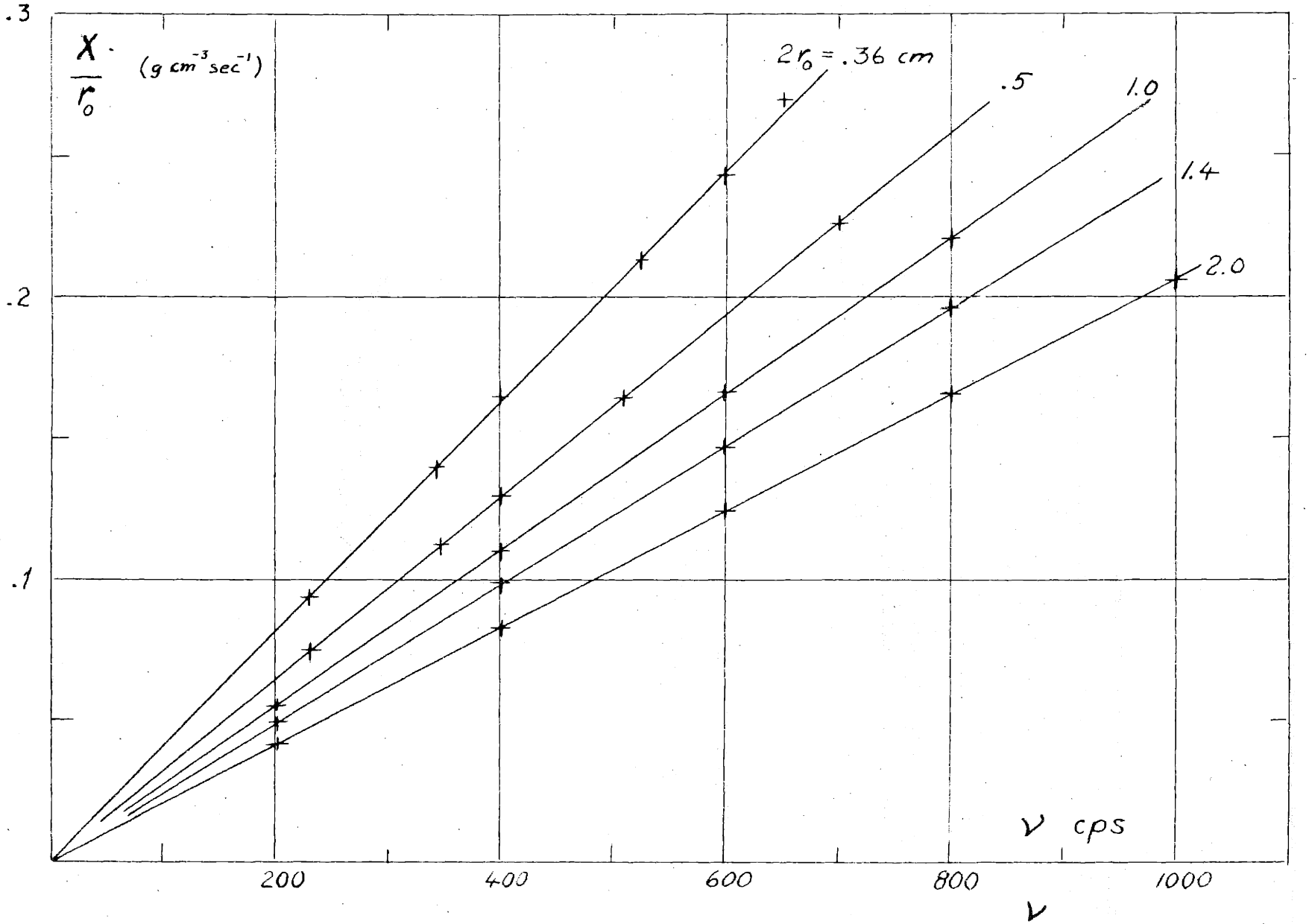
.3
.2
.1
$\frac{\chi}{r_0}$ (g cm^{-3} sec^{-1})
$2r_0$ = .36 cm
.5
1.0
1.4
2.0
ν cps
200
400
600
800
1000
ν

Figure 7

being the specific reactance of the aperture. The experimental values lie almost completely on straight lines, indicating that the kinetic mass is independent of frequency in the frequency range under consideration. It may be mentioned that a plot of $(x_o/r_o)=(16/3\pi)\omega$, representing the reactance for an aperture in an infinite wall, is independent of orifice diameter, whereas we get splitting in thetube case.

From the slope S of a reactance curve in figure 7, we get the total kinetic mass of the aperture $m_{tot}=(r_o S/2\pi)$, which expressed as an equivalent neck length is $l=(S/2\pi\varrho)r_o$. By subtracting the neck length t we obtain the total end correction $2\delta=l-t$, which is listed in table 3 together with the values calculated from (I.4)

Table 3.

Diameter $2r_o$ cm	Measured slope S of curves in fig.7	Total equivalent neck length l cm	Neck length t cm	End correction $2\delta = l - t$	2δ calculated from eq.(I.5)
0.36	0.406 10^{-3}	0.390	0.097	0.283	0.284
0.50	0.324 "	0.430	0.051	0.379	0.387
1.00	0.276 "	0.736	0.051	0.685	0.707
1.40	0.245 "	0.920	0.051	0.869	0.890
2.00	0.207 "	1.110	0.051	1.059	1.12

The agreement between theoretical and experimental values is evidently very good, the average percentage error for the five apertures being 2.6 %.

The measured values are consistently somewhat smaller than the calculated. This is expected from the fact that any assumed velocity distribution different from the correct one gives an end

correction which is always too big. However, the deviations found here are so small that the plane velocity distribution can be considered to yield the mass reactance of an aperture with an accuracy which is within the experimental error of most acoustic measurements.

§ 2. The aperture resistance.

The local increase in particle velocity caused by a constriction or a discontinuity in a tube causes a relatively large dissipation due to viscosity. The calculation of this dissipation can be done approximately by using an assumed velocity distribution and introducing a "skin" friction resistance R_s, which for a "smooth" surface may be set approximately equal to [14]

$$R_s = \frac{1}{2}\sqrt{2\rho\mu\omega} \qquad (I.12)$$

where μ is the viscosity of air and ρ the density. Aperture resistances calculated in this manner have been reported to be smaller than the measured [15] - [19]. However, these reported deviations seems to have been caused by disregarding the fact that not only the neck dissipation but also the contribution from other parts of the plate containing the aperture are included in the measured results. Before comparing the measured values with the expression for the specific neck resistance,

$$\rho c\theta_n = 2R_n t/r_o \qquad (I.13)$$

(R_n = surface resistance in the neck.)

these additional contributions have to be subtracted.

In the impedance measurements mentioned in the previous section the separation of the neck dissipation from the exterior contributions was obtained by measuring the aperture resistance as a function of neck length. A linear relation is found as shown in figure 8, and from the measured slopes of the curves, the resistance per unit length of the neck is found to be in reasonable agreement with (I.15) using $R_n = R_s$. The maximum deviation is 9 % (average 5 %) in measurements on three apertures with diameters 0.5, 1.0, 1.4 cm as seen in table 4.

Table 4.

Measurements of neck resistance.

Frequency cps.	Aperture diameter $d=2r_o$ cm	Measured slope $S=2R_s/r_o$ (see fig)	Surface resistance R_n obtained from measurements.	Calculated surface resistance from (I.12)
229	0.5	0.105	0.013(1)	0.0127
234	1.0	0.0570	0.014(1)	0.0129
234	1.4	0.0378	0.013(2)	0.0129

However, the residual part of the measured resistance, the "end correction", is found to be considerably larger than the calculated, using a surface resistance $R_w = R_s$ on the parallel walls of the aperture plate. The dissipation is obtained by integrating the squared tangential velocity

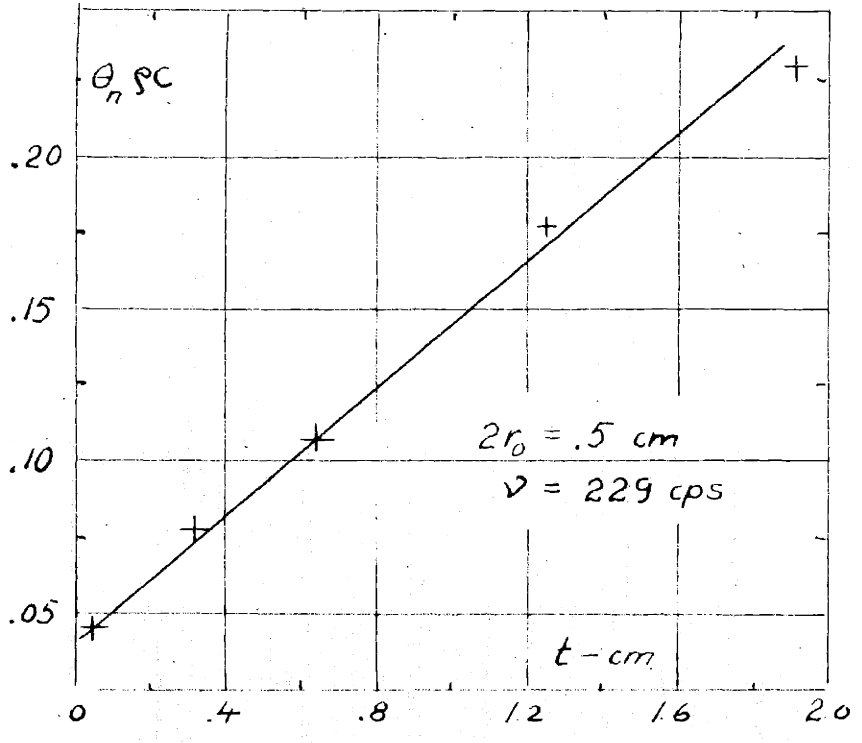
θ_n pc
.20
.15
.10
.05
$2r_0$ = .5 cm
ν = 229 cps
t - cm
0
.4
.8
1.2
1.6
2.0

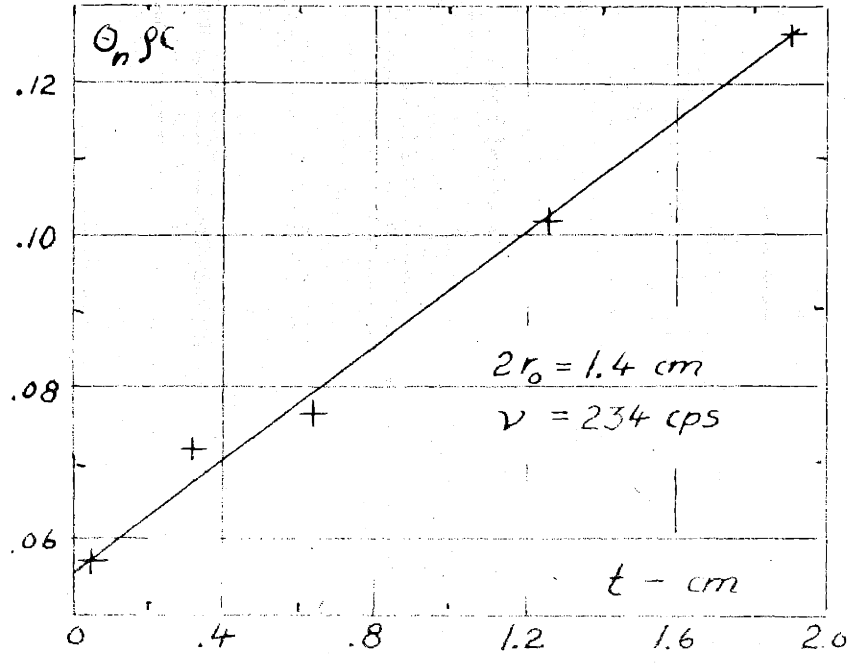
θ_n pc
.12
.10
.08
.06
$2r_0$ = 1.4 cm
ν = 234 cps
t - cm
0
.4
.8
1.2
1.6
2.0

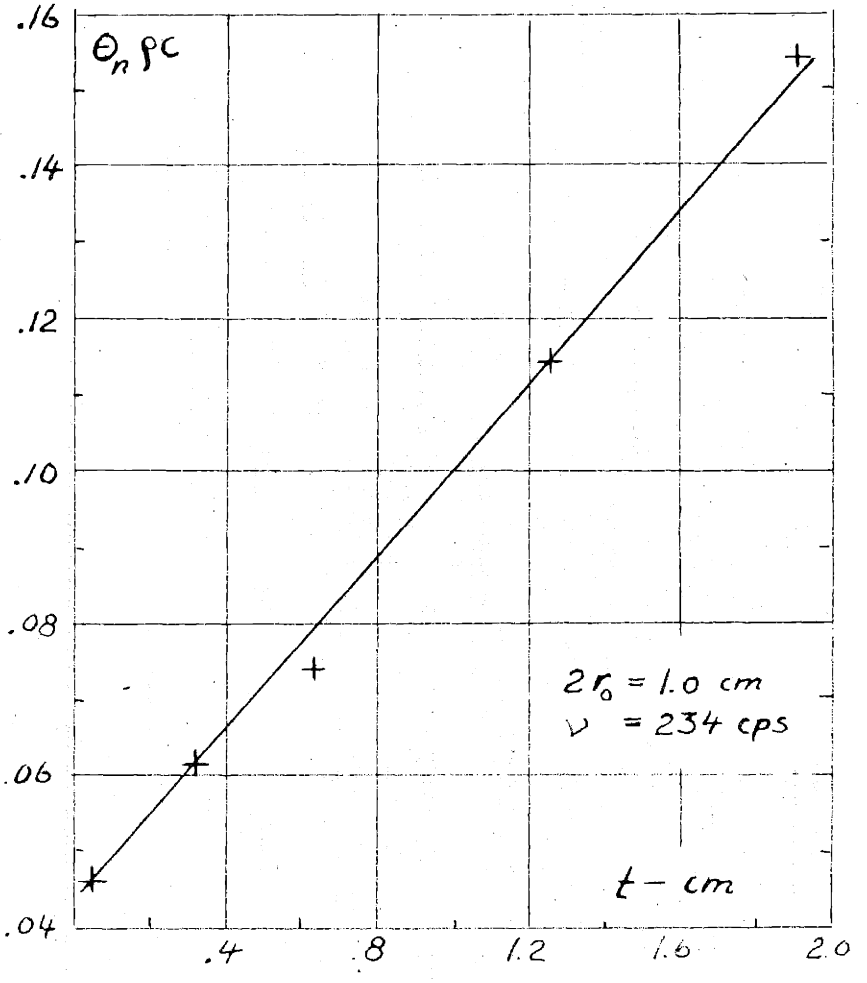
θ_n pc
.16
.14
.12
.10
.08
.06
.04
$2r_0$ = 1.0 cm
ν = 234 cps
t - cm
.4
.8
1.2
1.6
2.0

Figure 8

over the wall surfaces and for small apertures the corresponding specific resistance can be expressed approximately as [9]

$$\varrho c\theta_w \simeq \frac{4R_w}{U_o^2 r_o^2} \int_0^R \left[u-(r_o/R)^2 U_o\right]^2 r\, dr \qquad (I.14)$$

where u is the axial velocity distribution over the aperture plate, $u = u(r)$ for $r \leq r_o$ and $u = 0$ for $r > r_o$, and U_o is the average velocity in the aperture. For a uniform velocity distribution, $u(r) = U_o$, the expression (I.14) reduces to

$$\varrho c\theta_w \simeq 2R_w \left[1 - (r_o/R)^2\right] \qquad (I.14a)$$

All surfaces of the aperture plates considered had the same smoothness and we should reasonably expect that $R_w = R_n = R_s$. However, of this value of R_w is used in (I.14a) the resulting resistance θ_w becomes about 50 % smaller than the measured and in order to get approximate agreement with measurements we have to put $R_w \simeq 2R_s$.

A possible reason for this discrepancy may be that the surface resistance given in (I.12) does not apply when calculating the dissipation on the plate walls. This resistance is obtained by determining the force per unit area of an infinite plane vibrating in its own plane with simple harmonic motion in a semi-infinite body of viscous fluid. In

that case there is no velocity gradient in a direction parallel to the plate. Under the present conditions, however, we have a large velocity gradient along the plate surfaces in the radial direction in the vicinity of the aperture, which may lead to a different value of the surface resistance.

Although a further analysis of the surface resistance concept is required in this case, it does not seem likely that the large discrepancy found above can be accounted for in this way.

It seems more plausible that the effect of the velocity distribution in the aperture is more important in this connection. In order to investigate this possibility the following distribution was introduced in (I.14); $u(r)= \frac{1}{2} U_o \left[1-(r/r_o)^2\right]^{-1/2}$ for $r < r_1$, $u(r)=u(r_1)(r_o-r)/(r_o-r_1)$ for $r_1 < r < r_o$ and $u(r)=0$ for $r > r_o$; in other words, the steady flow distribution was assumed in the region between $0 < r < r_1$ and a linear decrease of $u(r)$ down to zero at $r = r_o$ in the region $r_1 < r < r_o$. This distribution yields a resistance which in addition to a term involving $\omega^{1/2}$ also contains a relatively large term proportioned to ω in disagreement with measurements, which give an almost perfect $\omega^{1/2}$- dependence of the resistance. The ω-term corresponds to the part between $r = r_1$ and $r = r_o$ of the integral in (I.14). If this is omitted, the frequency dependence of the calculated and measured resistance are in better agreement.

Since the integral goes to infinity when $r_1 = r_o$ one can always, by a proper choice of r_1, make the calculated resistance values (using $R_w = R_s$) for a single aperture agree with measured at least in a small frequency range. However, by expressing the resistance in terms of r_1 and R_w and choosing these two values as to make a best agreement between calculated and measured resistance curves for all the apertures studied over a frequency range between 200 - 1000 cps., a value $R_w \simeq 2R_s$ was again found. However, since these calculations are somewhat arbitrary and because of the omitted relatively large part of the integral and the divergence of the integral when $r_1 = r_o$, it seems plausible that the cause of the discrepancy is to be found in the effect of the velocity distribution.

The question of the meaning of "smooth surface" is also of importance in this connection. Preliminary experiments were performed to investigate the effect of the roughness of the surface. However, these measurements were not carried far enough to enable one to draw any general conclusions.

Finally the appearance of non-linear effects in the aperture region requires special attention since circulations and turbulence may occur even at low levels and contribute to the measured resistance Θ_w. A rather detailed study of these phenomena is presented in the following paragraph. It

is found that the non-linear contributions to the resistance are in general small at the low levels at which the measurements described above were performed.

§ 3. Acoustic circulations and jet-effects and the non-linear aperture impedance..

Introduction and summary.

The transmission of sound through an aperture as given in the preceeding section is actually much more involved than indicated there. Since there is going to be a considerable increase in the velocity in the aperture region due to the constriction, one may expect that second (or higher) order effects should occur even at relatively low sound levels in the tube.

The presence of such additional effects was first observed by Rayleigh in his candle experiment [20], and he stated that the observed motion of the air was pulsatory. This opinion is not shared by Eckart, however, who claims that the motion may have been steady. In his recent paper on streaming and vortices Eckart shows [21] that steady circulations necessarily follow as part of the wave equation, taking into account viscosity and second order terms. His treatment is mainly valid for liquids and for ultrasonic frequencies and it is claimed to give a correct explanation of the well-known "crystal wind". A qualitative and to some extent quantitative check of Eckarts theory has been

reported by Liebermann [22] who shows circulation effects in water at a frequency of 2 Mc. Steady circulations of this nature in air at audio frequencies was already predicted by Rayleigh in his treatment of the circular cylindrical tube [23] and experimental verification of circulations of this kind has been given by Andrade [24] who, in addition, shows circulations around a sperical obstacle in a tube. Bouasse [25] has reported similar findings including steady circulations at the mouth of an open tube and pulsatory motion around resonators in agreement with Rayleigh's experiment.

The presence of additional non-linear losses of sound in an aperture in a tube, indicating some kind of "turbulence", was first reported by Sivian in his study of the impedance of small orifices [26]. Non- linear behaviour also of the reactance of an aperture has later been observed by Labate [27]. Sivian assumed that the non-linear losses were connected with turbulence of the same type as that occuring in a tube at steady flow. It was found, however, that the onset of non-linearity was not sudden and the Reynolds number did not seem to be characteristic for the occurence of non- linearity. The quantitative results obtained by Sivian may be subject to some doubt for reasons discussed in § 4, page 48.

It is the purpose of this section to present an experimental investigation, leading to a description of different types of circulations and jet effects caused by an aperture at

different sound levels and frequencies, and to investigate the influence of these effects on the acoustic conductivity of the aperture.

It is found that there exist four definite types of "circulation effects" as the particle velocity in the aperture is increased. These regions have been represented by "phase diagrams", which show at what frequencies and levels the different types of circulation occur. Photographs of the various flow patterns in each region of the "phase diagrams" have been taken for a number of apertures.

A turbulence criterion for sound through an aperture is presented, based on the observation that the non-linear effects are velocity-determined in some cases, displacement-determined in others.

It is shown that the non-linear properties of the acoustic resistance of an aperture is closely connected with the circulation effects. Quantitative check in one of the circulation regions and a good qualitative overall agreement indicates that the non-linear properties of the resistance is due to the interaction between the sound field and the circulatory effects. The reactance of the aperture is independent of sound level until turbulence is obtained, where the reactance starts to decrease.

Experimental procedure.

The experimental set-up used in these studies is shown in figure 9. A steel plate with a circular orifice was placed between two cylindrical sections of tubing having an interior diameter of three inches. These sections contains two sets of windows, one for illumination and one for observation. The tubes were connected to a three inch precision impedance tube [13]. The aperture was backed with a cavity, the length of which was adjusted by a solid brass plunger. The cavity length was always adjusted to a value equal to a quarter wave length of the sound at which measurements were being made. This cavity length was selected only because it made measurements of acoustic impedance of the aperture more convenient; the circulation effects which are mainly of local character are independent of cavity length if the length is not too short. The acoustic impedance of the aperture was determined by the conventional standing wave measurement in the tube. The streamings around the aperture were made visible by means of smoke particles introduced into the cylindrical section immediately terminating the impedance tube.

In order to be able to observe the phenomena, it is necessary to illuminate only a thin layer of the smoke in the tube. This was accomplished by projecting a line source of light through cylindrical lenses, as shown in the figures. Both steady and stroboscopic illumination were used in determining whether the circulations were time-independent or of a pulsa-

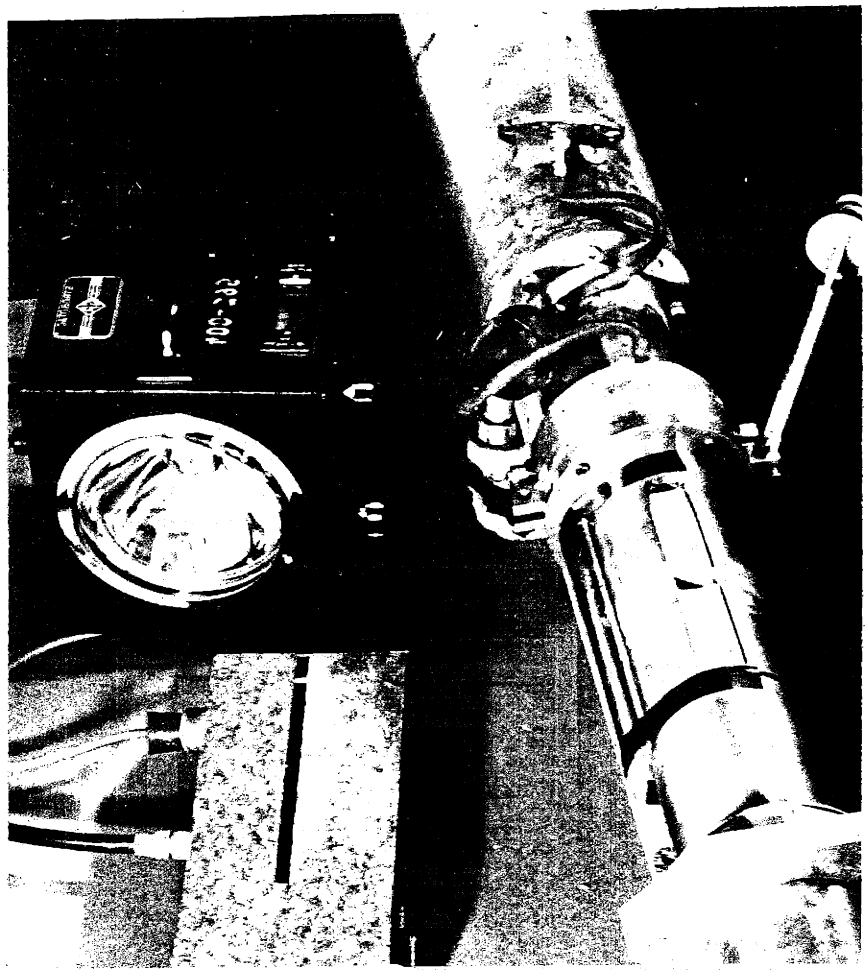

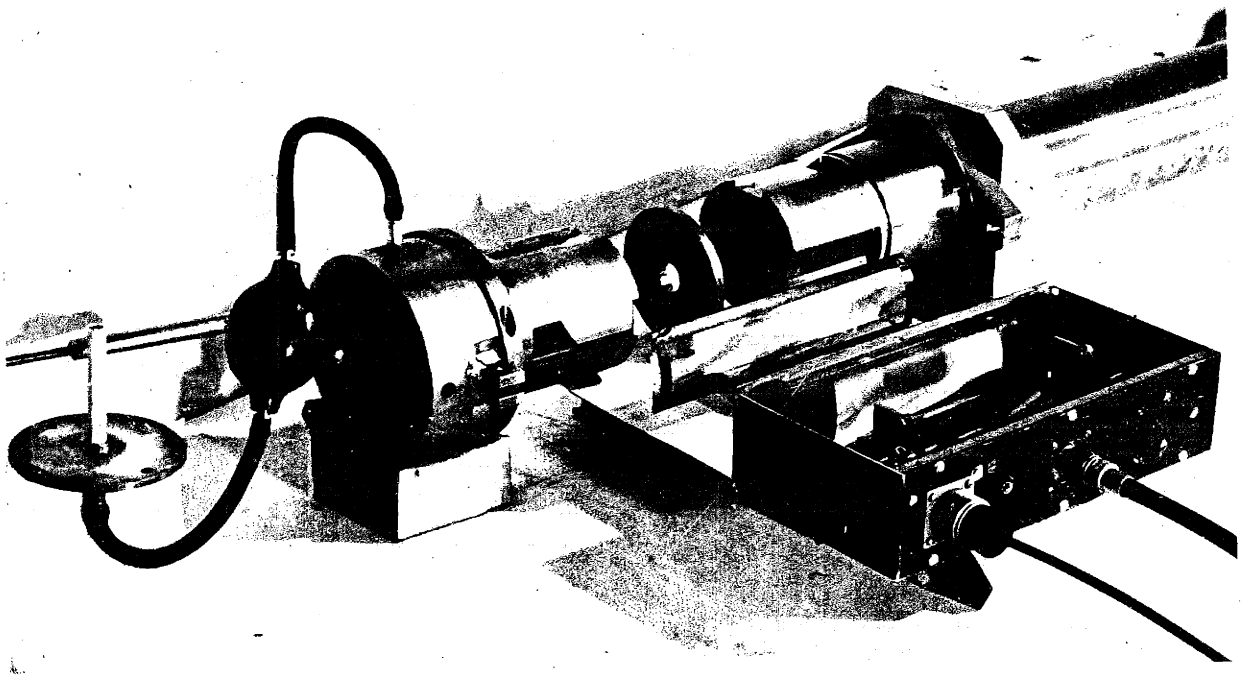

Figure 9

tory character.

These studies were made on a group of 25 apertures covering a range of thicknesses from 0.5 mm to 20 mm and diameter from 3.5 mm to 20 mm in the frequency range from 200 cps. to 1000 cps. Sound pressure levels were used which resulted in particle velocities in the aperture from a few centimeters per second to as high as 900 cm/sec.

Circulation patterns and "Phase diagrams".

The acoustical streaming around each aperture was closely investigated by both stroboscopic illumination and a strong steady light source throughout the entire range of sound pressure levels obtainable with the electronic equipment in use. Flow patterns were studied as a function of the particle velocity through the aperture. with frequency as a parameter. These studies disclosed that, in general, four different types of circulation exist as the sound level is increased from a low to a high value. These various types of circulation can be classified as definite regions of flow:

Region 1: A low particle velocity region with steady circulation; the flow is directed out from the aperture along the axis.

Region 2: A region of steady circulation in which the direction of flow is along the axis toward the aperture i.e. the revers of that in region 1.

Region 3: A region characterized by the onset of turbulence.

Region 4: A high particle velocity region characterized by the appearance of jets and vortex rings. The jet is pulsatory and is made up of air pulses contributed by each cycle of the sound wave. It appeares symmetrically on both sides of the aperture.

In order to show at what sound intensities and frequencies the different kinds of circulation effects occur, "phase-diagrams" have been made up from the measurements and observations made. These phase diagrams are shown in figures 10 - 13 . Figures 14 - 17 show the variation of the different regions with aperture thickness as the frequency kept constant at 224 and 238 cps.

It is evident from these curves that there is a consistent tendency for the steady circulations to become more pronounced with increasing frequency. This is in qualitative agreement with Eckart's theory. For sufficiently low frequencies, and sufficiently thin orifices, we see that it is possible to pass directly from region 1 to region 4, in which case the steady circulations are of importance only for low levels. It is interesting to notice the consistent displacement of the "eutectic point" towards the origin when the orifice diameter increases; a transition from region 1 to region 4

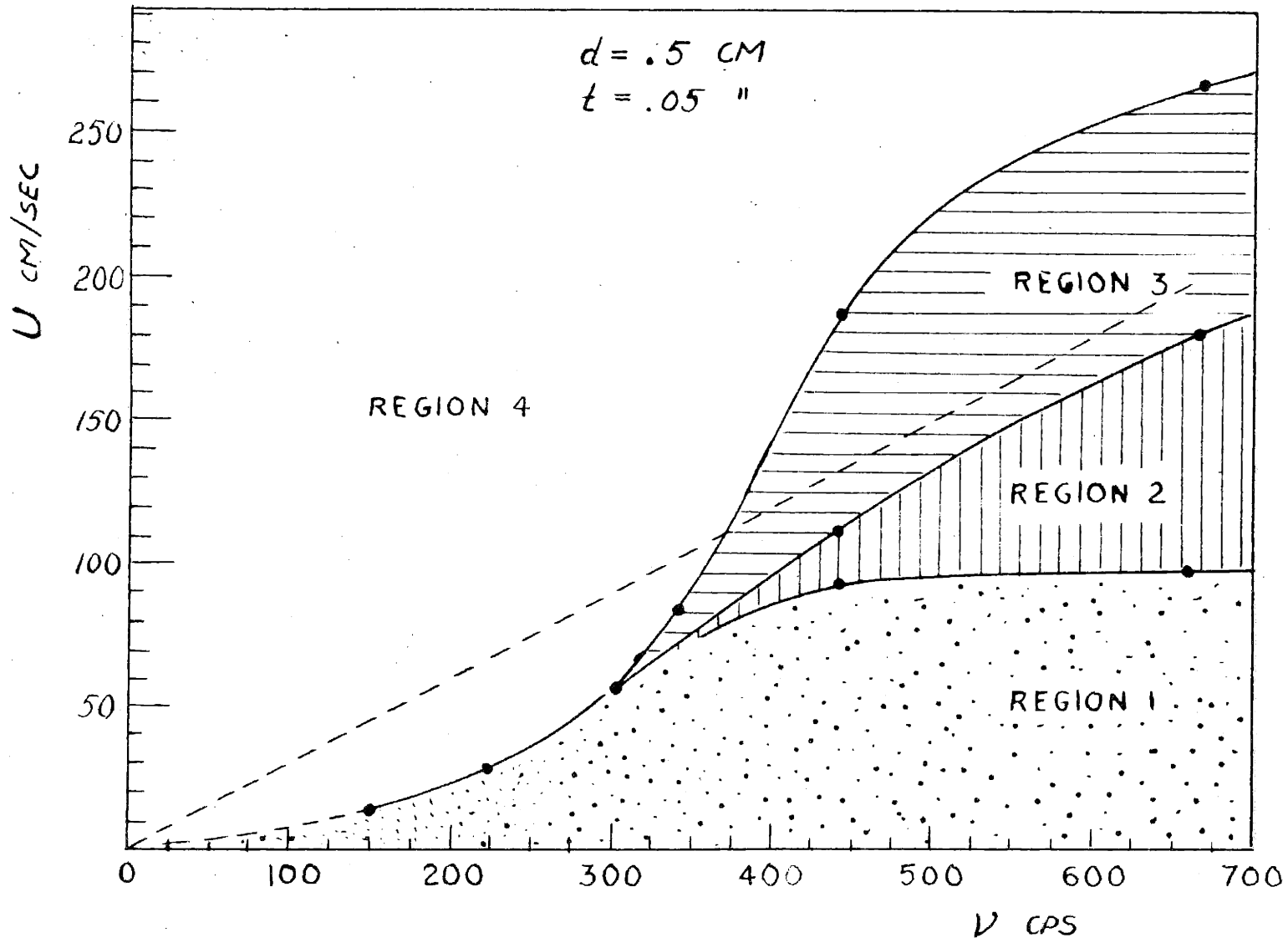
d = .5 CM
t = .05 "
U CM/SEC
250
200
150
100
50
REGION 4
REGION 3
REGION 2
REGION 1
0
100
200
300
400
500
600
700
V CPS

Figure 10

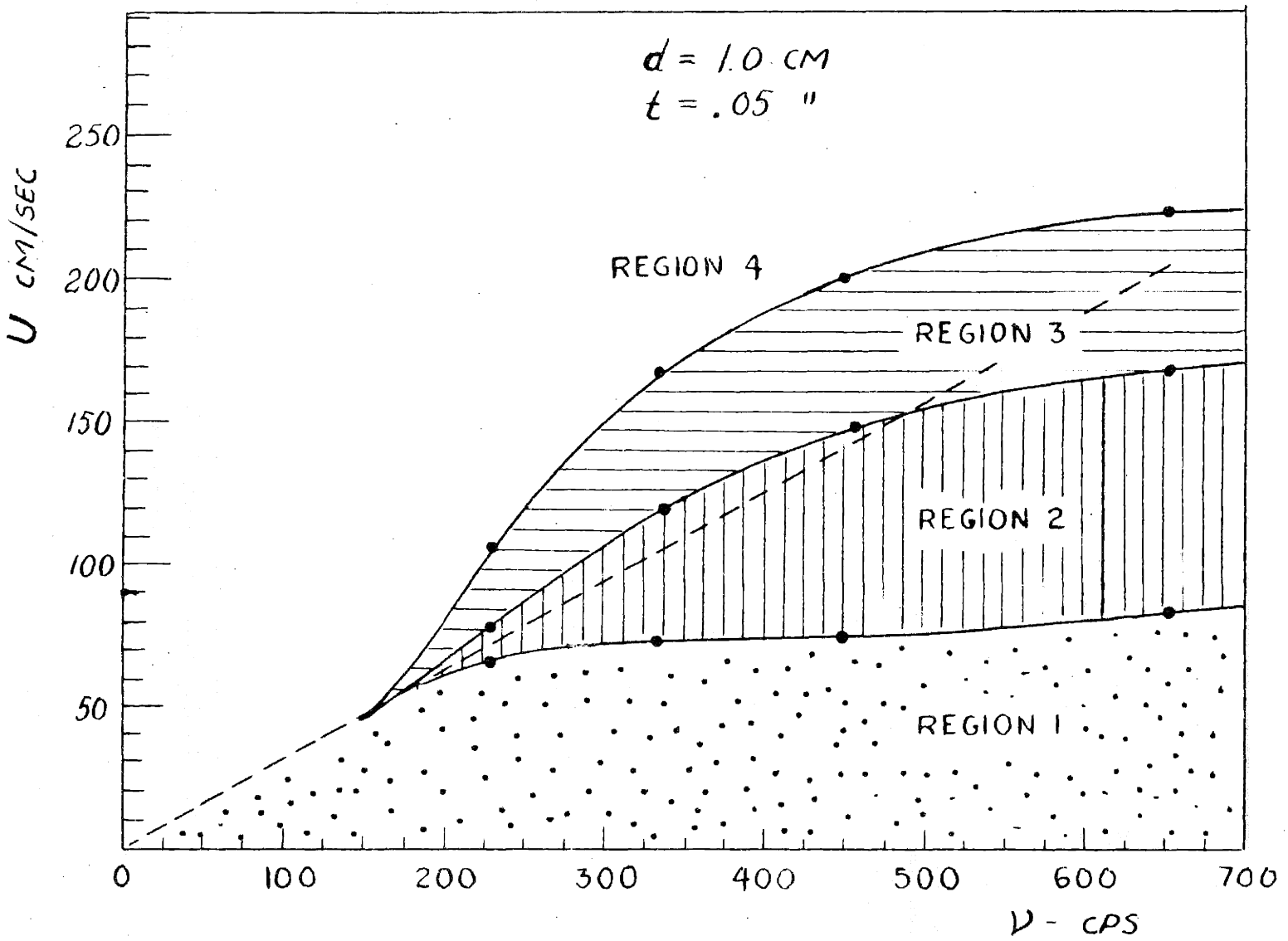
d = 1.0 CM
t = .05 "
REGION 4
REGION 3
REGION 2
REGION 1
U CM/SEC
V - CPS
250
200
150
100
50
0
100
200
300
400
500
600
700

Figure 11

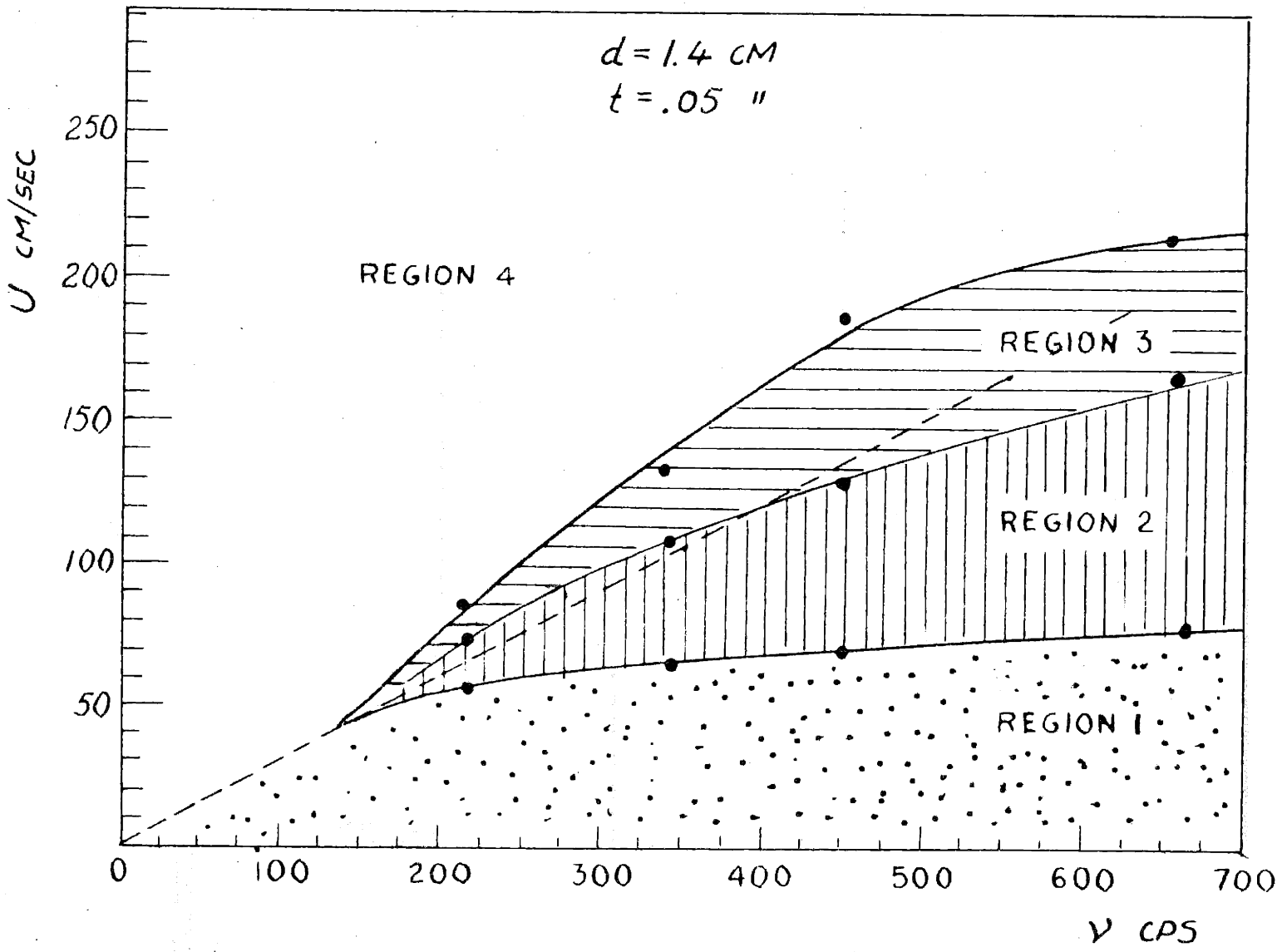
d = 1.4 CM
t = .05 "
U CM/SEC
250
200
150
100
50
REGION 4
REGION 3
REGION 2
REGION 1
0
100
200
300
400
500
600
700
ν CPS

Figure 12

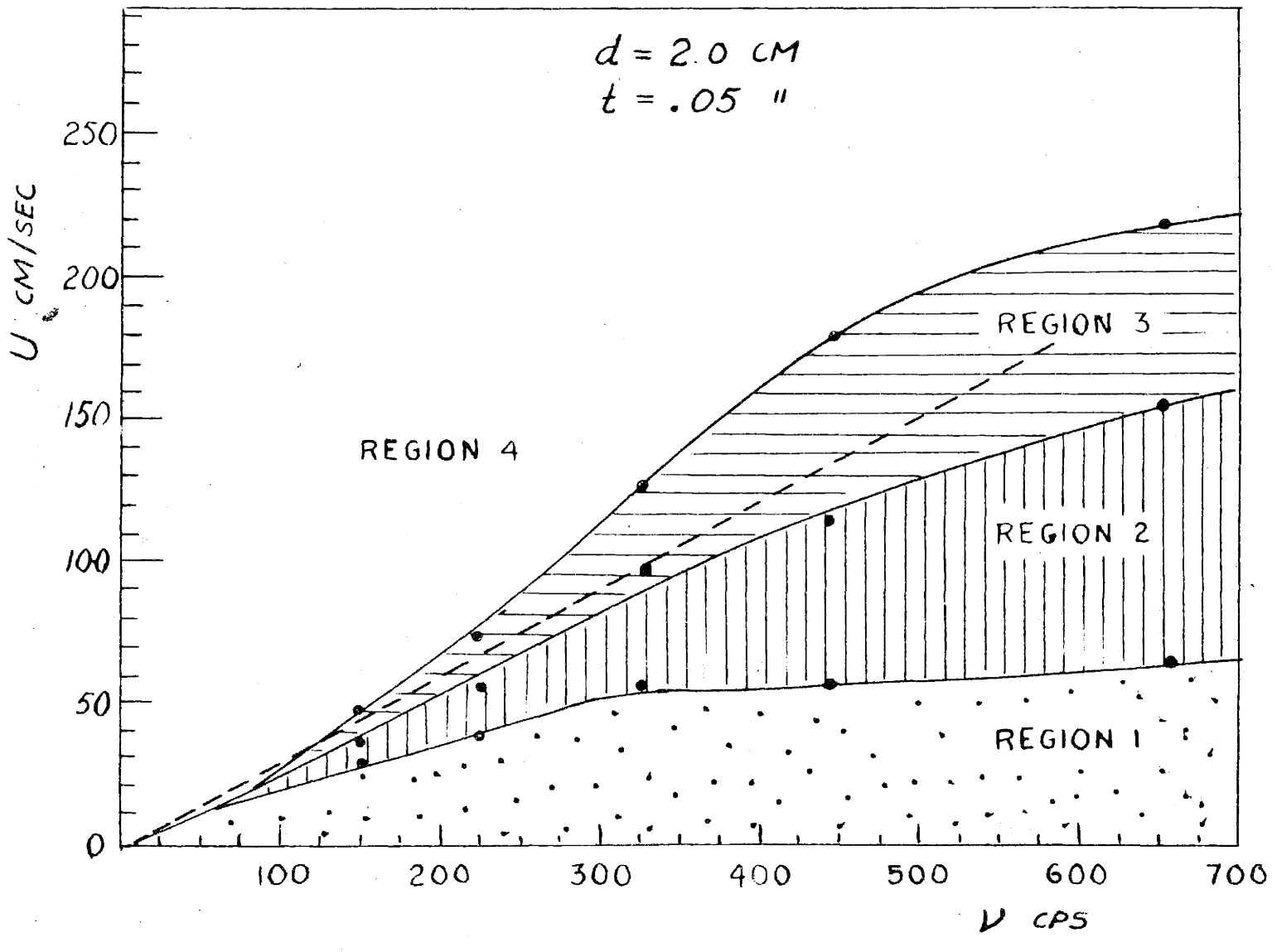
d = 2.0 CM
t = .05 "
250
200
150
100
50
0
U CM/SEC
REGION 4
REGION 3
REGION 2
REGION 1
100
200
300
400
500
600
700
ν CPS

Figure 13

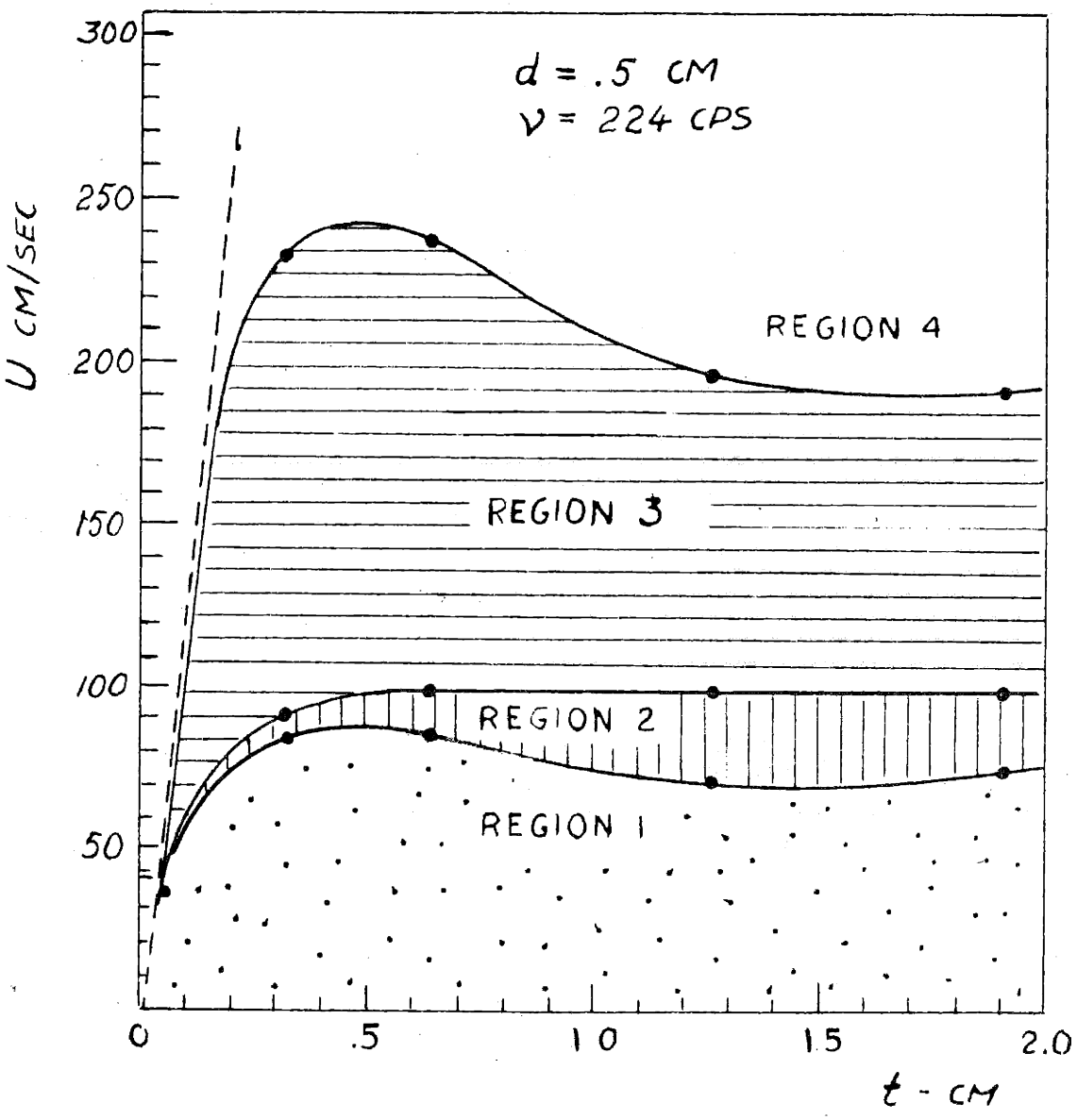
d = .5 CM
ν = 224 CPS
U CM/SEC
300
250
200
150
100
50
REGION 4
REGION 3
REGION 2
REGION 1
0
.5
1.0
1.5
2.0
t - CM

Figure 14

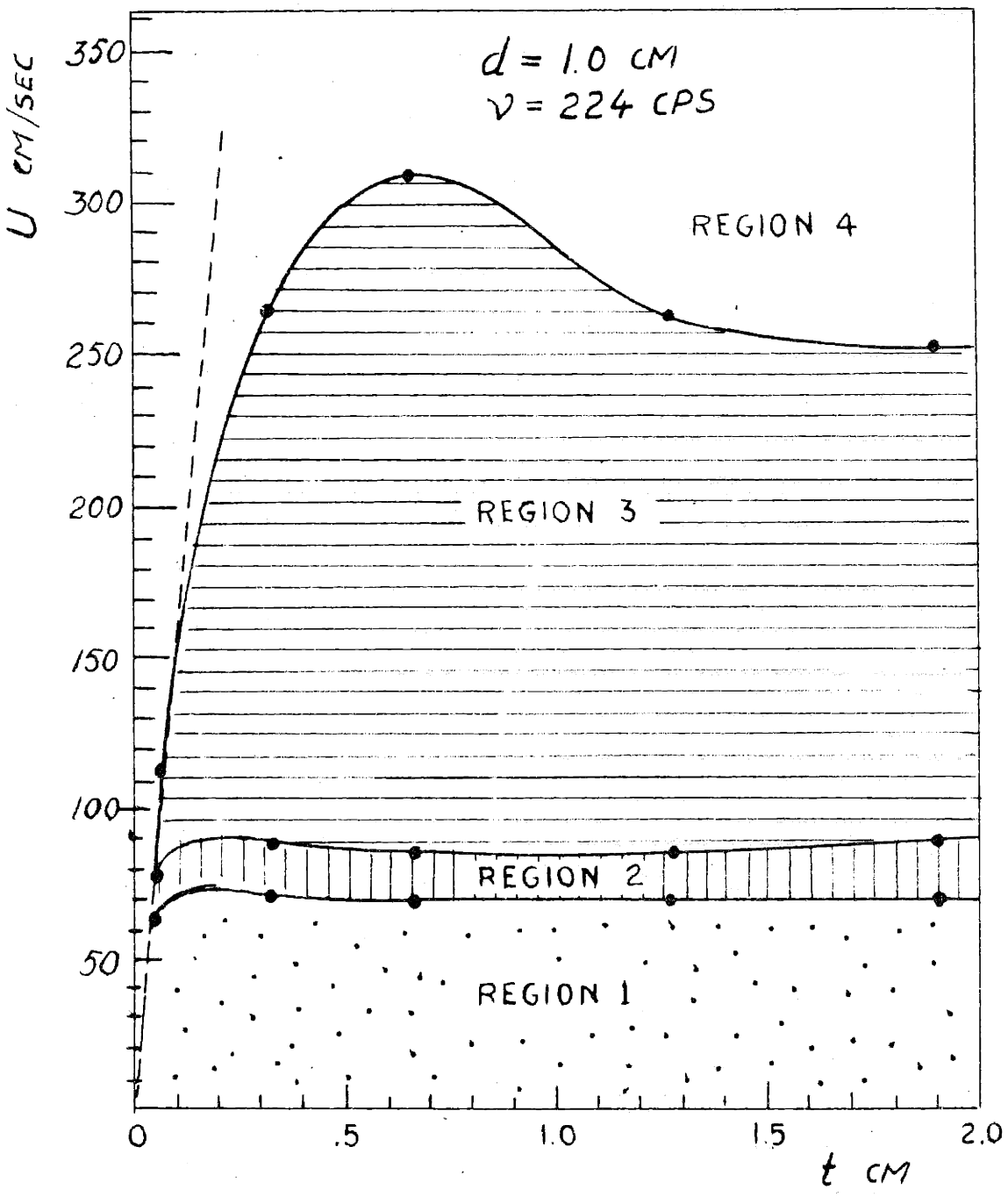
d = 1.0 CM
ν = 224 CPS
U CM/SEC
350
300
250
200
150
100
50
REGION 4
REGION 3
REGION 2
REGION 1
0
.5
1.0
1.5
2.0
t CM

Figure 15

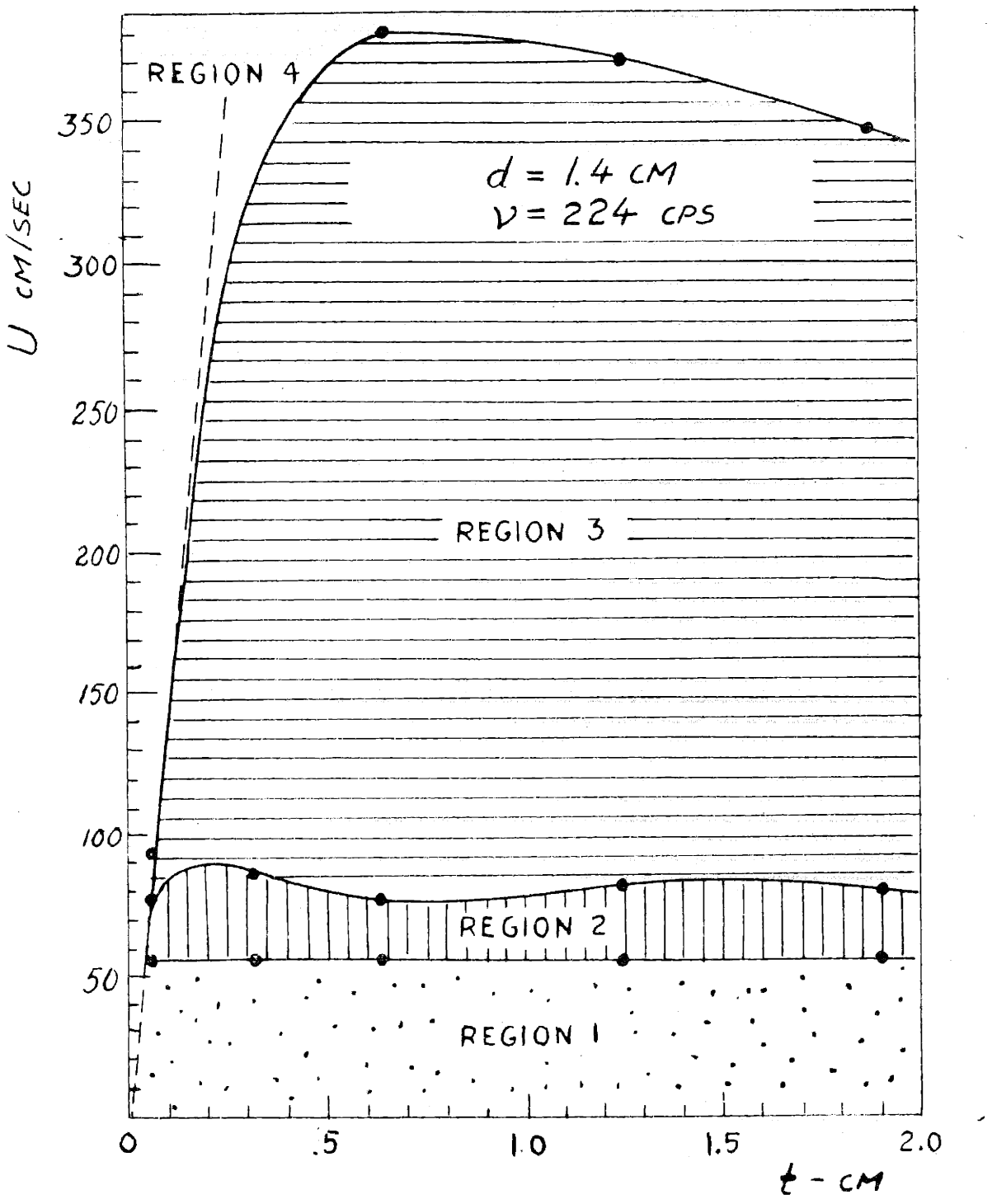
REGION 4
REGION 3
REGION 2
REGION 1
d = 1.4 CM
ν = 224 CPS
U CM/SEC
350
300
250
200
150
100
50
0
.5
1.0
1.5
2.0
t - CM

Figure 16

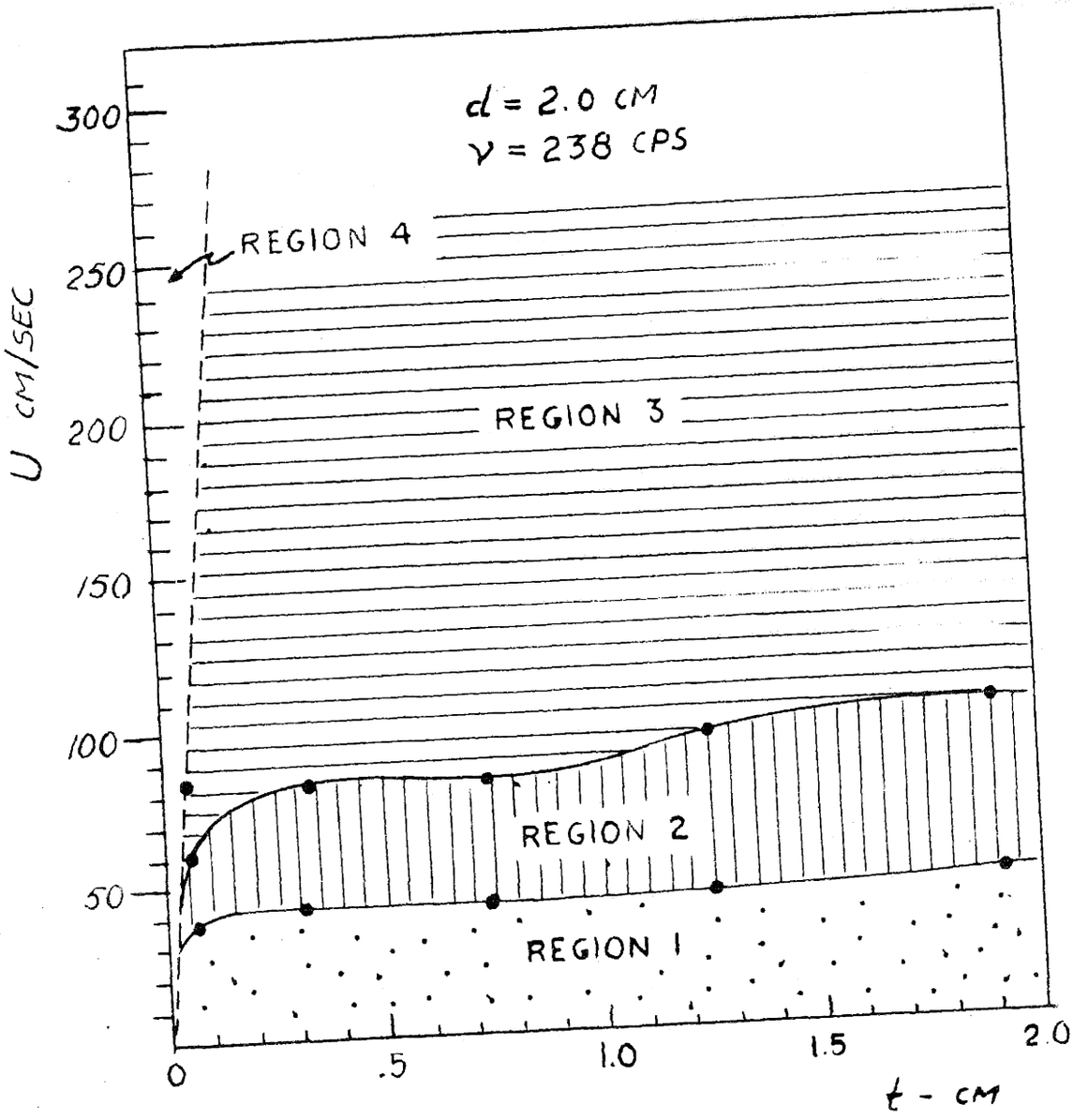
d = 2.0 CM
ν = 238 CPS
REGION 4
REGION 3
REGION 2
REGION 1
U CM/SEC
300
250
200
150
100
50
0
.5
1.0
1.5
2.0
t - CM

Figure 17

can generally be expected only for relatively small apertures.

The turbulent effects start with region 3. For a steady stream of air in a long tube the usual criterion for turbulence is a critical value of the Reynolds number. It is evident from the phase diagrams that such a criterion cannot properly be used in connection with effects of this kind. Its shortcomings, of course, result from the fact that nonlinearity is not due to turbulent effects alone, and even if it were, such a number would necessarily have to be function of frequency and the geometry of the aperture.

It is obvious that the average net amount of air going through the aperture is always zero. In region 1 and 2 this condition is immediately fulfilled because the circulations occur symmetrically on both sides, the separate flow-lines never crossing the orifice. In region 4, which is characterized by pulsations, air is drawn in diffusely from one side to the aperture and thrown out along the axis on the other side. This "breathing" effect alternates from one side to the other with the frequency of the sound, and the flow pattern is exactly symmetrical on both sides of the aperture. Since the air jet is concentrated along the axis, there exists an average out-flow of air along the axis and an average inflow at the edges of the aperture such that the total average is zero.

In the turbulent region 3, where sometimes pulsations and steady circulations are superposed and roughly of the same importance, the flow pattern is not always symmetrical. We may, for example, have an average inflow along the axis on one side and an outflow on the other, with compensating streams in opposite directions in other parts of the aperture. For apertures large enough (e.g. 2 cm in diameter) the geometry of these unstable flow patterns can be quite complicated. Their "direction" is not unique but probably depends on the phase of the sound wave in the orifice, when the cirtical level causing this kind of circulation is reached. It was found that the asymmetrical pattern could be exited in one "direction" as well as in the opposite.

Region 1.

Figure 18 represents a typical picture of the type of circulation that exists in region 1 of the phase diagram. Two centers of circulation just outside the edges of the orifice are visible in this picture. They appear at very low sound intensities and the circulation region increases with an increase in sound level. These two separate circulating regions very soon contact each other to give a relatively high velocity stream aong the centrum line. This can be seen in figure 19. The circulation region increases with increasing sound intensity until it reaches a maximum and then it begins to decrease, although its direction of flow is still the same.

Region 2.

After a certain velocity is reached, the circulation begins to change in character and enters region 2 of the phase diagram. A typical example of a flow pattern at the beginning of this region is shown in figure 20. This photograph represents a transition from region 1 to region 2. Both types of flow, typical of each region are evident; outflow from the aperture can be seen in the center, near the aperture, and a relatively strong inflow is seen outside of this region. The outflow ultimately disappears and the inflow becomes pure when the sound level is sufficiently increased, as shown in figure 21. In this type of flow, very high stream velocities are obtained and turbulence finally begins at the edges of the aperture.

Region 3.

This turbulence represents the beginning og region 3 and results in an exchange of particles between the stream on one side of the aperture and that on the other side. The exchange appears as "boiling" around tha aperture. At the same time, pulsatory effects start to superpose on the streams, but are not yet predominant. Figure 22 shows the streaming at a higher sound level, just before complete turbulence has set in. The pulsations, at this stage, are beginning to become more important and when the sound level has reached a certain value, a real pulsatory jet is formed which causes complete turbulence in the tube. This is the

beginning of region 4.

Region 4.

The jet usually starts on one side of the orifice. After additional increase in level the jet appears also on the other side, resulting in complete symmetry. The particle velocities representing the boundary line between region 3 and region 4 are those for which a jet was obtained in either direction. The onset of a jet is for most apertures very well defined, since at a certain level a sudden "break-through" occurs, in which every cycle of the sound wave gives a pulse. At lower levels (I.e. in region 3) the "breaks" occur only intermittently.

A typical jet in tube photographed under steady illumination is shown in figure 23. Figure 24 shows the jet when it is photographed with flash illumination with the terminating tube eliminated. This gives a clear indication of the lengths these jets can attain and also shows the pulsatory character. The pulsations, however, are more strikingly shown by figure 25 which gives a picture of the jet taken at a still higher sound intensity. Here we have separate vortex rings travelling out from the aperture with a speed of the order of the average sound particle velocity U in the aperture. Measurements at a distance of about 5 cm from the aperture gave values between $0.50\ U$ and $0.60\ U$. The formation of the pulsatory jet and the vortex rings can

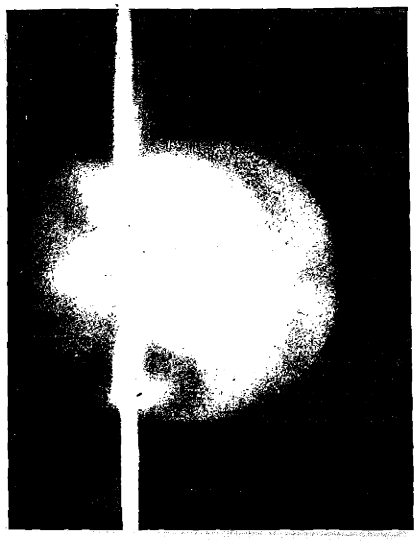

Figure 18

Figure 19

Figure 20

Figure 21

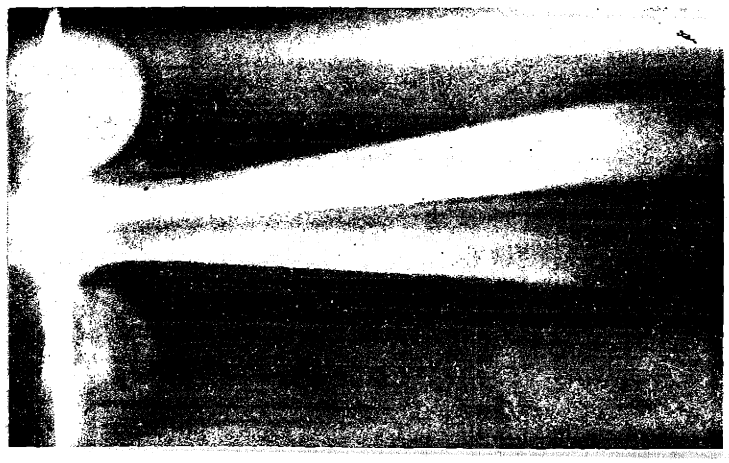

Figure 22

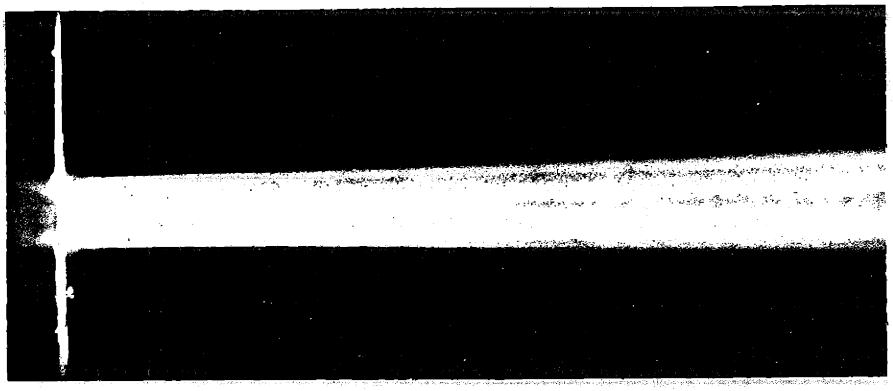

Figure 23

Figure 24

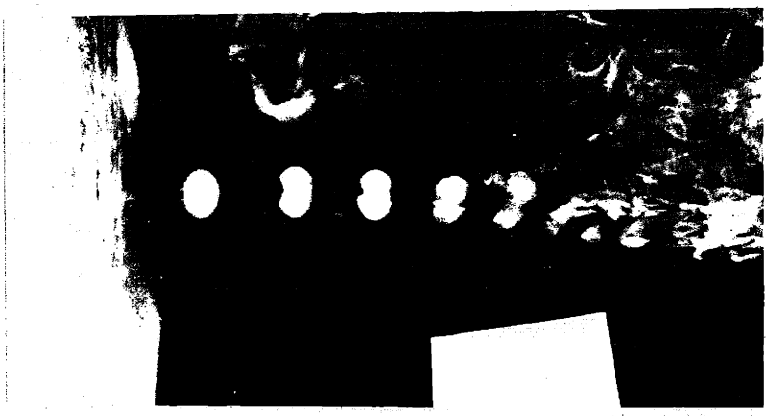

Figure 25

Figure 26

be easily followed under stroboscopic illumination.

It was found that an increase of particle velocity, corresponding to a vertical line in the phase diagram, produces a gradual development of the jet if the line is to the left of the "eutectic" point and a more sudden one if the line is to the right of the"eutectic" point. Figure 26 shows a phase of the smooth development of the jet for the case where the line is to the left of the "eutectic" point.

Turbulence criterion for sound through an aperture.

With the phase diagrams on hand we are now able to discuss the criterion for the onset of turbulence when sound passes through an aperture in a wall. The onset of turbulence is represented by the lower boundary line of region 3 in the phase diagrams in figures 10 - 17 . We call the velocities on this boundary the critical velocities U_c. It is interesting to see that for wall thicknesses large enough the onset occurs approximately at a constant value of U_c , independent of aperture diameter and thickness. The turbulence is then velocity determined, but the onset is not given by the Reynolds number valid for a steady stream in a long tube. This number $R = \rho dU/\mu = 2200$ leads to velocities which are inversely proportional to the diameter and considerably larger than the values found here. That this Reynolds number is not applicable in our case is expected because we have neither a long tube nor a steady flow.

Furthermore, the mechanism of the onset of turbulence seems to be different in the two cases. From what can be learned by merely watching the flow pattern around the aperture it seems as if the first indication of turbulence is caused by the breakdown of the steady circulations around the aperture. In such a case the constant value found above as critical velocity can be better understood, since the circulations are velocity determined. And the invalidity of the Reynold number as a criterion is apparent.

From figures 14 - 17 it is clear that when the plate thickness t is decressed far enough, the critical velocity starts decreasing and seem to approach a straight line through the origin. That is, from being a constant independent of t for large t, the critical velocity finally becomes proportional to t when t approaches zero. Disregarding the transition between these two regions we may define a critical thickness t_c, and say that $U_c = \text{const} = C_1$ for $t > t_c$ and $U_c = C_2 t$ for $t < t_c$. The critical thickness is then given by $t_c = C_1/C_2$. Both from the phase diagrams and the impedance measurements, discussed later, it becomes evident, that for $t < t_c$ turbulence starts when the displacement amplitude in the aperture becomes approximately equal to the wall thickness. That is, the constant C_2 equals ω and we have $U_c = \omega t$ for $t < t_c$, which is shown as a dashed line in the diagrams 14 - 17. At the special frequency for which these diagrams are valid we have $C_1 \approx 85$ and with $\omega = 2\pi \cdot 224$ the critical thickness is $t_c = 0.06$ cm.

In order to be able to generalize this criterion we need more information about C_1. Although any complete experimental evidence is not presented here, we can, however, start with the assumption that C_1 is only frequency dependent $C_1 = C_1(\omega)$, and independent of thickness and diameter of the aperture, which is true at the frequency corresponding to figures 14 - 17. Some information about $C_1(\omega)$ may be obtained from the phase diagrams 10 - 13, where the frequency dependence of the critical velocity for a thin aperture is given. The dashed line appearing in the diagrams is $U_c = t\omega = 0.05\omega$. The results indicate that U_c is roughly proportional to ω at least for frequencies below 500 cps. At higher frequencies the increase is slower.

Within these approximation we can then formulate the turbulence criterion for sound through an aperture as

$$U_c = C(\omega) \quad \text{for} \quad t > t_c \qquad (I.22)$$

$$U_c = t\,\omega \quad \text{for} \quad t < t_c$$

For $\omega \leq 2\pi\ 500$ we have $C_1(\omega) \simeq \text{const} \cdot \omega \simeq 0.06\ \omega$ and $t_c = 0.06$ cm ($t_c = C(\omega)/\omega \to 0$ when $\omega \to \infty$).

We see from figures 10 - 13 that, especially for the smallest aperture, $d = 0.5$, the values of U_c at low frequencies are smaller than ωt, predicted by the criterion. This may be explained by the non uniform velocity distribution

yielding higher velocities at the periphery of the aperture, which becomes more pronounced the smaller the aperture.

Of special interest is the displacement determined part of the criterion, which inherently emphasizes the fact that we are dealing with acoustics and not with steady flow in hydrodynamics. The velocity determined part is more connected with steady flow phenomena and not specifically characteristic for acoustics. It seems physically reasonable, that in addition to a velocity criterion for turbulence onset valid for steady flow, we have in acoustics a displacement criterion coming into play when the obstacles in the field have dimensions of the same order of magnitude as the particle displacement. And it seems reasonable to think about this statement not only in connection with aperture walls but also other obstacles which can be sonsidered stationary in the sound field. And the possibility of turbulence of this kind should not be left without consideration in dealing with cases of sound propagation often met, where higher attenuation than expected is found.

Returning to the aperture problem we want to amphasize the fact that the sound pressure required to cause turbulence goes to zero when wall thickness goes to zero. That means that any experiment intended to check a "thin wall" theory is necessarily going to be uncertain in the respect that the closer the thin wall requirement is fulfilled, the

greater the difficulty of avoiding turbulence. The question how to make the compromise in actual measurements then suggests itself. The answer is, that the wall thickness has to be taken so large, that the critical level for turbulence, given by ωt, is well above the noise level in the measuring system. For it seems to be more important to avoid turbulence than to fulfill closely the thin wall requirement.

Non- linear aperture impedance.

In order to determine the effect of the circulation on the sound field in the aperture region, the acoustic impedance of the aperture was measured over a large range of sound levels (up to 140 db in the tube), using the same technique as described in (I.1).

The previous results illustrated by the phase diagrams indicate that if there is any close connection between the non- linear part of the impedance and the circulation phenomena, then the non-linearity of the impedance should be in some cases velocity -determined, in other displacement-determined. That is, when plotting the results, we may sensibly choose as variable the particle displacement ξ in the aperture for sufficiently thin walls and the velocity U for thicker. (The velocity in the aperture is given by

$$U = \left(\frac{2p_{\pm}}{\rho c}\right)(R/r_o)^2\left[(\theta + 1)^2 + \chi^2\right]^{-1/2}, \text{ where } \zeta = \theta - i\chi$$

is the measured specific impedance ratio).

We may start giving an example on the correlation between steady circulations and the resistance of the aperture. In figure 27 the measured resistance of an aperture 0.5 cm in diameter, is given as a function of U for some different thicknesses. The frequency is 224 cps. We see that the resistance in all cases passes through a maximum at velocities corresponding to region 1 in the phase diagram. As mentioned before, the "intensity" of the circulation in region 1 reaches a maximum and goes through a minimum at the boundary to region 2 where we have a "stagnation", due to the change in direction of the circulations. The measured resistance goes through maxima and minima correspondingly and then increases steadily with increasing velocity as does the circulation intensity. This consistancy between the changes in the steady circulations and the resistance was found to be true in general.

In contrary to this smooth variation of resistance the onset of turbulence causes in general a sudden change in slope of the resistance curve. This is illustrated in figures 28-31, where the non-linear part $\varrho c\theta_{NL}$ of the measured resistance is expressed in terms of an equivalent aperture thickness $\Delta_{NL} = (r_o/2)(\varrho c\theta_{NL}/R_s)$ and plotted against ξ/t, ξ being the particle displacement in the aperture. The quantity Δ_{NL} was chosen because it makes the curves relatively independent of frequency and aperture diameter.

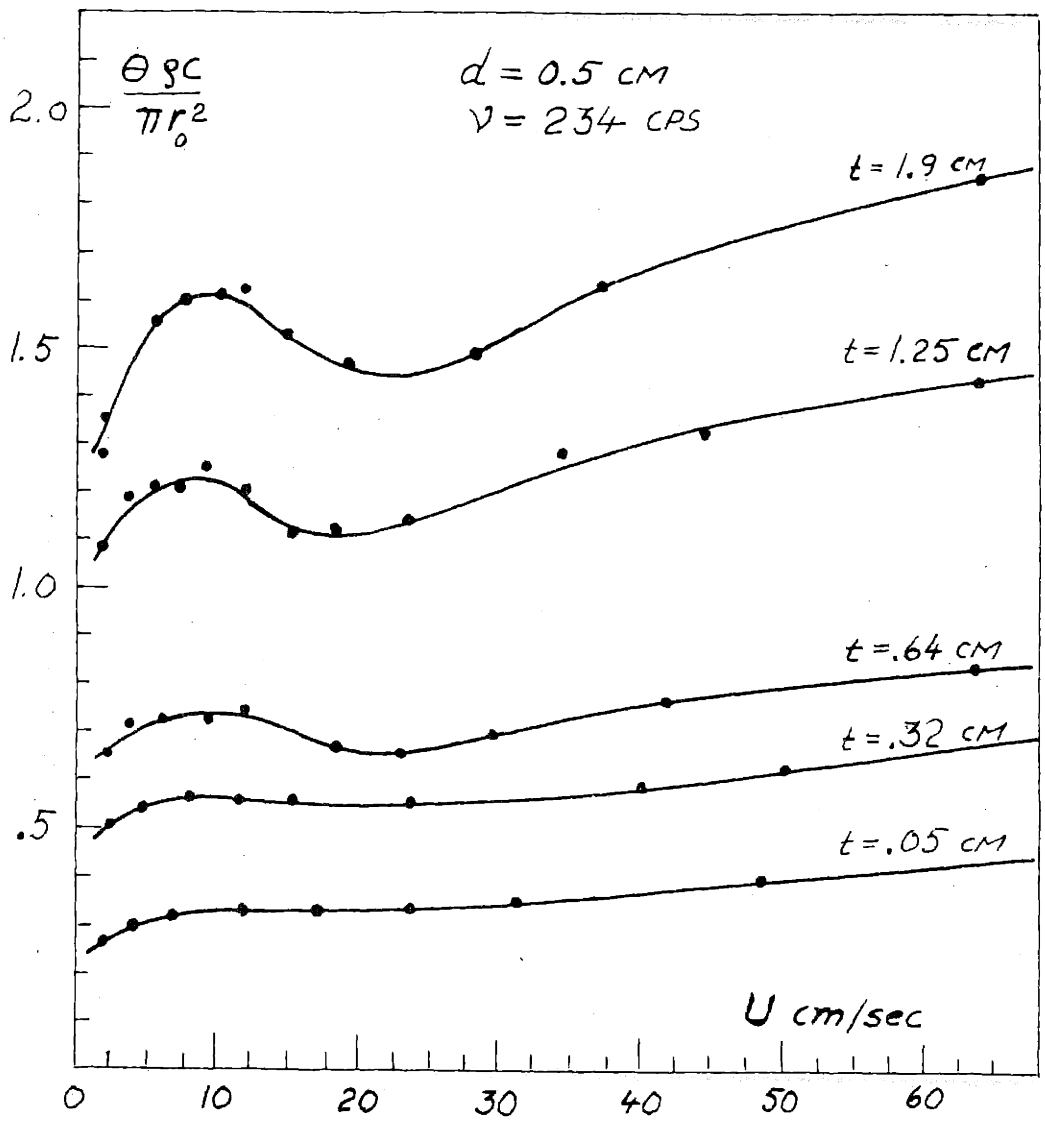
θgc / πr₀²
d = 0.5 cm
ν = 234 CPS
t = 1.9 cm
t = 1.25 cm
t = .64 cm
t = .32 cm
t = .05 cm
2.0
1.5
1.0
.5
U cm/sec
0
10
20
30
40
50
60

Figure 27

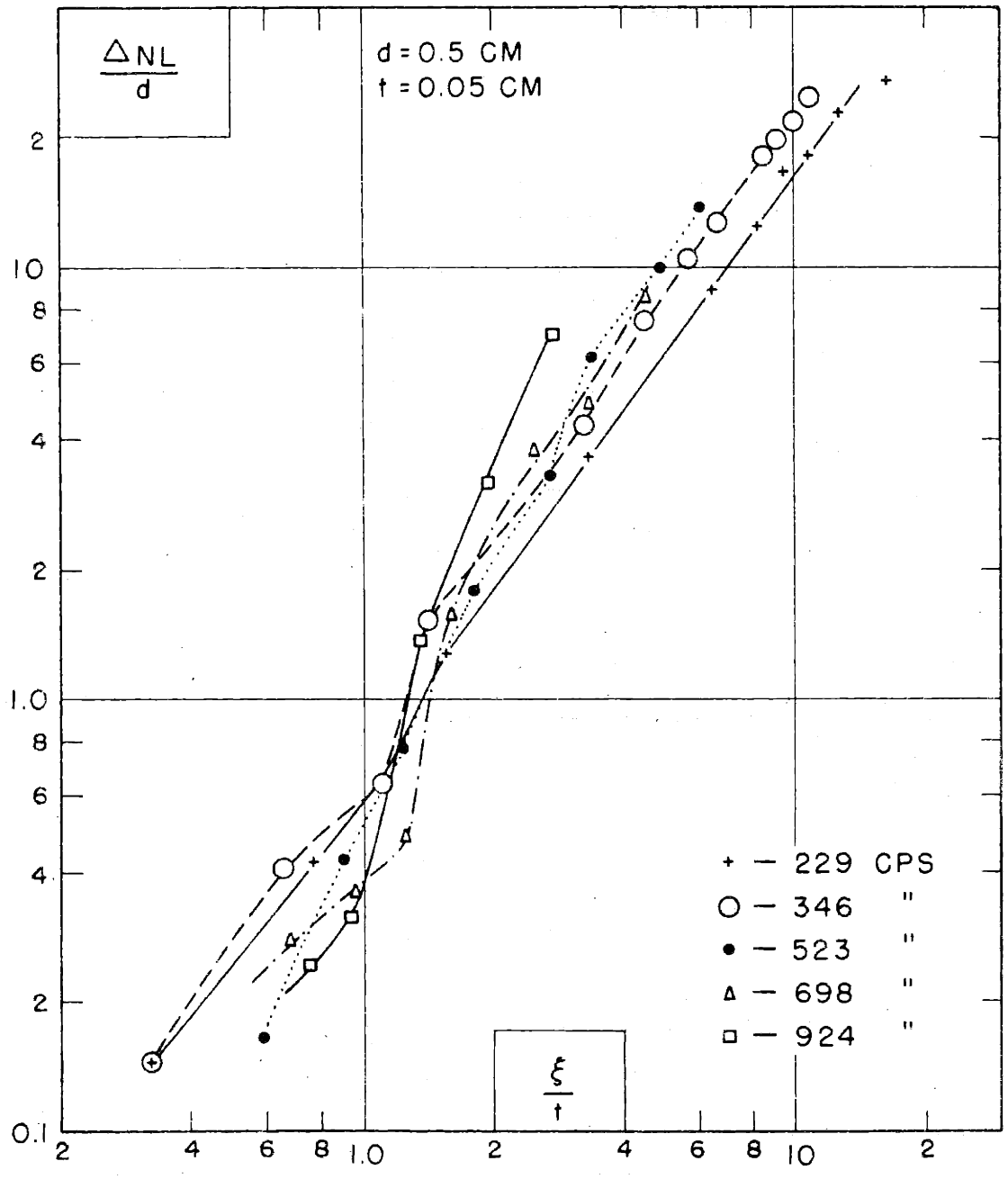
ΔNL/d
d = 0.5 CM
t = 0.05 CM
2
10
8
6
4
2
1.0
8
6
4
2
0.1
2
4
6
8
1.0
2
4
6
8
10
2
+ — 229 CPS
O — 346 "
• — 523 "
Δ — 698 "
□ — 924 "
ξ/t

Figure 28

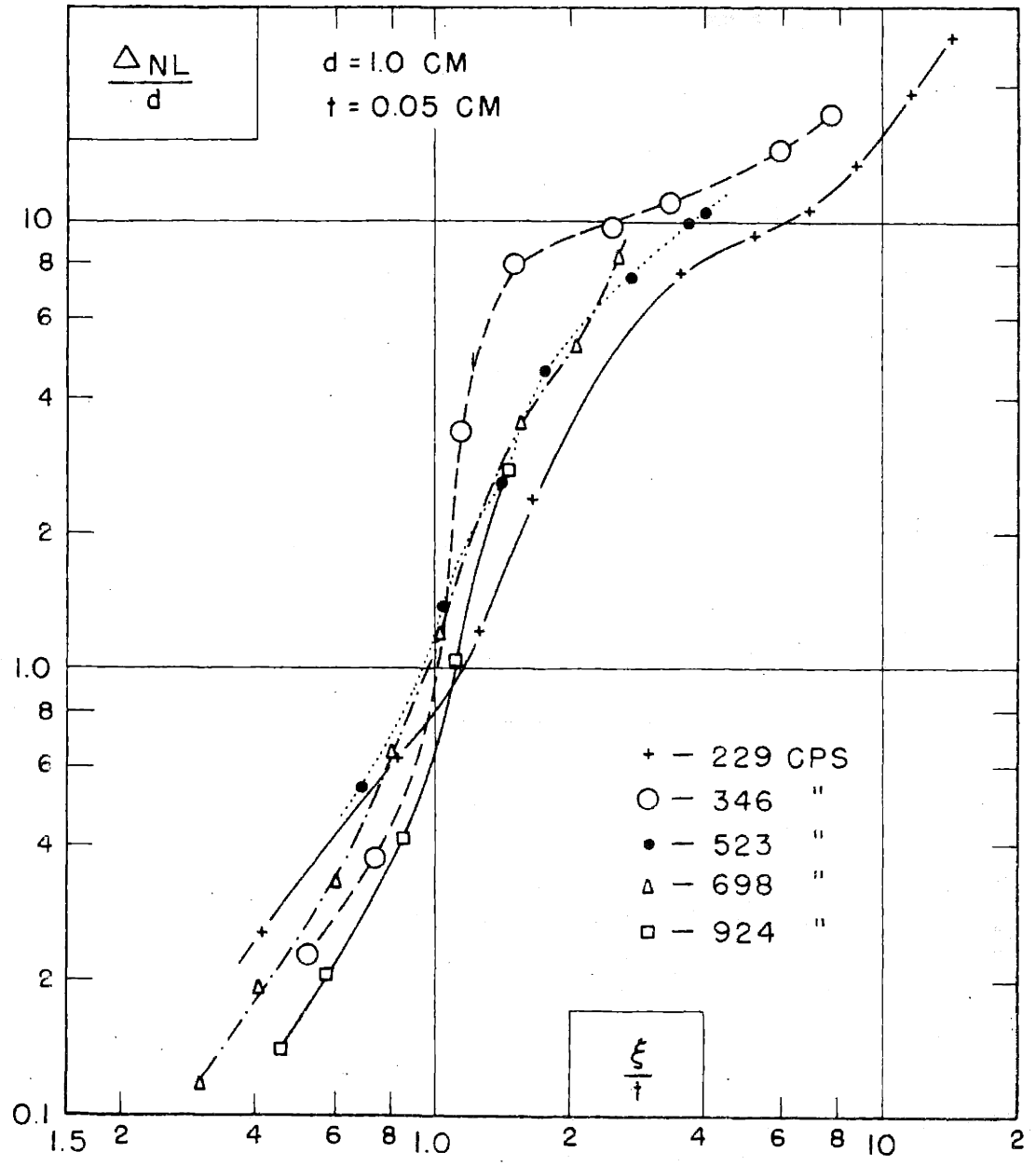
ΔNL / d
d = 1.0 CM
t = 0.05 CM
10
8
6
4
2
1.0
8
6
4
2
0.1
1.5
2
4
6
8
1.0
2
4
6
8
10
2
+ — 229 CPS
○ — 346 "
● — 523 "
△ — 698 "
□ — 924 "
ξ / t

Figure 29

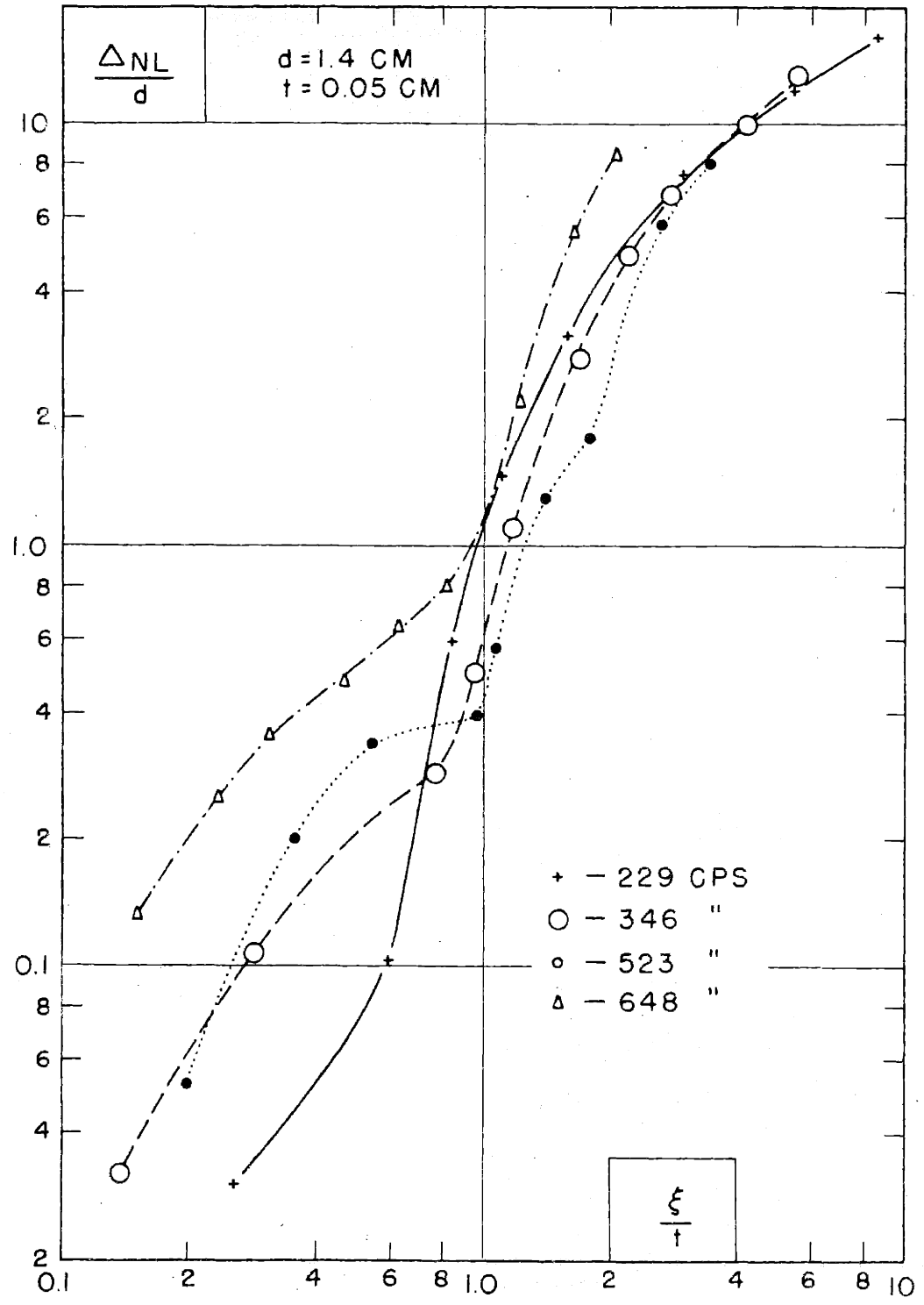
ΔNL / d
d = 1.4 CM
t = 0.05 CM
10
8
6
4
2
1.0
8
6
4
2
0.1
8
6
4
2
0.1
2
4
6
8
1.0
2
4
6
8
10
+ — 229 CPS
○ — 346 "
o — 523 "
Δ — 648 "
ξ / t

Figure 30

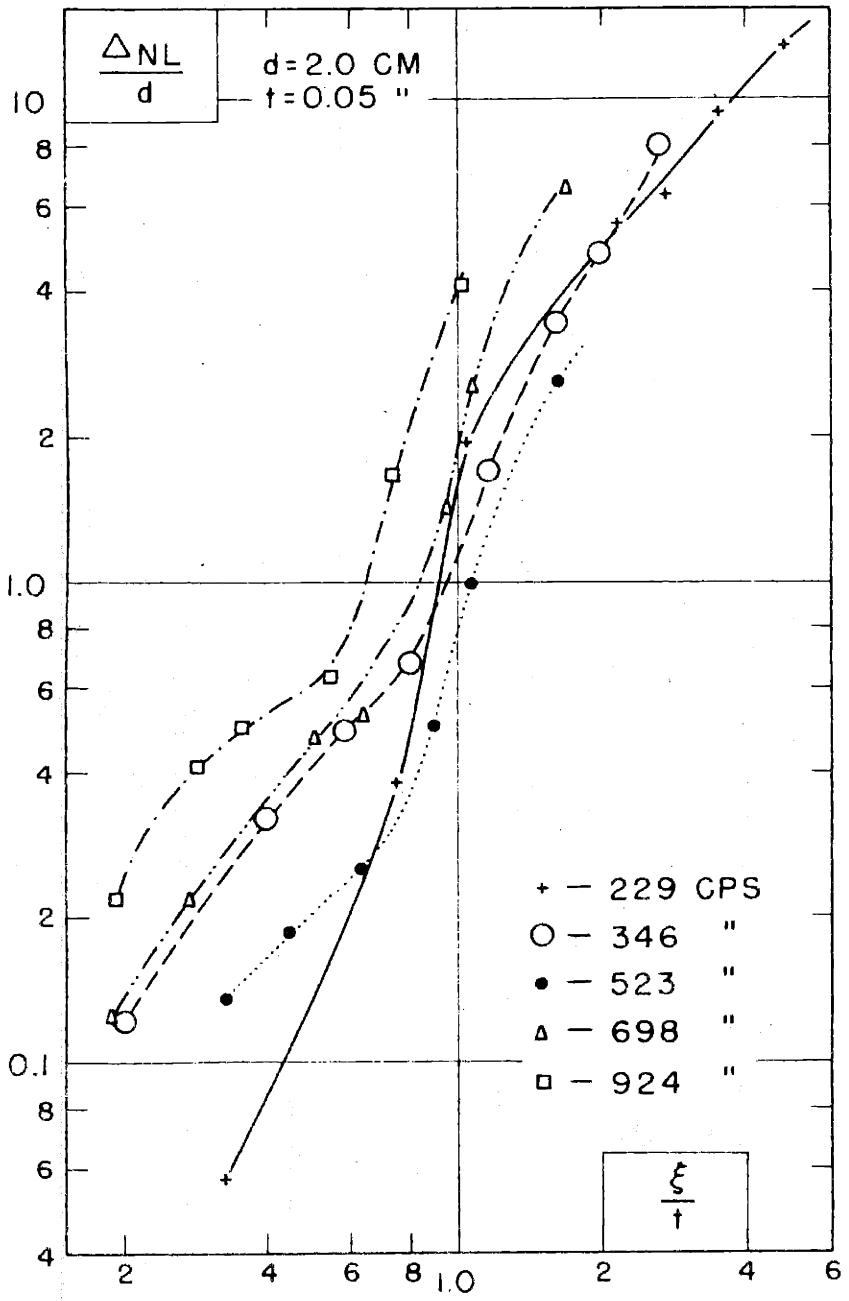

Figure 31

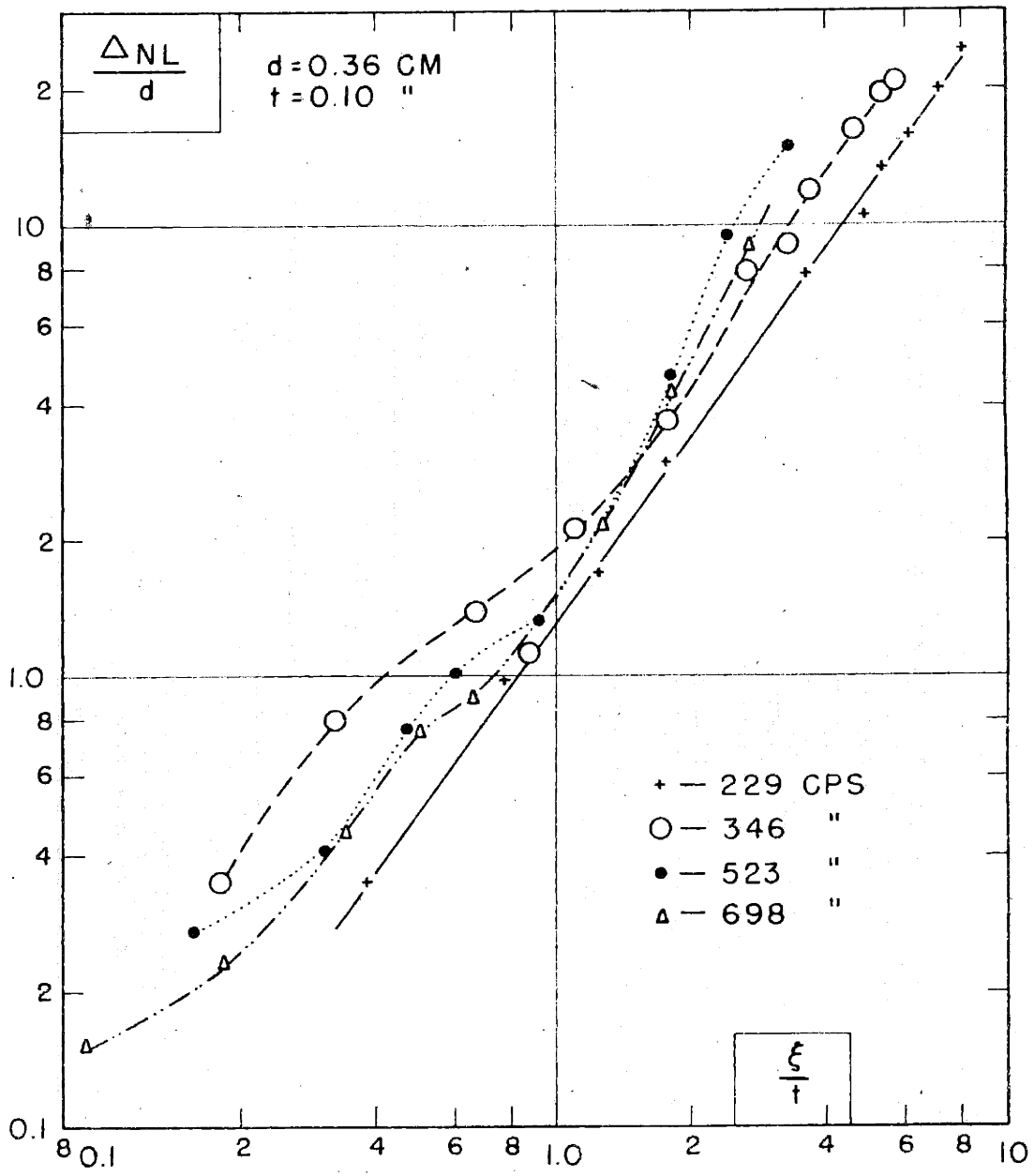

Figure 32

The wall thickness is $t = 0.05$ cm, so the displacement amplitude should be the proper variable to choose, at least as far as turbulence is concerned. From the criterion we know, that turbulence sets in when $\xi/t = 1$, and we now see that this is consistent with the results of the measurements, which show a discontinuity in the slope of the resistance curve at $\xi = t$. This discontinuity is larger for large apertures, and we see furthermore that there is a general tendency of the curves to be velocity-determined below furbulence and displacement-determined above turbulence.

For wall thicknesses well above the critical value we expect the non-linear part of the resistance to be velocity-determined, and the measured resistance curves shown in figures 33 - 35 also indicate that. It is interesting to see that Δ_{NL}/d is, roughly speaking, independent of diameter and thickness of the aperture. There is no longer any sharp change in slope of the resistance curves when turbulence sets in, which may be explained by the fact that the turbulence in this case is of another character, now being caused by the steady circulations.

We are then in a position to express the non-linear resistance empirically for a "velocity determined aperture". We can write $\Delta_{NL}/d = C(U/100)^n$ where n and C are practically independent of aperture dimensions but probably slightly frequency dependent. We have measurements only at

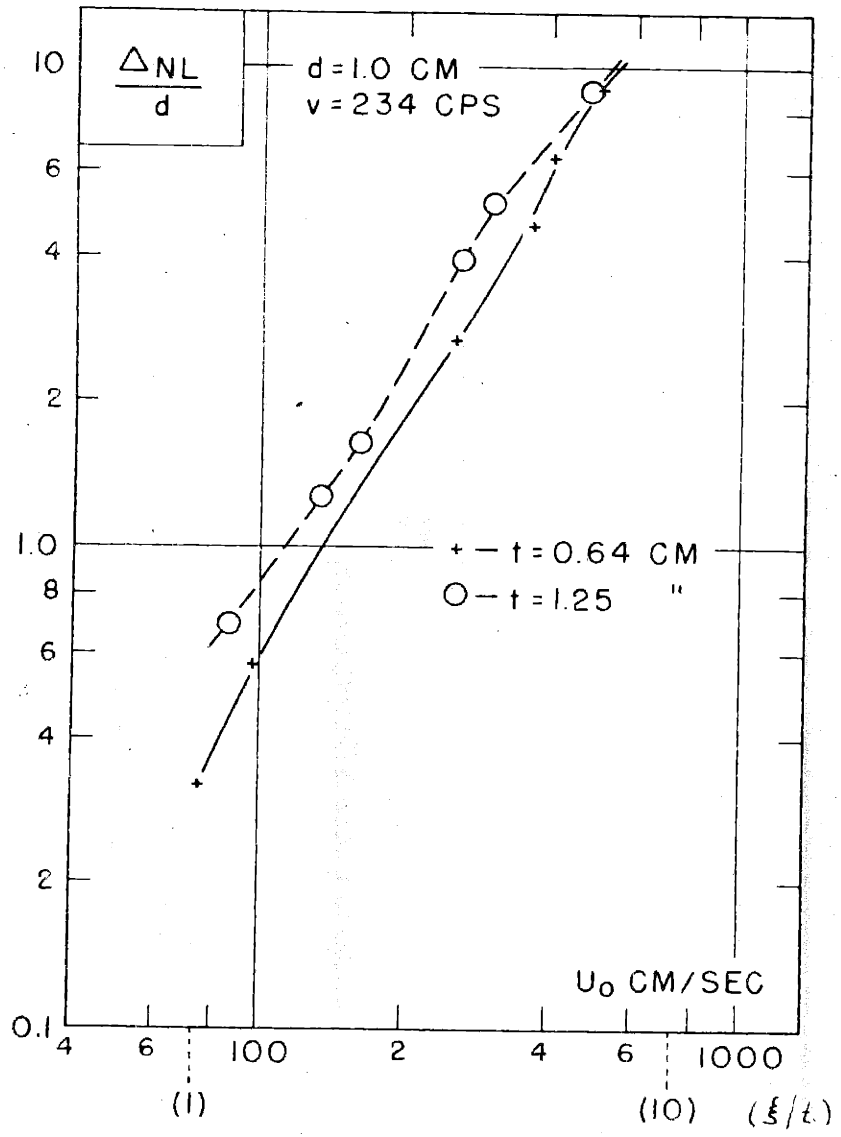

Figure 33

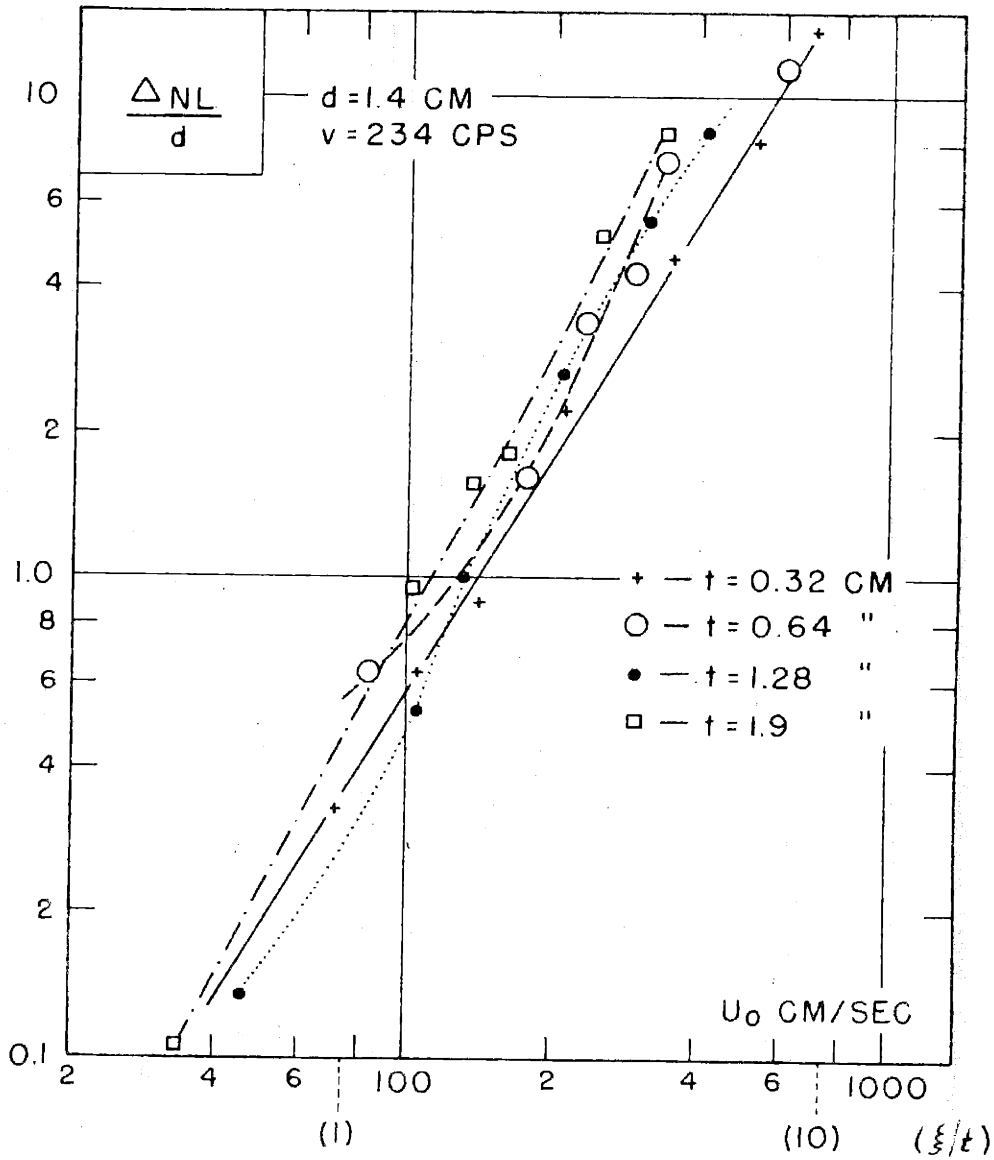

Figure 34

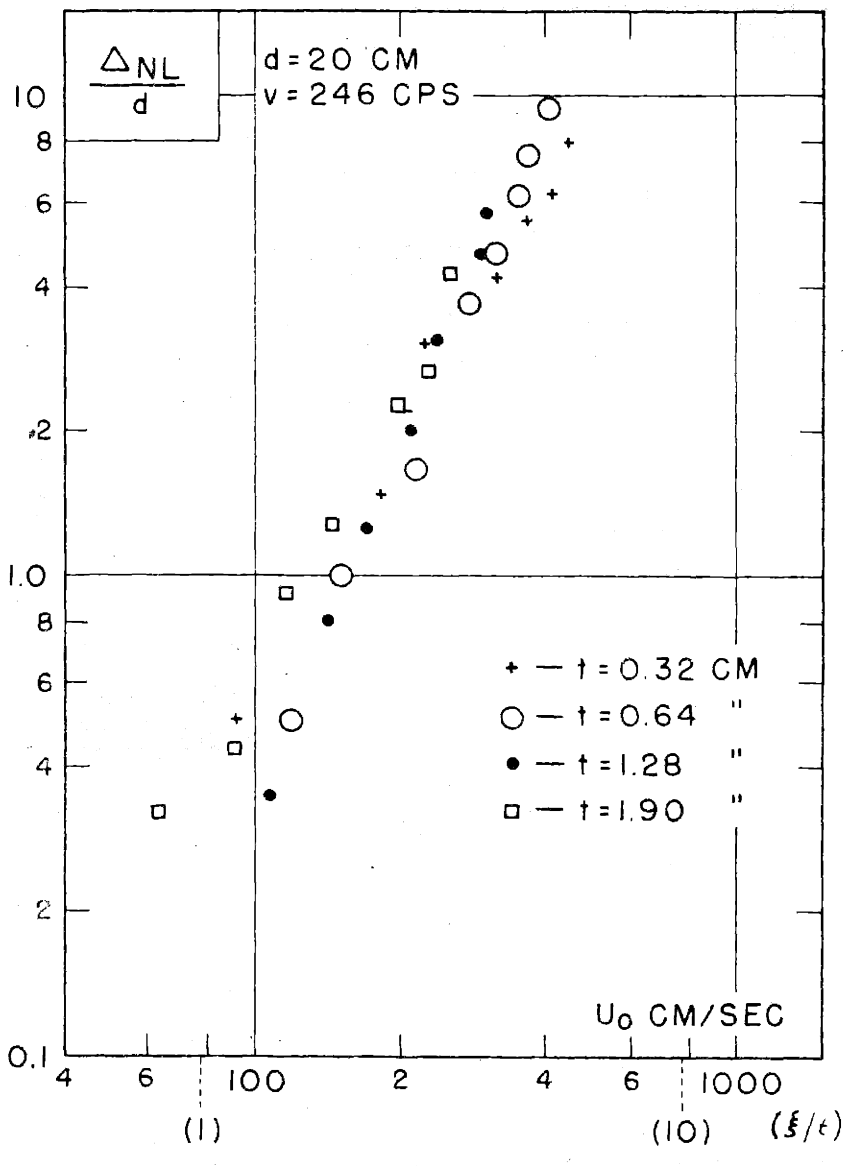
ΔNL/d
d = 20 CM
v = 246 CPS
10
8
6
4
2
1.0
8
6
4
2
0.1
+ — t = 0.32 CM
○ — t = 0.64 "
● — t = 1.28 "
□ — t = 1.90 "
U0 CM/SEC
4
6
100
2
4
6
1000
(1)
(10)
(ξ/t)

Figure 35

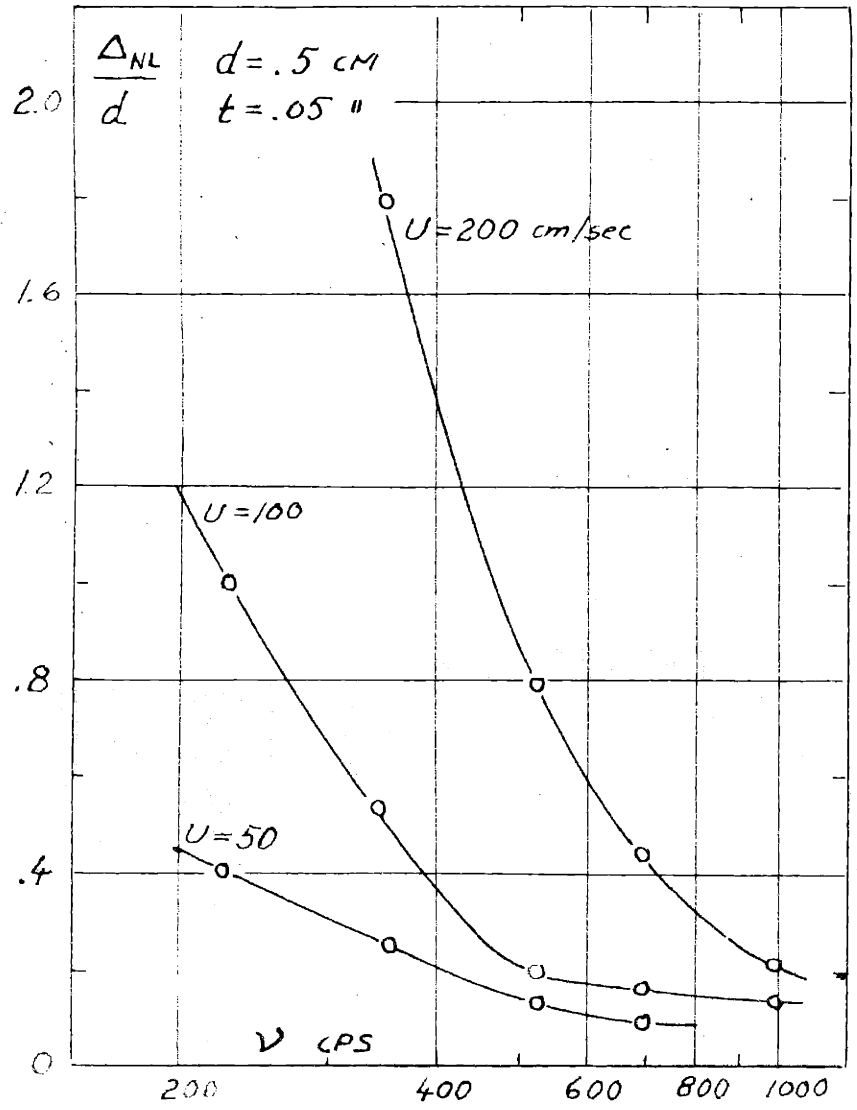

Figure 36

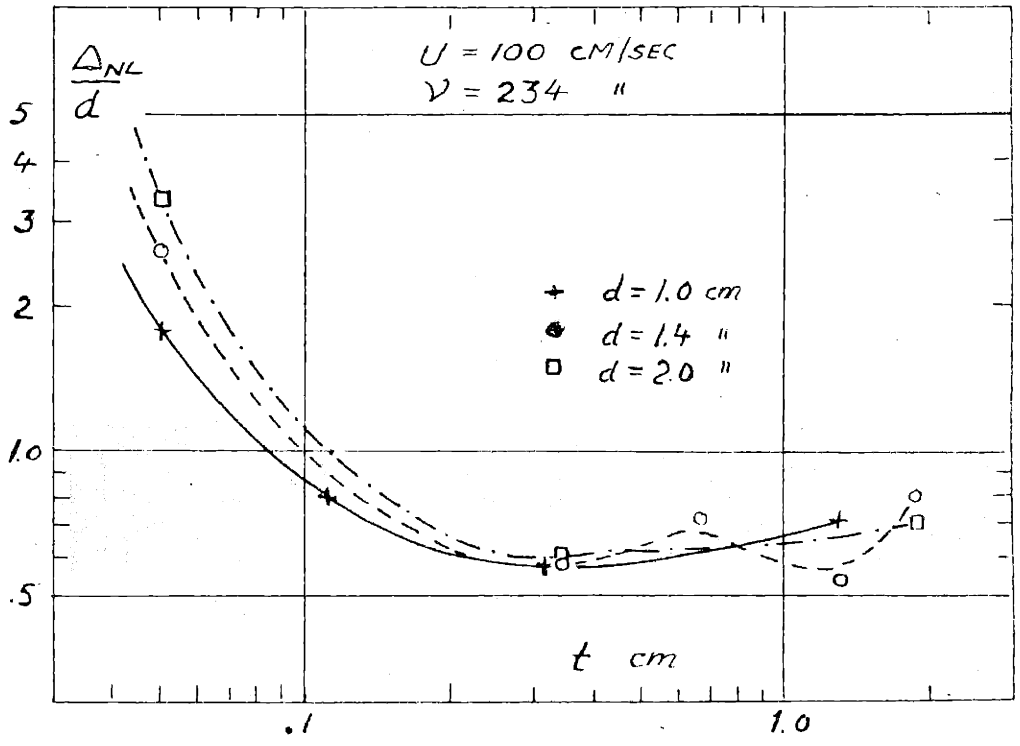

Figure 37

one single frequency, 234 cps., at which the constants are $C = 0.7$, $n = 1.7$.

Figure 36 serves to illustrate the frequency dependence of the non- linear part of the resistance for an aperture with a wall thickness less than the critical. Keeping velocity U constant and varying the frequency brings us through the phase diagram in figure 12 on a horizontal line, from the left to the right; from regions of high dissipation to regions of low dissipation. And the resistanc is first amplitude-determined and later velocity -determined. Similar curves with the thickness as variable are shown in figure 37.

A quantitative comparison.

A quantitative comparison was made between the measured non-linear part of the resistance and the energy transformed from sound to translatory kinetic energy of a vortex jet shown in figure 25. If the air pulse forming the vortex rings have a velocity v and a mass m, the force on a wall placed in the stream should be, assuming inelastic collision,

$$F = (\omega/2\pi)mv \qquad (I:15)$$

The rate with which kinetic energy is carried away from one side of the orifice can then be written as

$$E_t = \frac{1}{2} F_v \qquad (.16)$$

Since the stream is broken up into vortex rings, which have a rotational velocity, a rotational kinetic energy

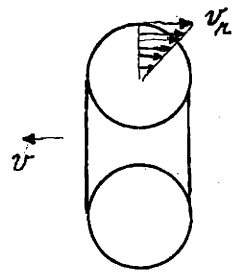

Figure 38

E_r must be added to the translational energy E_t. To estimate its value, let us assume that the rotational velocity on the surface of the vortex ring is v_r, With a linear velocity distribution as indicated in figure 38 we obtain then for the rotational energy

$$E_r = \frac{1}{2} \frac{F}{v} (v_r)^2 \qquad (I.17)$$

Taking into account that the jet exists on both sides of the aperture, we obtain for the rate of total kinetic energy carried away from the aperture

$$E_k = 2(E_t + E_r) = Fv \left[1 + \frac{1}{2} \left(\frac{v_r}{v}\right)^2\right] \qquad (I.18)$$

Expressing this in terms of acoustic resistance for the orifice we can define an equivalent acoustic resistance R_k from

$$\frac{1}{2} R_k (\pi r_o^2 U)^2 = E_k \qquad (I.19)$$

The force F was measured by a torsion balance consisting of a thin aluminum disc suspended by a wire as shown in figure 39. The equilibrum was first determined, and then the torsion angle required to keep the disc in the equilibrum position when acted upon by the jet. The disc was

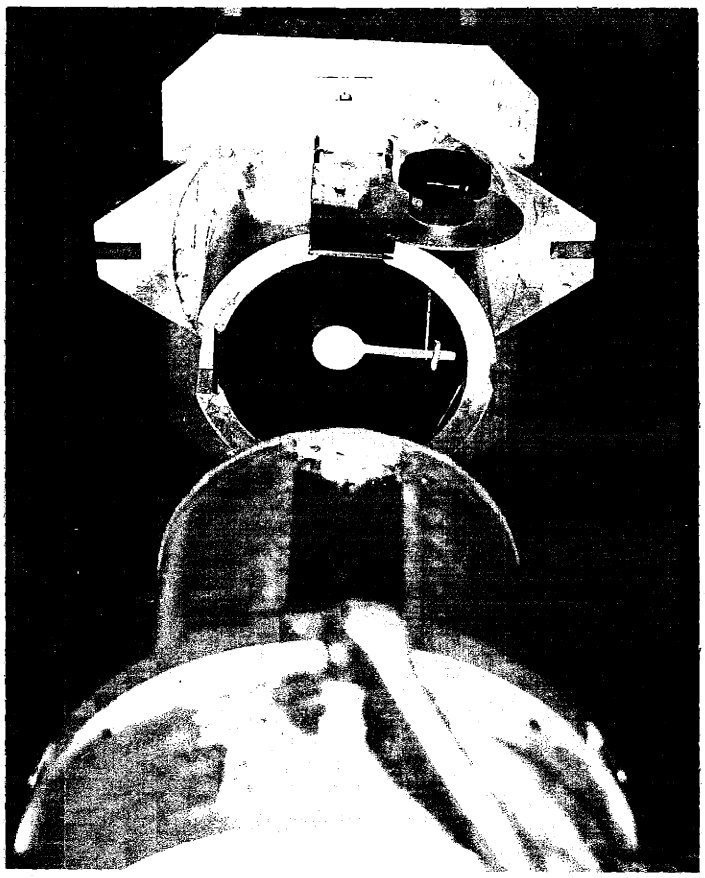

Figure 39

placed about 3 cm from the aperture. The torsion constant of the wire was determined in the usual way by pendulum experiment, replacing the disc by a thin rod of the same weight as the disc.

The velocity of the vortex jet was determined by measuring the distance d between two successive vortex rings under stroboscopic illumination. The velocity is then given by $v = (\omega/2\pi)\, d$. Experiments were carried through only with one aperture, diameter 0.5 cm, thickness 0.05 cm. Larger apertures require an inconveniently large disc, and apertures with walls thicker than 0.05 cm give very diffuse vortex rings and their velocity is then hard to measure. The results obtained are shown in table 5.

In the expression for E_k in (I.25) the second term corresponding to the rotational kinetic energy is small compared with the translational energy and may be neglected in a first approximation. We then obtain the dashed curve for R_k shown in figure 40. There is evidently a rather good agreement with the curve for R_{NL} obtained from the impedance measurement, even if R_k is somewhat smaller than R_{NL}. The relatively large difference at low levels is expected because the jet is divergent at these levels, as seen in figure 26, and only part of it strikes the torsion balance. The smaller difference between R_k and R_{NL} at higher levels can be eliminated almost completely on

Table 5.

Orifice diameter 0.5 cm, orifice thickness 0.05 cm

Frequency 234 cps.

Average sound particle velocity in the aperture U cm/sec.	Vortex velocity v cm/sec.	Stagnation force F dynes
113	-	-
232	100	3.70
340	190	13
450	270	26
515	312	40
565	355	52
607	380	64
656	405	81
692	412	95
726	420	108
805	455	137
418	512	-

account of the rotational energy. Assuming $v_r = \alpha U$ and using the known values of U and v from table 5, we get for $\alpha = 0.3$ the values of R_k represented by the solid circles in figure 40. For this value of v_r, an almost perfect agreement is obtained.

The qualitative agreement between the behavior of the non-

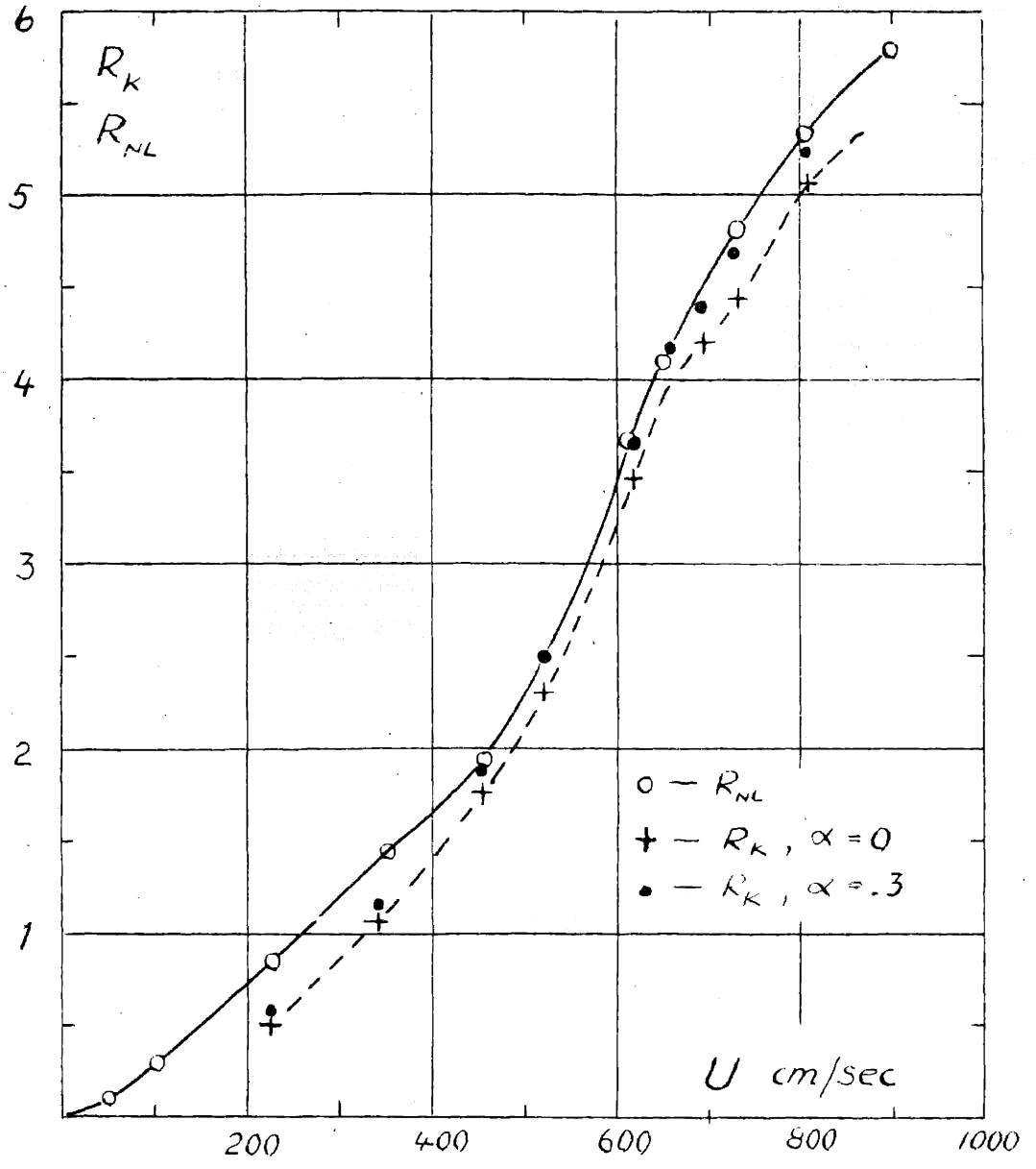
6
5
4
3
2
1
R_K
R_{NL}
o — R_{NL}
+ — R_K, $\alpha = 0$
• — R_K, $\alpha = .3$
U cm/sec
200
400
600
800
1000

Figure 40

linear acoustic losses and the circulations in general and this quantitative check in the jet region, makes it very plausible that the non-linear losses at all levels may be explained as the energy required to drive the circulation currents or the jets.

The non-linear reactance.

The reactance of an aperture stays constant independent of the sound level until turbulence is reached; that means the steady circulations are superposed upon the sound vibration outside the orifice without affecting the kinetic mass. (The vibration of the flow pattern can actually be seen under stroboscopic illumination). The turbulence causes a decrease of the reactance which continues steadily with increasing level. The non-linearity of the mass reactance is best observed with thin apertures for which the end correction is the major part of the kinetic mass. A series of curves showing the decrease in the kinetic mass, expressed as equivalent end correction δ_{NL}, are shown in figures 41 - 43. The thickness of the aperture is here 0.05 cm and the curves are plotted against ξ/t. All curves indicate a start at $\xi/t = 1$, where the turbulence sets in. It is clear that δ_{NL}/d never can exceed the corresponding value for the linear mass, which for small apertures is about 0.8. As seen in figure 44, the mass reactance for the aperture with $d = 0.36$ is almost canceled by the non-linear effects, with δ_{NL}/d approaching 0.7 at high levels.

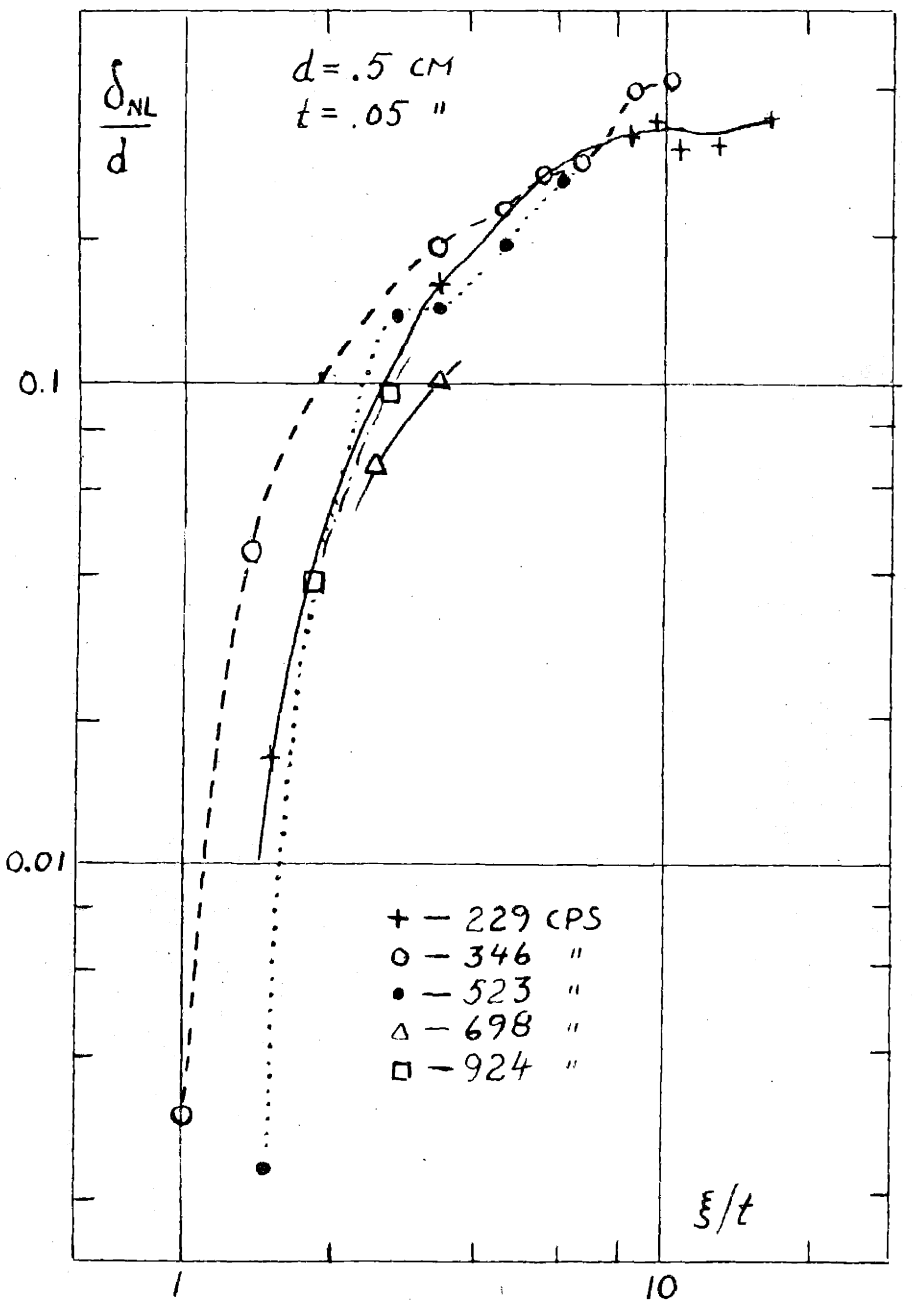

Figure 41

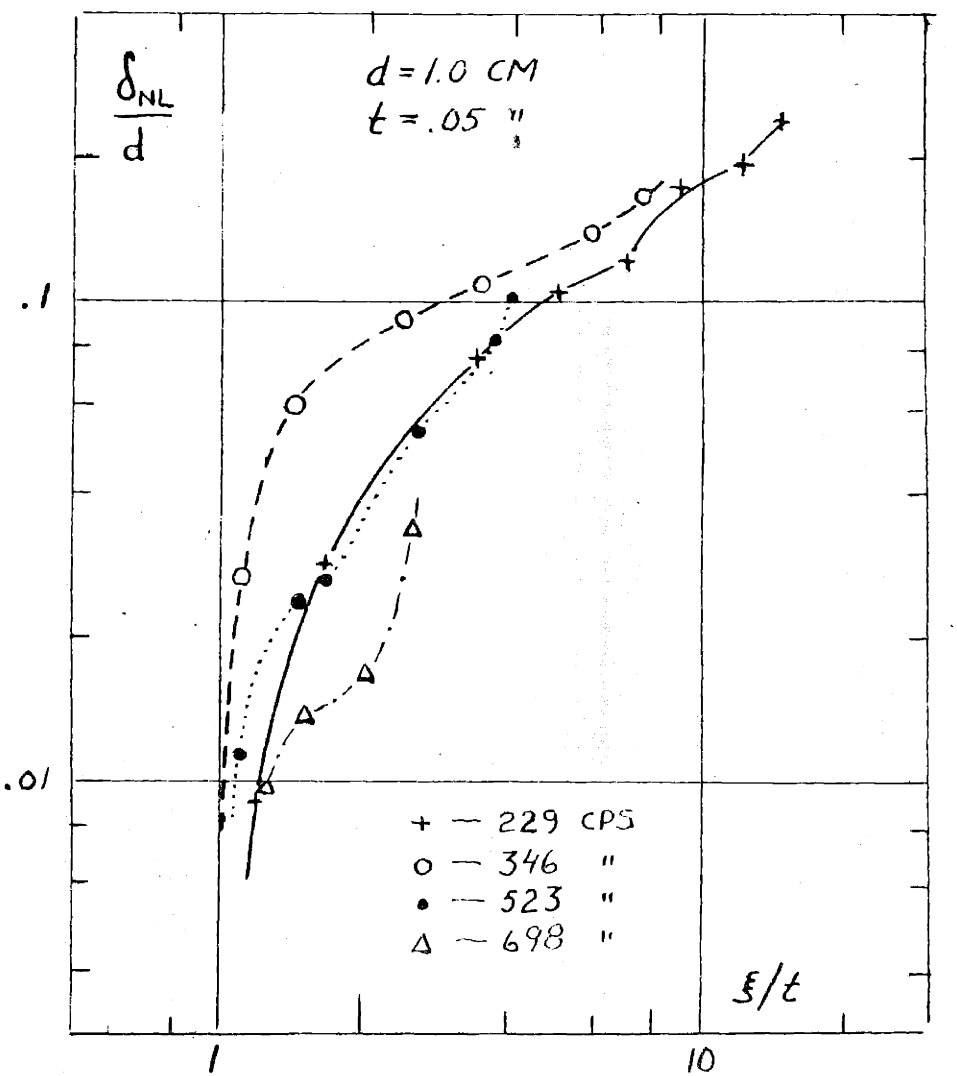

Figure 42

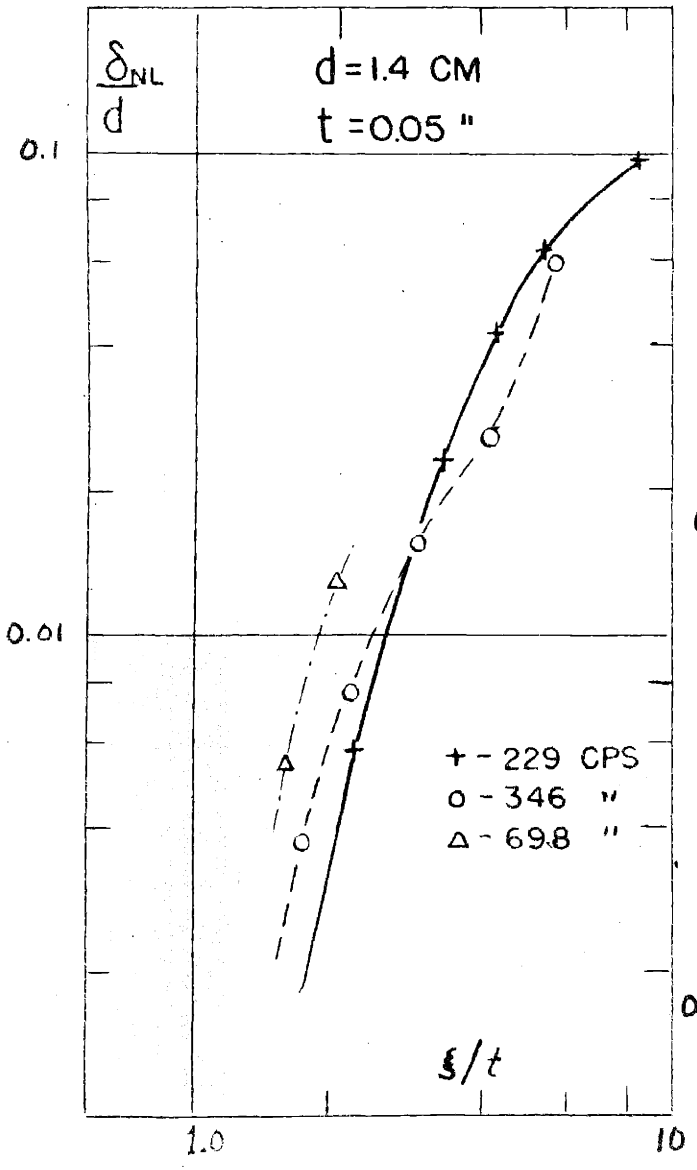

Figure 43

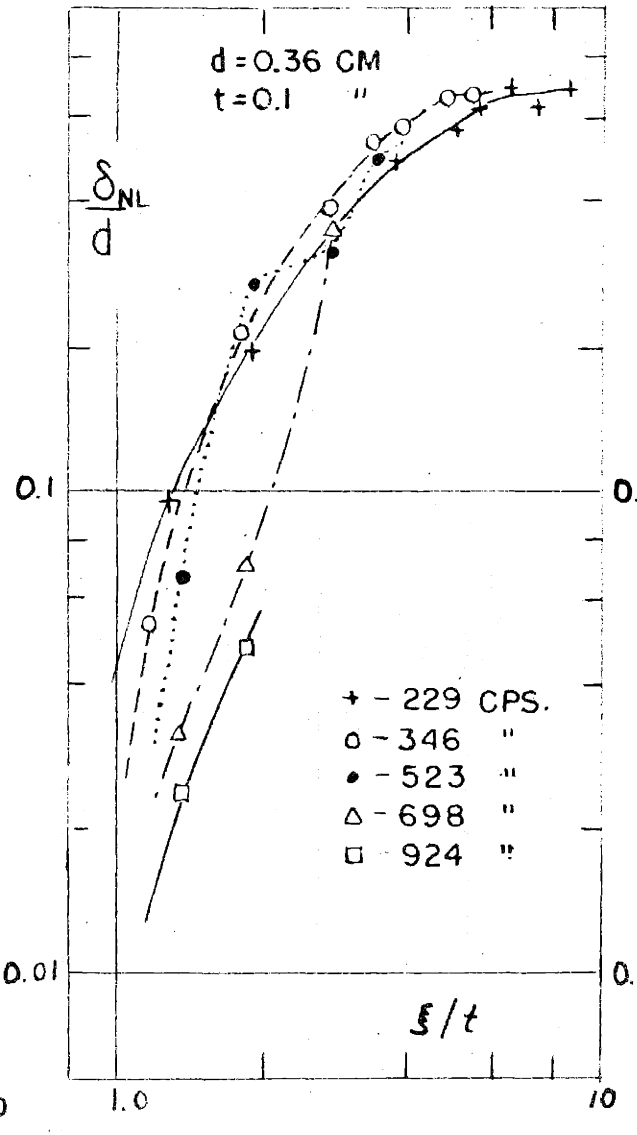

Figure 44

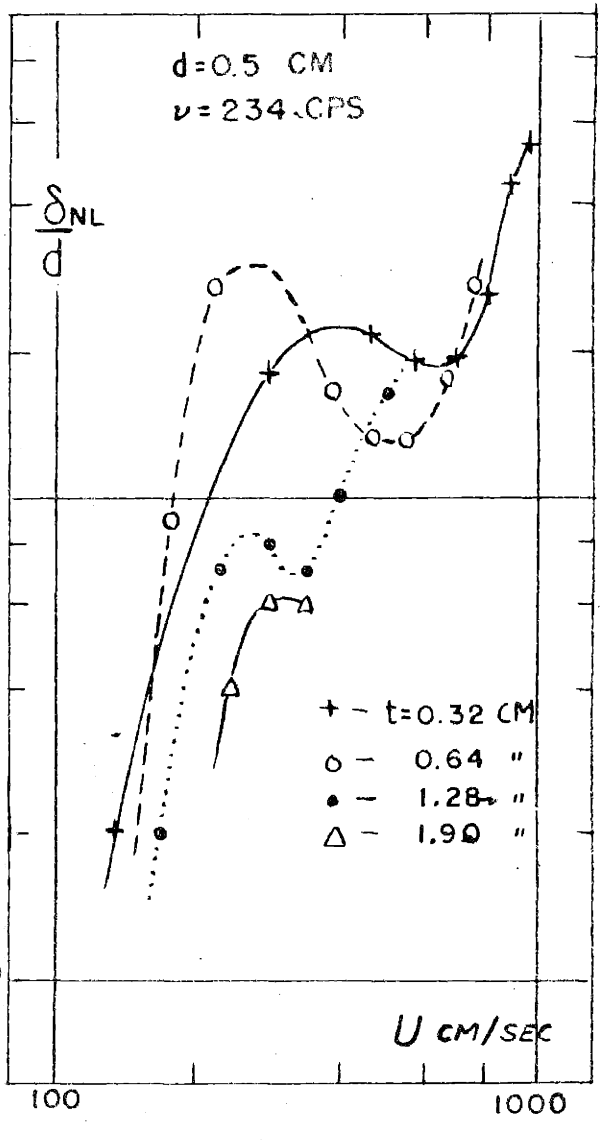

Figure 45

The results for thicker apertures of diameter 0.5 cm, in figure 45, shows an interesting fluctuation, which seems to be connected with the onset of the jet.

The value of the non-linear kinetic mass decreases rather rapidly with increasing diameter of the aperture and also with the increasing thickness.

§ 4. The resonator as a tube termination.

In order to give an illustration of the pressure distribution around an aperture, we consider the case of a circular cylindrical tube terminated by a circular resonator as shown in figure 1. With a cavity length L and an aperture radius r_o the resonance frequency ν_o is determined from the relation

$$\frac{\cot k_o L}{k_o L} = \frac{2\delta}{(r_o/R)^2 L} \qquad (I.20)$$

$$k_o = \omega_o/c$$

where δ is the mass end correction on one side of the aperture obtained from figure 2, or the approximate expression (I.8). The total aperture impedance $\zeta_{tot} = \zeta + 2\zeta_s$, mentioned on page 7, is

$$\zeta_{tot} = \theta - i(r_o/R)^2 \left[\gamma \cot(k_o L) - \cot(k_o L \gamma)\right] \qquad (I.21)$$

$$(\gamma = \omega/\omega_o)$$

where θ may be obtained from (I.11).

The pressure in the tube to the left of the aperture can be written

$$p_e = 2P_+ e^{-\Psi}\left[\sinh(ikx + \Psi) + i \cosh\Psi \sum(+)\right] \tag{I.22}$$

and the pressure inside the cavity is

$$p_i = 2P_+ e^{-\Psi}\left[i \cosh\Psi \frac{\cos k(L - x)}{\sin k L} - i \cosh\Psi \sum(-)\right] \tag{I.23}$$

where $\sum(\pm) = 4\pi \frac{R}{\lambda} \frac{R}{r_o} \sum' \frac{J_1(b_n r_o)}{(b_n R)^2 J_o^2(b_n R)^2} J_o(b_n r) e^{\pm b_n R\, x/R}$

$J'(b_n R) = 0$

and $\operatorname{tgh} \Psi = (R/r_o)^2 \zeta_{tot}$ (I.24)

Only the pressure along the axis of the tube is now considered and we take the case of a thin aperture $t << r_o$, and choose $r_o = 1.52$ cm, $R = 3.82$ cm ($2R = 3"$) and $L = 7$ cm. The resonance frequency is then 415 cps, and the resistance obtained from (I.15) and (I.12) is $\zeta_c\theta = 0.066$. The total impedance (I.16) can be written

$$\zeta_{tot} = 1.57\ 10^{-3}\left[\sqrt{\gamma} - i46(\gamma - 1/\gamma)\right] \tag{I.25}$$

This resonator offers practically no absorption because the resistance is much too low. The case when the resonator is

matched to the line impedance will be considered below.

Using (I.17)-(I.20) the pressure distribution for a number of frequencies between $\gamma = 0.6$ and $\gamma = 1.8$ has been calculated and drawn in figure 46. We notice the discontinuity in the calculated pressure at the aperture caused by the incorrect assumption of a uniform velocity distribution. The true pressure, which hardly can be calculated, must be continous and is probably given quite closely by the smoothened curves drawn solid in the figures.

At frequencies lower than the resonance frequency the plane wave pressure p_1 inside the cavity is in phase with and larger than the outside plane wave pressure p_e. The "scattered" waves are in phase with p_e and out of phase with p_i and thus serves to join the two pressures smoothly at the aperture, (disregarding the discontinuities mentioned above.) The biggest difference between p_i and p_e occurs at resonance $\gamma = 1$, in which case the total pressure drops to zero just outside the orifice. The phase difference between p_e and p_{s1} right at the aperture is then 90° but increases rapidly to 180° at a small distance away from the aperture. The highest inside pressure occurs at a frequency somewhat lower than ν_o.

When $\gamma = 1$ we have p_i and p_e out of phase, and a pressure mode appears first slightly outside, then slightly in-

side the aperture when the frequency increases, as shown in figure 46.

When the resonator is matched to the line impedance there is 100 % absorption at resonance. The pressure distribution in this case is shown in figure 47. The general behaviour of the total pressure is the same as in the previous case but the effect of the scattered pressure is not so pronounced. The phase relations between the component waves are now more involved and even if the scattered and the plane waves are of the same magnitude in the neighborhood of the aperture we do not get any points of zero pressure.

The reason for having plotted these pressure distributions was primarily to investigate the influence of the higher order modes in connection with measurements on apertures and resonators. In most cases one is then interested in the plane wave pressure and has to make sure that higher order modes are avoided, which otherwise may cause considerable errors as seen in figure 46. This point seems to have escaped Sivian in his measurements of the impedance of orifices [26].

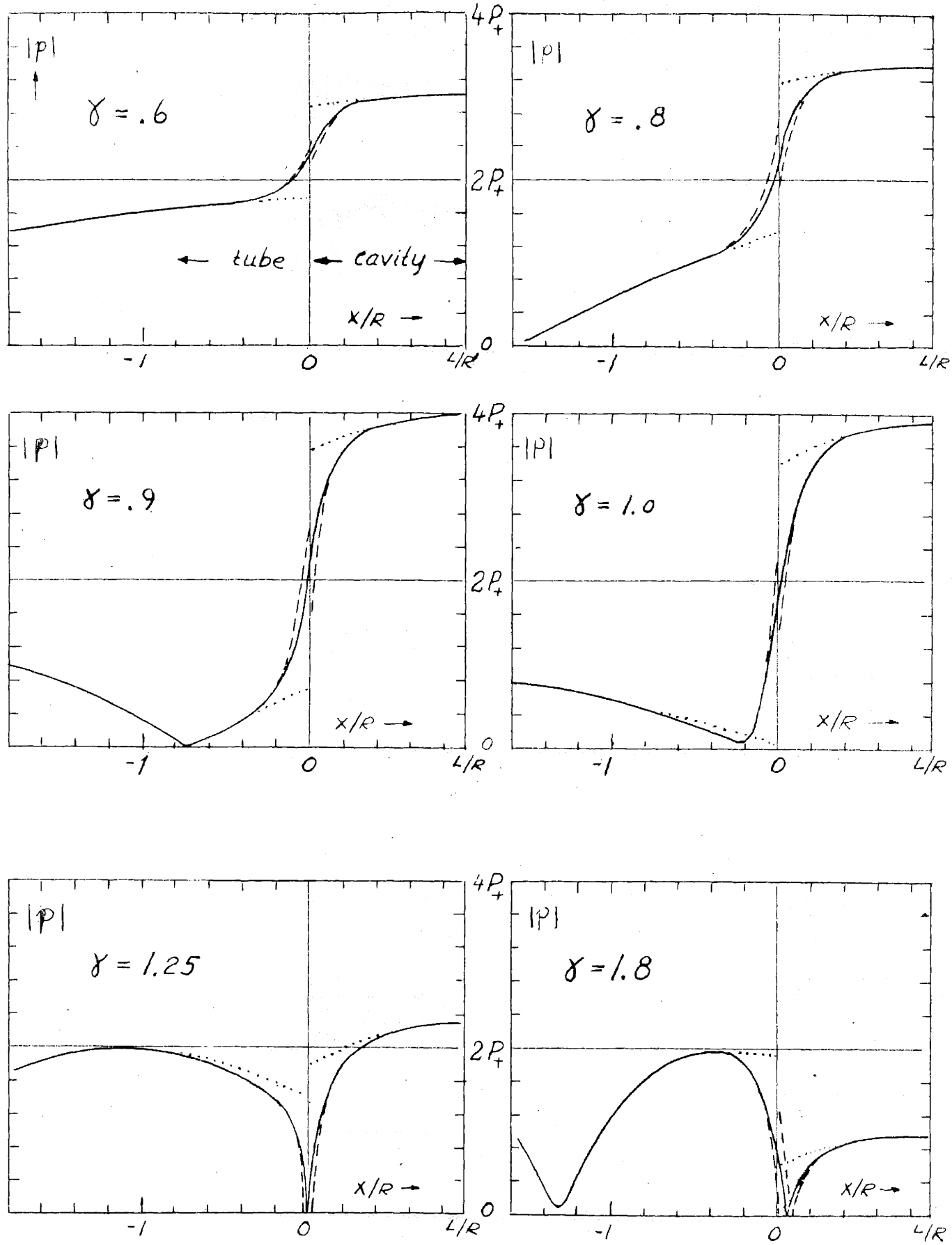
|p|
γ = .6
tube
cavity
x/R
4P+
2P+
0
-1
0
L/R
|p|
γ = .8
x/R
-1
0
L/R
|p|
γ = .9
x/R
-1
0
L/R
|p|
γ = 1.0
x/R
-1
0
L/R
|p|
γ = 1.25
x/R
-1
0
L/R
|p|
γ = 1.8
x/R
-1
0
L/R

Figure 46

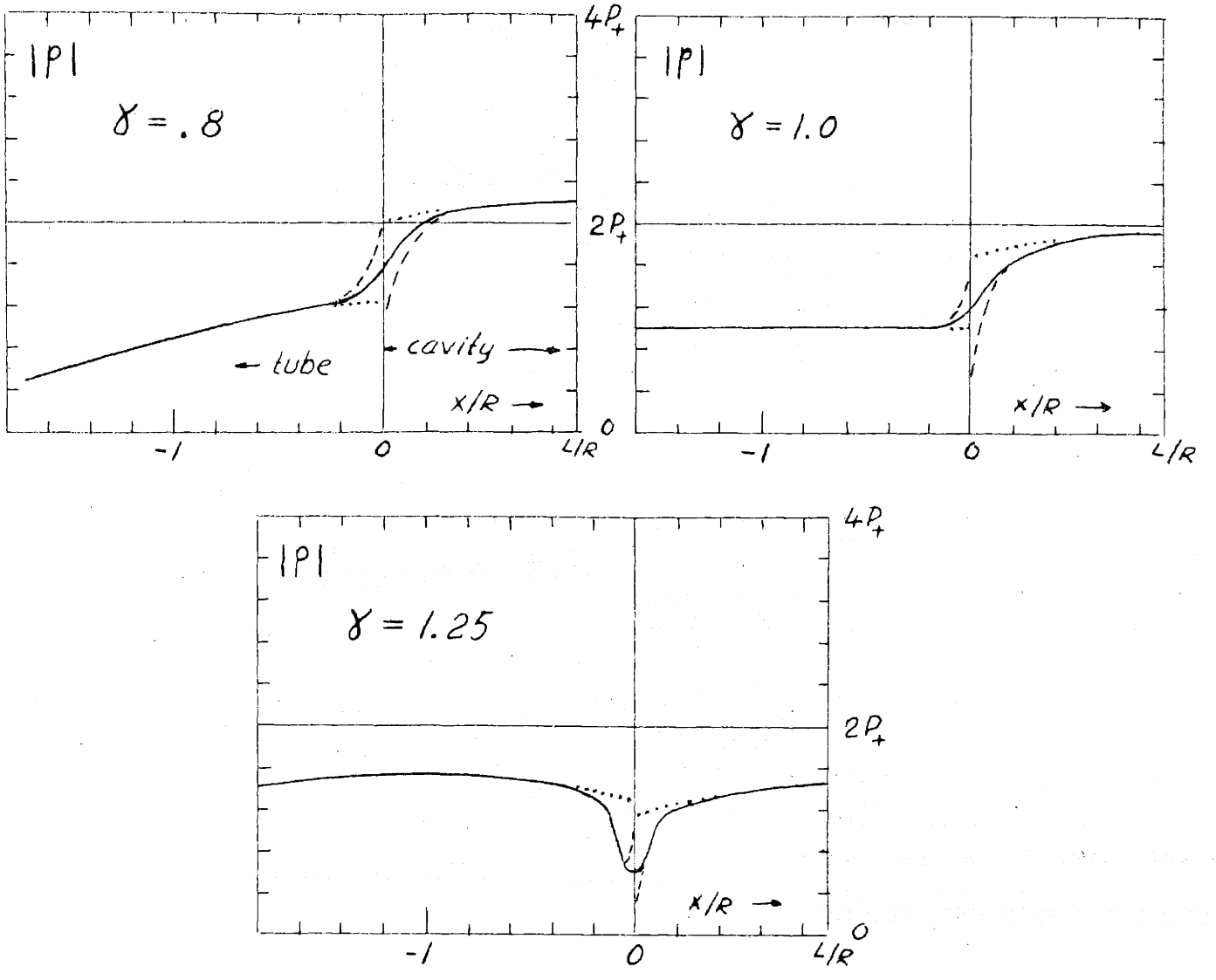
|P|
γ = .8
4P+
2P+
0
tube
cavity
x/R
-1
0
L/R
|P|
γ = 1.0
x/R
-1
0
L/R
|P|
γ = 1.25
4P+
2P+
x/R
-1
0
L/R
0

Figure 47

II. The acoustic resonator in free field.

Introduction.

The analysis of the absorption and scattering by an acoustic resonating system is of course analogous to that of an electrical antenna system. When the dimensions of the resonator are very small compared to the wave length of the primary plane wave the expressions for the scattered and absorbed energy are exactly the same as for the electrical dipole, when written in terms of internal and radiation impedance. The system can then be represented by a resonant circuit in which the resistance is the sum of the internal and radiation resistance and the driving voltage corresponds to the "blocked" pressure at the resonator, which then equals the pressure P_o of the primary plane wave. In systems like a Helmholtz resonator this long wave length approximation is often a good one.

Our study in this section is limited to a single cavity resonator and in order to be able to carry through an analysis with no restriction on the frequency, we choose the spherical cavity. The investigation of the scattering from a rigid sphere has been treated in some detail by Morse and others [28] - [31]. The analysis of the spherical resonator follows the same lines. An exact solution may be obtained in the

same way as for an aperture in a plane wall, as mentioned in chapter I, using for example the variational method for determining the coefficients in the expansion of the velocity in the hole. However, by assuming a certain velocity distribution at the start the calculations become simplified but still accurate enough for practical purposes. An exact solution is probably going to lead to iteration calculations which converge too slowly to be of any practical value.

Before making any detailed analysis we write down the expressions for the scattering cross section σ_s and the absorption cross section σ_a valid in the limit of infinite wave length

$$\sigma_s = \frac{\theta_i}{|\zeta|^2} A_o = \frac{R_i}{|Z_i|^2} \qquad \text{(II.1)}$$

$$\sigma_a = \frac{\theta_r}{|\zeta|^2} A_o = \frac{R_r}{|Z_r|^2} \qquad \text{(II.2)}$$

($R = \theta/A_o$; $Z = \zeta/A_o$; A_o = area of the hole in the resonator)

These expressions follow directly from the simple analogue circuit in which θ_i is the "internal" specific resistance ratio of the hole (considered as a moving piston), θ_r the corresponding radiation resistance and ζ the sum of the internal and the radiation impedance. At resonance the σ_a

reduced to

$$\sigma_a = \frac{\theta_i}{|\theta_i + \theta_r|^2} A_o = \frac{\lambda^2}{4\pi} \frac{4(\theta_i/\theta_r)}{(1+\theta_i/\theta_r)^2} \qquad (II.3)$$

where we have introduced the radiation resistance $R_r = \pi/\lambda^2$ for a piston in a sphere (or a simple source). A similar expression holds for the scattering cross section. The absorption cross section has a maximum equal to $\lambda^2/4\pi = 0.0796\,\lambda^2$ when $\theta_i = \theta_r$, which is the same as for the corresponding maximum value for the electric dipole [32]. The scattering cross section, which then has the same value, without being a maximum, increases monotonically with decreasing internal resistance.

It is the purpose of this section to investigate the scattering and absorption somewhat more generally and to determine their dependence on the dimensions of the resonator and on frequency. In doing this, the air in the hole of the resonator is assumed to move as a piston with uniform velocity and the field inside and outside the cavity are fitted together at the boundary of the sphere. The viscous dissipation on the surfaces of the sphere is determined by integrating the squared tangential velocity over the total surface of the resonator. The scattering and absorption cross section, the "Q", and the reverberation time are then studied as functions of the dimensions of the resonator. It is found that there exist optimum values of the resonator dimensions giving

maximum values of absorption, Q-value and reverberation time. Conditions for turbulence are then discussed and on analysis of the near field of the resonator is made. Finally some notes on arrays of resonators in free field are presented.

1. The boundary conditions.

The primary plane wave $P_o e^{ikr\cos\vartheta}$ is first assumed to strike the spherical resonator under "normal" incidence, that is, the direction of propagation coincides with a diameter of the sphere through the centrum of the hole as indicated in figure 48.

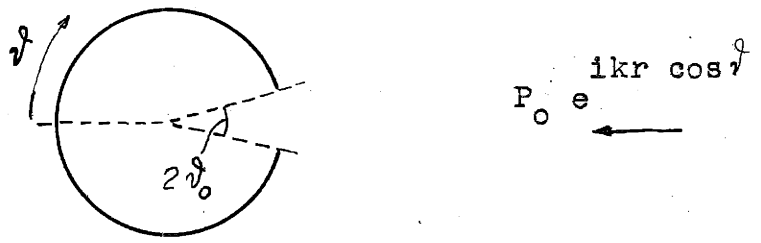

Figure 48

The inner and the outer radii of the sphere are b and a and the hole radius is r_o. With the arrangement shown in figure 48 the hole is placed at $\vartheta = \pi$ and covers an angle $2\vartheta_o$. We assume now that the sphere shell is thin, $a - b = t \ll r_o$.

If the radial velocity over the sphere at $r = a$ equals $u(\vartheta)$ we have the first boundary condition for the external field

$$u_{rp} + u_{rs} = u(\vartheta) \qquad (r = a) \qquad (II.4)$$

The continuity of average pressure over the hole yields

$$\int_{\pi-\vartheta_o}^{\pi} (p_p + p_s)_{r=a} \sin\vartheta \, d\vartheta = - U_o \varrho c \zeta_i (1-\cos\vartheta_o) \qquad (II.5)$$

where average pressure calculated from the inside field has been expressed in terms of the "internal" specific hole impedance $\varrho c \zeta_i$ discussed below. The velocity across the hole has then been assumed uniform and equal to U_o, positive in the positive r-direction, of course.

We consider the scattered wave made up of two parts, $p_s = p_{s1} + p_{s2}$, where p_{s1} is the contribution from the hole and p_{s2} is the scattered wave from the sphere when the hole is blocked. From the definition of the specific radiation impedance $\varrho c \zeta_r$ of the air piston in the hole we have

$$\int_{\pi-\vartheta_o}^{\pi} p_{s1} \sin\vartheta \, d\vartheta = U_o \zeta_r \varrho c (1-\cos\vartheta_o) \qquad (II.6)$$

The boundary condition (II.5) can therefore be written

$$(1-\cos\vartheta_o)^{-1} \int_{\pi-\vartheta_o}^{\pi} (p_p + p_{s2})_{r=a} \sin\vartheta \, d\vartheta = - U_o \varrho c (\zeta_i + \zeta_r) \qquad (II.7)$$

where the expression to the left represents the average "blocked" pressure over the surface of the hole. The pressure $p_r + p_{s2}$ can be written [33]

$$(p_p+p_{s2})_{r=a} = P_o e^{-i\omega t} \frac{1}{(ka)^2} \sum_{m=o} \frac{2m+1}{D_m} P_m(\cos\vartheta) e^{-i(\delta_m - \frac{\pi}{2} m)}$$

where $$tg\ \delta_m = j_m'(ka)/n_m'(ka) \qquad (II.8)$$

$$D_m^2 = |j_m'(ka)|^2 + |n_m'(ka)|^2$$

and the average value over the hole is

$$p_{av} = \frac{1}{1-\cos\vartheta_o} e^{-i\omega t} \sum_{m=o} \frac{(-i)^m e^{-i\delta_m}}{(ka)^2 D_m} \left[P_{m-1}(\cos\vartheta_o) - P_{m+1}(\cos\vartheta_o)\right] \qquad (II.9)$$

When $(ka) << 1$, we obtain

$$p_{av} = P_o e^{-i\omega t}\left[1 - \frac{3}{4} ika(1+\cos\vartheta_o)\right] \qquad (II.10)$$

The expressions for p_{av} given in [34] seem to have a sign error in the imaginary part. This does not affect the magnitude of p_{av}, but is of great importance in connection with the study of the near field of the resonator presented in paragraph 5.

Calculation of ζ_i and ζ_r.

The internal impedance ζ_i consists of the stiffness reactance of the volume of the resonator cavity, the mass reactance caused by the higher order modes in the cavity and the resistance due to dissipation on the surfaces of the resonator. If the wall of the resonator has a finite thickness we have in addition to consider the mass reactance of the air

plug in the neck and the neck resistance. The radiation impedance ζ_r is defined in (II.6) and has been calculated in [35], where, however, a factor $(\cos\vartheta_o)^{-1}$ is missing.

In order to determine ζ_i we have to start from the general expression of the pressure inside the cavity

$$p_i = \sum_o^\infty C_m P_m(\cos\vartheta)\, j_m(kr)$$

Expanding the velocity of the orifice piston in the spherical harmonics and applying the boundary conditions at the surface of the sphere, we obtain

$$p_i = \tfrac{1}{2}\varrho c\, U \sum_o^\infty (-1)^m \frac{P_{m-1}(\cos\vartheta_o)-P_{m+1}(\cos\vartheta_o)}{j_m(ka)}\, j_m(kr)P_m(\cos\vartheta)$$

The reactive part $-i\chi_i$ of the internal impedance is now obtained from

$$(1-\cos\vartheta_o)(-i\chi_i)\varrho c = (-U_o)^{-1}\int_{\pi-\vartheta_o}^{\pi} p_i \sin\vartheta\, d\vartheta$$

which yields

$$\chi_i = \frac{1}{2(1-\cos\vartheta_o)} \sum_o^\infty \frac{\left[P_{m-1}(\cos\vartheta_o)-P_{m+1}(\cos\vartheta_o)\right]^2}{(2m+1)} \frac{j_m(ka)}{j_m'(ka)} \qquad \text{(II.11)}$$

Since $j_o(ka)/j_o'(ka) \approx -3/ka$ for small values of ka, we see that the first term of the sum gives the contribution $-(1/\omega)(\varrho c^2/V)(\pi r_o^2)^2 \frac{1}{\varrho c}$, which is the capacitive reactance of the fundamental mode in the cavity, as expected. All

other modes give a mass contribution to the reactance as long as the frequency is well below the first resonance frequency of the cavity, determined by $j_o'(ka) = 0$. At frequencies slightly below this resonance the mass reactance is very large. Since we are mainly interested in relatively low frequencies, we can put $j_m(ka)/j_m'(ka) = (ka)/m$, and the mass reactance ofthe higher order modes expressed as an end correction is

$$\delta_i = \frac{(\rho c \chi_i/\omega)}{\rho} = \frac{1}{2}\,\frac{a}{1-\cos\vartheta_o}\sum_{m=1}^{\infty}\frac{\left[P_{m-1}(\cos\vartheta_o)-P_{m+1}(\cos\vartheta_o)\right]^2}{(2m+1)m} \tag{II.12}$$

The corresponding expression for the external end correction is

$$\delta_r = \frac{(\rho c \chi_r/\omega)}{\rho} = \frac{1}{2}\,\frac{a}{1-\cos_o}\sum_{m=o}^{\infty}\frac{\left[P_{m-1}(\cos\vartheta_o)-P_{m+1}(\cos\vartheta_o)\right]^2}{(2m+1)(m+1)} \tag{II.13}$$

where $P_{-1}(\cos\vartheta_o) = 1$.

The value of δ_i and δ_r in the limit of small ϑ_o can be obtained in the following way: we approximate the sum in (II.12) by an integral and introduce then the asymptotic value of $P_n(\cos\vartheta_o)$ for large n [36].

$$\lim_{n\to\infty} P_n(\cos\vartheta_o) = \sqrt{\frac{2}{n\pi\sin\vartheta_o}}\cos\left[(n+\tfrac{1}{2})\vartheta_o - \frac{\pi}{4}\right]$$

Replacing $\sin\vartheta_o$ by ϑ_o and introducing the continous variable $z = n\vartheta_o$ yields

$$\lim_{\vartheta_o \to 0} \left\{ \lim_{n \to \infty} P_n(\cos \vartheta_o) \right\} = \sqrt{\frac{2}{\pi}} \; \frac{\cos(z - \frac{\pi}{4})}{\sqrt{z}} = J_o(z)$$

The difference $P_{m+1}(\cos \vartheta_o) - P_{m-1}(\cos \vartheta_o)$ appearing in the sum, is now written as the differential

$$P_{m+1}(\cos \vartheta_o) - P_{m-1}(\cos \vartheta_o) \simeq 2 \vartheta_o \, J_o'(z) \, dz = -2 \vartheta_o \, J_1(z) \, dz$$

and the sum can then be transformed to a well-known integral

$$\lim_{\vartheta_o \to 0} \sum_{m=1} \frac{\left[P_{m-1}(\cos \vartheta_o) - P_{m+1}(\cos \vartheta_o) \right]^2}{(2m + 1)m} =$$

$$= 2 \vartheta_o^3 \int_0^\infty \frac{J_1^2(z)}{z^2} \, dz = \frac{8}{3\pi} \vartheta_o^3$$

where we have used $\int_0^\infty (J_1^2(z)/z^2) \, dz = \frac{4}{3\pi}$ [39]

Multiplying by the factor $\frac{1}{2} \frac{a}{1 - \cos \vartheta_o} \simeq a/\vartheta_o^2$ appearing in front of the sum in (II.12) we obtain

$$\lim_{\vartheta_o \to 0} \delta_i = \lim_{\vartheta_o \to 0} \delta_r = \frac{8}{3\pi} r_o = \delta_o \qquad \text{(II.14)}$$

which is the same value for a piston in an infinite wall. A closed form for the sums in (II.12) and (II.13) was not found beyond this limit value for small ϑ_o, and the plots of δ_i/δ_o, δ_r/δ_o and $(\delta_i + \delta_r)/2\delta_o$ appearing in figure 49 were obtained by a direct summation of the series in (II.12-13). However, Morse has shown [38] that if the distribution

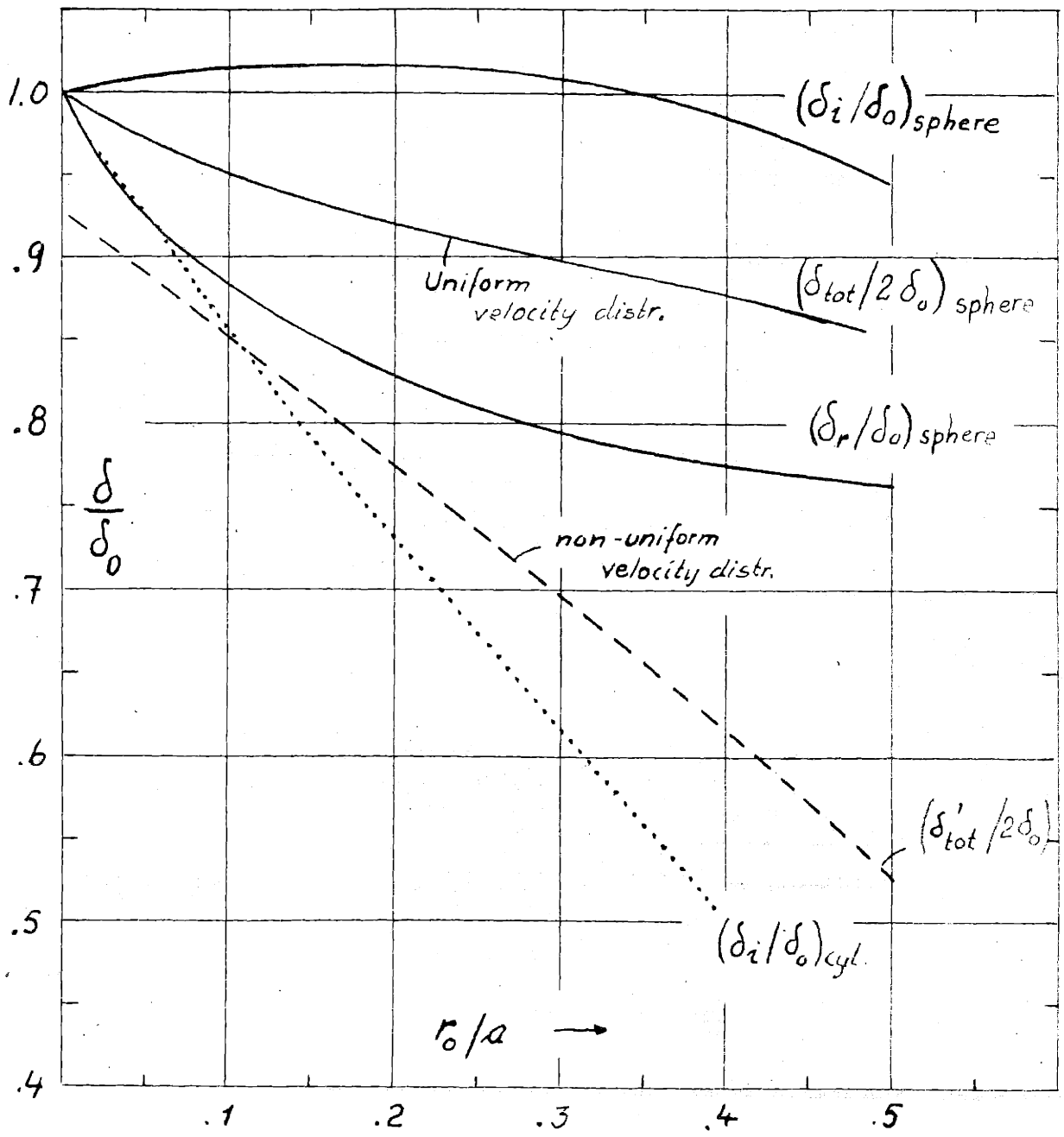
1.0
.9
.8
.7
.6
.5
.4
δ/δ0
.1
.2
.3
.4
.5
r0/a
(δi/δo)sphere
(δtot/2δo) sphere
(δr/δo) sphere
Uniform velocity distr.
non-uniform velocity distr.
(δ'tot/2δo)
(δi/δo)cyl.

Figure 49

$$u(\vartheta) = U_o/\sqrt{\cos\vartheta - \cos\vartheta_o} \qquad \text{(II.15)}$$

is used for the particle velocity in the hole of the resonator, the end correction can be expressed in the closed form

$$\delta'_{tot} = \delta'_i + \delta'_r = a\left[(\pi - \vartheta_o)\cos(\tfrac{1}{2}\vartheta_o) - \sin(\tfrac{1}{2}\vartheta_o)\right]\sin(\tfrac{1}{2}\vartheta_o) \qquad \text{(II.16)}$$

which is represented by the dashed curve in figure 49. For small ϑ_o we get

$$\delta'_{tot} \simeq \frac{\pi}{2} r_o \qquad \text{(II.17)}$$

Comparison with (II.14) yields $\delta'_{tot} = \frac{3\pi^2}{32}\delta_{tot}$, or in other words, the velocity distribution (II.15) gives about 8 % smaller end correction than the uniform one, when $\delta_o << 1$ and the difference increases with δ_o. Since $\delta' < \delta$, it follows that (II.15) is theoretically closer to the true distribution than the uniform one. However, in practice, the viscosity and also non-linearity in the high velocity region near the edges of the hole affects the distribution, and measurements of resonance frequencies reported in § 4 are in favour of the uniform distribution.

It is interesting to see (figure 49) that the internal end correction $(\delta_i)_{cyl.}$ for a cylindrical resonator is considerably smaller than for the spherical one, and assuming that

the external end corrections are the same in the two cases, it follows that a cylindrical resonator has a higher resonance frequency than a spherical of the same volume and with r_o/a equal to ξ . (ξ is defined in table 1.)
If the value $2\vartheta_o$ is used as end correction for a cylindrical resonator in free field, the resonance frequency obtained is clearly going to be too small, the error for $r_o/a = 0.25$, for example, being about 17 % if the neck length is small compared with the radius of the hole. This may explain reported deviations between measured and computed resonance frequencies for cylindrical resonators in free field 39.

The viscous dissipation.

The resistive part of the impedance $\zeta = \zeta_i + \zeta_r$ contains two parts, the radiation resistance θ_r and the resistance θ_i caused by viscous dissipation at the surfaces of the sphere and in the neck. To obtain the surface dissipation caused by a piston-like motion of the air in the hole, we have to start from the corresponding tangential velocity u_ϑ on the surfaces of the sphere.

$$(u_\vartheta)_{r=a} = \sum_{m=0} B_m \sin\vartheta P_m'(\cos\vartheta)$$

where for the outer surface

$$B_m = -\frac{U}{2}\frac{(-1)^m}{(ka)}\frac{h_m(ka)}{h_m'(ka)}\left[P_{m-1}(\cos\vartheta_o) - P_{m+1}(\cos\vartheta_o)\right]$$

The coefficients B_m for the inner surface are obtained by

replacing $h_m(ka)/h_m'(ka)$ by $j_m(ka)/j_m'(ka)$.

The viscous dissipation is given by $(1/2) \int R_w u^2 \, dA$ where the integration has to be taken over the inner and outer surfaces of the sphere. Introducing the expression for u_ϑ yields integrals of the type [40]

$$I_{mn} = \int_{-1}^{+1} (1 - z^2) P_m'(z) P_n'(z) \, dz = \begin{cases} 0 & m \neq n \\ \frac{2n(n+1)}{2n+1} & m = n \end{cases} \qquad \text{(II.18)}$$

The dissipation on one of the surfaces of the sphere is therefore

$$\text{Dissipation} = \pi a^2 \sum_{m=1}^{\infty} B_m^2 \frac{2m(m+1)}{2m+1} \equiv \frac{1}{2} \varrho c \, \Theta_i \, \pi r_o^2 \, U^2 \qquad \text{(II.19)}$$

from which the corresponding resistance Θ_i is obtained as shown. Introducing the low frequency approximations for B_m and adding the contributions from the inner and outer surfaces, the internal resistance becomes

$$\Theta_i \varrho c = R_w (r_o/a)^{-2} \sum_{1}^{\infty}{}' \frac{(m+1)^2 + m^2}{m(m+1)(2m+1)} \left[P_{m-1}(\cos \vartheta_o) - P_{m+1}(\cos \vartheta_o) \right]^2$$

We can determine the value of the total resistance in the limit of small ϑ_o in the same way as for the mass end correction on page 52. We then get

$$\lim_{\vartheta_o \to 0} (\Theta_i \varrho c) = 4 R_w \int_0^{\infty} \frac{J_1^2(x)}{x} \, dx = 2 R_s \qquad \text{(II.20)}$$

where we have used $\int_0^{\infty} \frac{J_1^2(x)}{x} \, dx = \frac{1}{2}$ given in [37]. This is

approximately the same value of the hole resistance as that found for the circular aperture in the circular tube.

If the resonator has a wall thickness t we get in addition the neck resistance $2R_n\, t/r_o$ so that the total resistance is

$$\varrho c\theta_i = (2R_n/r_o)(t + \frac{R_w}{R_n} r_o) = 2R_w(1 + \frac{R_n}{R_w}\frac{t}{r_o}) = 2R_w(1 + \alpha t/r_o)$$

$$\alpha = R_n/R_w \qquad \text{(II.21)}$$

In (I. 2) we found that the neck resistance $2R_n t/r_o$ is in agreement with measurements if the classical value $R_n = R_s$ is used for the surface resistance. The remaining part, however, obtained from the assumption of a uniform velocity in the aperture and represented by $2R_w$ in (II.21), was found to be in fair agreement with measurements only if we put $R_w \simeq 2R_s$.

In cases where we need a numerical expression for the total resistance θ_i we have then to use $R_n = R_s$ and empirically set $R_w = 2R_s$ so that $\alpha = 0.5$ in (II.21) and hence

$$\theta_i \varrho c = 4R_s(1 + 0.5\, t/r_o) \simeq 3.4\, 10^{-3}/\sqrt{\nu}\,(1 + 0.5\, t/r_o) \qquad \text{(II.21a)}$$

<u>The absorption and scattering cross section.</u>

The absorbed and scattered power equal $(1/2)U_o^2\, \pi r_o^2\, \theta_i\, \varrho c$ and $(1/2)U_o^2\, \pi r_o^2\, \theta_r\, \varrho c$ respectively. Using (II.7) and

(II.10) the corresponding cross sections become

$$\sigma_a = \frac{\Theta_i}{|\beta|^2}\,\pi r_o^2\left[1 + \frac{9}{16}(ka)^2(1+\cos\vartheta_o)^2\right] \qquad (II.22)$$

$$\sigma_s = \frac{\Theta_r}{|\beta|^2}\,\pi r_o^2\left[1 + \frac{9}{16}(ka)^2(1+\cos\vartheta_o)^2\right] \qquad (II.23)$$

when $ka << 1$.

These quantities represent only the effect of the hole in the sphere, however. In order to obtain the total absorption and scattering we have to add the corresponding quantities for a rigid sphere in a free field, and in addition consider some interaction terms. To see this we start from the expression for the total scattered pressure

$$p_s = \sum_{o}^{\infty} A_m P_m(\cos\ ) h_m(kr) \qquad (II.24)$$

We know that we can set $A_m = A_{1m} + A_{2m}$, where A_{1m} gives the scattered pressure from the hole and A_{2m} corresponds to the scattering from a rigid sphere. For large r one has $h_m(kr) \simeq (1/kr)\exp\left[i(kr - \frac{m+1}{2}\pi)\right]$ and the velocity is $u = p_s/\rho c$. The scattered power can then be expressed as

$$\Gamma_s = \frac{2\pi}{k^2}\frac{1}{\rho c}\sum_{m=o}\frac{1}{2m+1}\left|A_{1m} + A_{2m}\right|^2$$

which contains the scattered power from the hole, represented by $|A_{1m}|^2$, the scattered power from a rigid sphere, represented by $|A_{2m}|^2$ and the interaction effect given by the cross terms $2\mathrm{Re}(A_{1m}\cdot A_{2m}^*)$. The coefficients A_{1m} and A_{2m} are

$$A_{1m} = \frac{\varrho c}{2} U (-1)^m \left[P_{m-1}(\cos\vartheta_o) - P_{m+1}(\cos\vartheta_o) \frac{1}{D_m} e^{-i\delta_m} \right]$$

$$A_{2m} = -P_o(2m+1) \sin\delta_m \, e^{-i\delta_m} \qquad \text{(II.25)}$$

The contribution in scattered power from the hole alone is given above in equation (II.23). The scattering from the rigid sphere becomes $(P_o^2/2\varrho c)(4/9)\pi a^2(ka)^4$ (The expression for the rigid sphere scattering in [41] seems to contain a factor 4 too much.)

The lowest term in the interaction is proportional to $(ka)^5$ and corresponds to $m = 1$. Since this term involves U as a factor, it exceeds generally the rigid sphere scattering at frequencies in the neighborhood of the resonance frequency of the resonator. However, the "hole" scattering is in general so large compared with the other parts that they can be neglected anyway at frequencies up to about twice the resonance frequency.

Correspondingly, the total absorbed power is obtained by integrating the total tangential velocity squared over the surface of the sphere.

$$\text{(Total dissipation)} = \frac{\pi a^2}{(\varrho c)^2} \frac{R_w}{(ka)^2} \sum_{m=o} |A_{1m} + A_{2m}|^2 \frac{2m(m+1)}{2m+1} |h_m|^2$$

which in addition to the prodominant part, given by equation (II.22) contains the contribution from $|A_{2m}|^2$, i.e. the dissipation on a rigid sphere in free field, and also

interaction terms. The rigid sphere dissipation becomes

$$(P_o^2/2\,\varrho c)(4\pi a^2 R_w/\varrho c)$$

The corresponding absorption cross section, $(4\pi a^2 R_s/\varrho c)$, is generally much smaller than the fundamental contribution (II.22). The first term of the interaction goes as $(ka)^8$ and can be neglected.

The expressions for σ_s and σ_a as given by expressions (II.22) and (II.23) are therefore adequate for most cases. The maximum value of the absorption cross section is obtained for $\theta_i \simeq \theta_r$

$$(\sigma_a)_{max} \simeq \frac{\lambda^2}{4\pi}\left[1 + \frac{9}{16}(ka)^2(1 + \cos\vartheta_o)^2\right] \qquad \text{(II.22a)}$$

with the same value for σ_s under the same conditions

§ 2. Investigation of characteristic quantities and optimum design.

We want now to investigate such characteristic quantities as the absorption and scattering cross sections, the Q-value and the reverberation time as a function of the dimensions of the resonator, and study the conditions for "optimum" design of resonators. When writing down the expressions for these quantities it seems to be practical to use $k_o a$, r_o/a and t/r_o as the three independent variables required to describe a resonator.

The equation for the resonance frequency is then

$$k_o a = 0.666 \sqrt{(r_o/a)}(\beta + 0.59\ t/r_o)^{-1/2} \qquad \text{(II.26)}$$

in which $\beta = \delta_{tot}/\delta_o$ is obtained from (II.12) or from figure 49. The relation (II.25) is represented in the "frequency chart" in figure 50.

In order to include the possibility of introducing an additional resistance $\varsigma c\theta_e$ in the hole of the resonator, we rewrite the expression for the specific hole resistance, given in (II.21), and introduce $\xi = 1 + \varsigma c\theta_e/2R_w$, so that

$$\theta_1 = 2(R_w/\varsigma c)(\xi + \alpha t/r_o)$$

If now the radiation resistance $(1/4)(kr_o)^2$ is added, the total hole resistance at resonance can be written

$$\theta = 2(R_w/\varsigma c)(\xi + \alpha t/r_o)\left[1 + C(k_o a)^6\right] \qquad \text{(II.27)}$$

where we have put $(k_o r_o) = (k_o a)(r_o/a)$ and used the relation (II.26). The parameter C is then

$$C = 0.632(R_w/\varsigma c)^{-1}\ \frac{(\beta + 0.59\ t/r_o)^2}{(\xi + \alpha t/r_o)} =$$

$$= 0.632(R_s/\varsigma c)^{-1} h(t/r_o) \qquad \text{(II.28)}$$

$$h(t/r_o) = \frac{(\beta + 0.59\ t/r_o)^2}{(\xi + t/r_o)}$$

The "hole parameter" h is practically equal to unity for small values of t/r_o, and with no extra resistance introduced, i.e. $\xi = 1$. A plot of h as a function of ξ with t/r_o as parameter is shown in figure 51. An average value of β has then been used, $\beta \simeq 0.9$, and α has been set equal to 0.5 in accordance with (II.21a).

The expression for the absorption cross section at resonance given in (II.21) can now be written

$$\sigma_a = \frac{\lambda_o^2}{4\pi} \frac{4C(k_o a)^6}{[1+C(K_o a)^6]^2} F \qquad (II.29)$$

where $F = 1 + (9/16)(k_o a)^2(1 + \cos\vartheta_o)^2$, and the scattering cross section $\sigma_s = (\theta_r/\theta_i)\,\sigma_a$ can be expressed similarly.

Starting from the definition $Q = \omega m/\theta\rho c$ and introducing $m = 1.7\, r_o(\beta + 0.59\, t/r_o)$ and the resistance given by (II.21), we obtain for the Q-value

$$Q = 3.03 \frac{C(k_o a)^2}{1 + C(k_o a)^6} \qquad (II.30)$$

Finally, from the exponential decay of the pressure in the resonator, determined by the factor $\exp\left[(-r/2m)t\right]$, the reverberation time becomes

$$T = 13.8\, m/\rho c\theta = 41.8\, \frac{1}{\omega} \frac{C(k_o a)^3}{1 + C(k_o a)^6} \qquad (II.31)$$

We want to investigate how a resonator shall be designed in order to give maximum value of any of these quantities.

Since we are dealing with three independent variables we have to vary one at a time. We may consider first the case where we have the sphere radius given, and ask for the optimum resonance frequency (or hole dimension), which makes any of the quantities in (II.29-32) a maximum. Or in the case of more practical interest we may have the resonance frequency given, and ask for the "best" resonator volume. In dealing with the first case we must recognize that the quantity C which appears in the expressions is frequency dependent because $R_w \sim \sqrt{\nu_o}$. We introduce then

$$K_1 = C\sqrt{k_o a} \ ,$$

which is independent of frequency, in (II.28-31) and the absorption cross section, for example, becomes

$$\sigma_a = 4\pi a^2 \ \frac{K(k_o a)^{7/2}}{\left[1 + K(k_o a)^{11/2}\right]^2} \ F$$

In the following list of results we have given the optimum values of the resonator parameters which maximize the characteristic quantities in (II.29-31). These optimum values are denoted by a star index. The numerical values given are obtained by using $R_w = 2R_s$ in accordance with the discussion given in connection with equation (II.21a). (The figures appearing within parenthesis refer to a single resonator in a wall, which is discussed in (III.§1)).

a) Optimum values of the resonance frequency (or hole radius) with sphere radius kept constant.

Absorption cross section:

$$k_o^* a = \left(\frac{7}{15}\ \frac{1}{K}\right)^{2/11} \underset{(0.835)}{=} 0.948\ \theta_w^{2/11}\ h^{-2/11} \qquad \text{(II.32)}$$

$$\theta_w = (R_w/\varrho c)(k_o a)^{-1/2}$$

$$r_o^* \underset{(1.58)}{=} 2.03\ \theta_w^{4/11}\ a h^{-4/11}\ (\beta + 0.59\ t/r_o) \qquad \text{(II.33)}$$

$$\sigma_a^* = 1.15\ \pi a^2\ K^{4/11}\ F = 0.845\ \pi a^2 \theta_w^{-4/11}\ h^{4/11}\ F \qquad \text{(II.34)}$$

Normalized expression for σ_a

$$\sigma_a/\sigma_a^* = \left(\frac{22}{15}\right)^2 \frac{(r_o/r_o^*)^{7/4}}{\left[1 + \frac{7}{15}(r_o/r_o^*)^{11/4}\right]^2} = \qquad \text{(II.35)}$$

$$= \left(\frac{22}{15}\right)^2 \frac{(\nu_o/\nu_o^*)^{7/2}}{1 + \frac{7}{15}(\nu_o/\nu_o^*)^{11/2}\ 2}$$

Numerical values:

$$k_o^* a \underset{(0.303)}{=} 0.344\ V^{-1/33}\ h^{-2/11} \underset{(0.298)}{=} 0.328\ a^{-1/11}\ h^{-2/11} \qquad \text{(II.32a)}$$

$$r_o^* \underset{(0.189)}{=} 0.242\ a^{9/11}\ g^{-4/11}\ (\beta + 0.59\ t/e_o) = \qquad \text{(II.33a)}$$

$$= 0.163\ V^{2/11}\ h^{-4/11}\ (\beta + 0.59\ t/r_o)$$

$$\sigma_a^* \underset{(18.2)}{=} 7.1\ \pi a^2\ a^{2/11} h^{4/11} F \qquad \text{(II.34a)}$$

Example: $V = 1000\ cm^3$ and $t << r_o$ gives

$$k_o^* a = \underset{(0.246)}{0.279}; \qquad r_o^* = \underset{(0.82)}{1.05}\ cm \qquad \sigma_a^* = \underset{(25)}{11.5}\ \pi a^2$$

Q-value.

$$Q = 3.03\ K\ \frac{(k_o a)^{5/2}}{1 + K(k_o a)^{11/2}} \tag{II.35}$$

$$k_o^* a = \left(\frac{5}{6}\frac{1}{K}\right)^{2/11} = \underset{(0.93)}{1.05}\ \theta_w^{2/11}\ g^{-2/11} \tag{II.36}$$

$$r_o^* = \underset{(1.94)}{2.49}\ \theta_w^{4/11} a h^{4/11} (\beta + 0.59\ t/r_o) \tag{II.37}$$

$$Q^* = \underset{(0.87)}{1.19}\ \theta_w^{-6/11} h^{6/11} \tag{II.38}$$

Normalized expression for Q.

$$Q/Q^* = \frac{5}{11}\ \frac{(\nu_o/\nu_o^*)^{5/2}}{1 + \frac{5}{6}(\nu_o/\nu_o^*)^{11/2}} = \frac{5}{11}\ \frac{(r_o/r_o^*)^{5/4}}{1 + \frac{5}{6}(r_o/r_o^*)^{11/4}} \tag{II.35a}$$

Numerical values:

$$k_o^* a = \underset{(0.321)}{0.365}\ a^{-1/11} g^{-2/11} = \underset{(0.336)}{0.382}\ V^{-1/33} h^{-2/11} \tag{II.36a}$$

$$r_o^* = \underset{(0.232)}{0.298}\ a^{4/11} g^{-4/11} = \underset{(0.156)}{0.200}\ V^{2/11} h^{-4/11} (\beta + 0.59\ t/r_o) \tag{II.37a}$$

$$Q^* = \underset{(18.3)}{25}\ V^{1/11} h^{6/11} \tag{II.38a}$$

Example: $V = 1000\ cm^3$ and $t << r_o$ gives

$$k_o^* a = \underset{(0.27)}{0.31}, \qquad r_o^* = \underset{(1.01)}{1.3}\ cm \quad \text{and} \quad Q^* = \underset{(31.5)}{43}$$

Reverberation time.

$$T = 41.8\ \frac{a}{c}\ \frac{K(k_o a)^{3/2}}{1 + K(k_o a)^{11/2}} \tag{II.30a}$$

$$k_o^* a = \left(\frac{3}{8}\ \frac{1}{K}\right)^{2/11} = \underset{(0.815)}{0.912}\ \theta_w^{2/11}\ h^{-2/11} \tag{II.39}$$

$$r_o^* = \underset{(1.50)}{1.87}\ \theta_w^{4/11}\ a\ h^{-4/11}\ (\beta + 0.59\ t/r_o) \tag{II.40}$$

$$T^* = \underset{(13.7)}{16.6}\ \frac{a}{c}\ \theta_w^{-8/11}\ h^{8/11} \tag{II.41}$$

Normalized expression for T.

$$T/T^* = \frac{11}{8}\ \frac{(\nu_o/\nu_o^*)^{3/2}}{1 + \frac{3}{8}(\nu_o/\nu_o)^{11/2}} = \frac{11}{8}\ \frac{(r/r_o^*)^{3/4}}{1 + \frac{3}{8}(r/r_o^*)^{11/4}} \tag{II.30b}$$

Numerical values:

$$k_o^* a = \underset{(0.281)}{0.315}\ a^{-1/11}\ h^{-2/11} = \underset{(0.295)}{0.330}\ V^{-1/33}\ h^{-2/11} \tag{II.39a}$$

$$r_o^* = \underset{(0.12)}{0.150}\ V^{3/11}\ h^{-2/11} \tag{II.40a}$$

$$T^* \underset{(0.0144)}{=} 0.0175\, V^{5/11} h^{8/11} \underset{(0.0276)}{=} 0.0335\, a^{15/11} h^{8/11} \qquad \text{(II.41a)}$$

Example: $V = 1000\ cm^3$ and $t \ll r_o$ gives

$k_o^* a = 0.27 \qquad r_o^* = 1.0\ cm \qquad T^* = 0.41\ sec.$

b) Optimum values of the sphere radius with the resonance frequency kept constant.

Absorption cross section.

$$k_o a^* = C^{-1/6} \underset{(0.965)}{=} 1.08 (R_w/\rho c)^{1/6} h^{-1/6} \qquad \text{(II.42)}$$

$$\sigma_a^* = \frac{\lambda_o^2}{4\pi} F \qquad \text{(II.43)}$$

Normalized expression for σ_a:

$$\sigma_a/\sigma_a^* = 4 \frac{(a/a^*)^6}{\left[1 + (a/a^*)^6\right]^2} \qquad \text{(II.28a)}$$

Numerical value:

$$a^* = \frac{(965)}{1080} \nu_o^{-11/12} h^{-1/6} \qquad \text{(II.42a)}$$

Example: $\nu_o = 200$ cps. and $t \ll r_o$ gives $a^* = 9.4$ cm.

Q-value.

$k_o a^*$: see (II.40)

$$Q^* \underset{(0.85)}{=} 1.20 (R_s/\rho c)^{-1/2} h^{1/2} \qquad \text{(II.44)}$$

Normalized expression for Q:

$$Q/Q^* = 2\,\frac{(a/a^*)^3}{1 + (a/a^*)^6} \qquad \text{(II.29a)}$$

Numerical values:

a^*: see (II.40a)

$$Q^* \underset{(134)}{=} 189\ \nu_o^{-1/4}\ h^{1/2} \qquad \text{(II.44a)}$$

Reverberation time.

$k_o a^*$: see (II.40)

$$T^* \underset{(1.86)}{=} 2.64(R_s/\varrho c)^{-1/2}\ \nu^{-1}\ h^{1/2} \qquad \text{(II.45)}$$

Normal expression for T.

$$T/T^* = 2\,\frac{(a/a^*)^3}{1 + (a/a^*)^6} \qquad \text{(II.30a)}$$

Numerical values:

a^*: see (II.40a)

$$T^* \underset{(293)}{=} 415\ \nu_o^{-5/4}\ g^{1/2} \qquad \text{(II.45a)}$$

Example: $\nu_o = 100$ $\quad T^* \simeq 1.3$ sec.

There are a few remarks referring to these results which may be worth mentioning. First we see that the maximum absorption cross section in (II.34), obtained when varying

the resonance frequency and keeping the sphere radius a constant, does not occur when the internal resistance equals the radiation resistance, but at a value somewhat larger than the radiation resistance. It is also interesting to realize the magnitude of the optimum cross section which is around 11-12 times the sphere cross section for resonators of "normal" size, i.e. with a volume of about 1000 cm^3. The value increases slowly with the volume.

From (II.41a) it is apparant that the maximum Q-value increases slowly with decreasing resonance frequency tending to infinity when $\nu \to 0$. At 50 cps., for example, the Q should be as high as 71 and at 25 cps. 85. This rise of Q is presumably going to be considerably reduced in practice by non-linear effects, which at low frequencies are going to be important even at very low levels as shown in (I. § 3).

In order to make the analysis complete we have to investigate the case when a and k_o are kept constant and t/r_o is considered as variable. We find then, that in order to obtain an optimum value we must have $dC/d(t/r_o) = 0$, or in other words $h' = 0$, which leads to the condition

$$(t/r_o)^* = \frac{\beta\alpha - 1.18\,\varepsilon}{0.59\,\alpha}$$

However, $\beta\alpha$ cannot exceed unity and there is no positive value of t/r_o for which any of the quantities discussed

is a maximum or a minimum.

If we are going to show the relations presented above graphically we have of course two choices. We may consider the sphere volume given and ask for the proper resonance frequency to choose in order to obtain maximum of any of the quantities discussed. In such a case it may be preferable to use the results under a). Howewer, it seems to be both simpler and of more practical value to plot the results as presented under b). Starting with a given resonance frequency ν_o and a hole parameter h, we obtain the optimum sphere radius from (II.42) or (II.42a), and the maximum values σ_a^*, Q^* and T^* from (II.43), (II.44) and (II.45). Finally the σ, Q and T for an arbitrary a are obtained from the normalized expressions (II.28a) and (II.29a). The hole radius is in any case obtained from the general frequency chart in figure 50. The set of curves representing these results are drawn in figure 52-55.

As an illustration of the use of these charts we may design a resonator with a resonance frequency 200 cps. for largest possible absorption cross section σ_a, and with no restrictions on Q and T, (which both are maximum when σ_a is a maximum). We suppose that there is no extra resistance in the hole and that $t \ll r_o$, so that the hole parameter is $h \simeq 0.9$. From figure 52 we obtain the optimum sphere radius $a^* = 8.4$ cm and the frequency chart in figure 50 yields

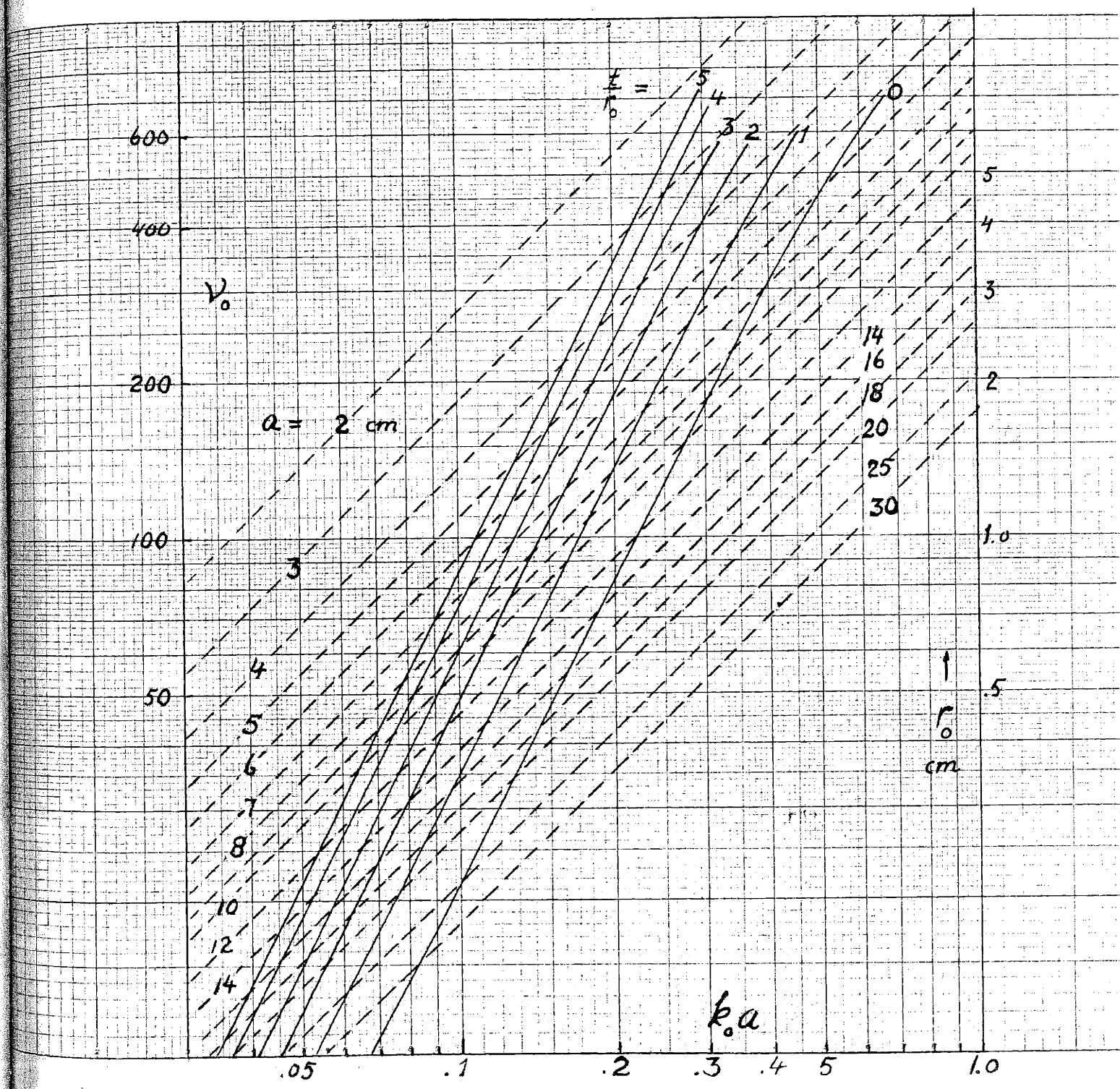

Figure 50

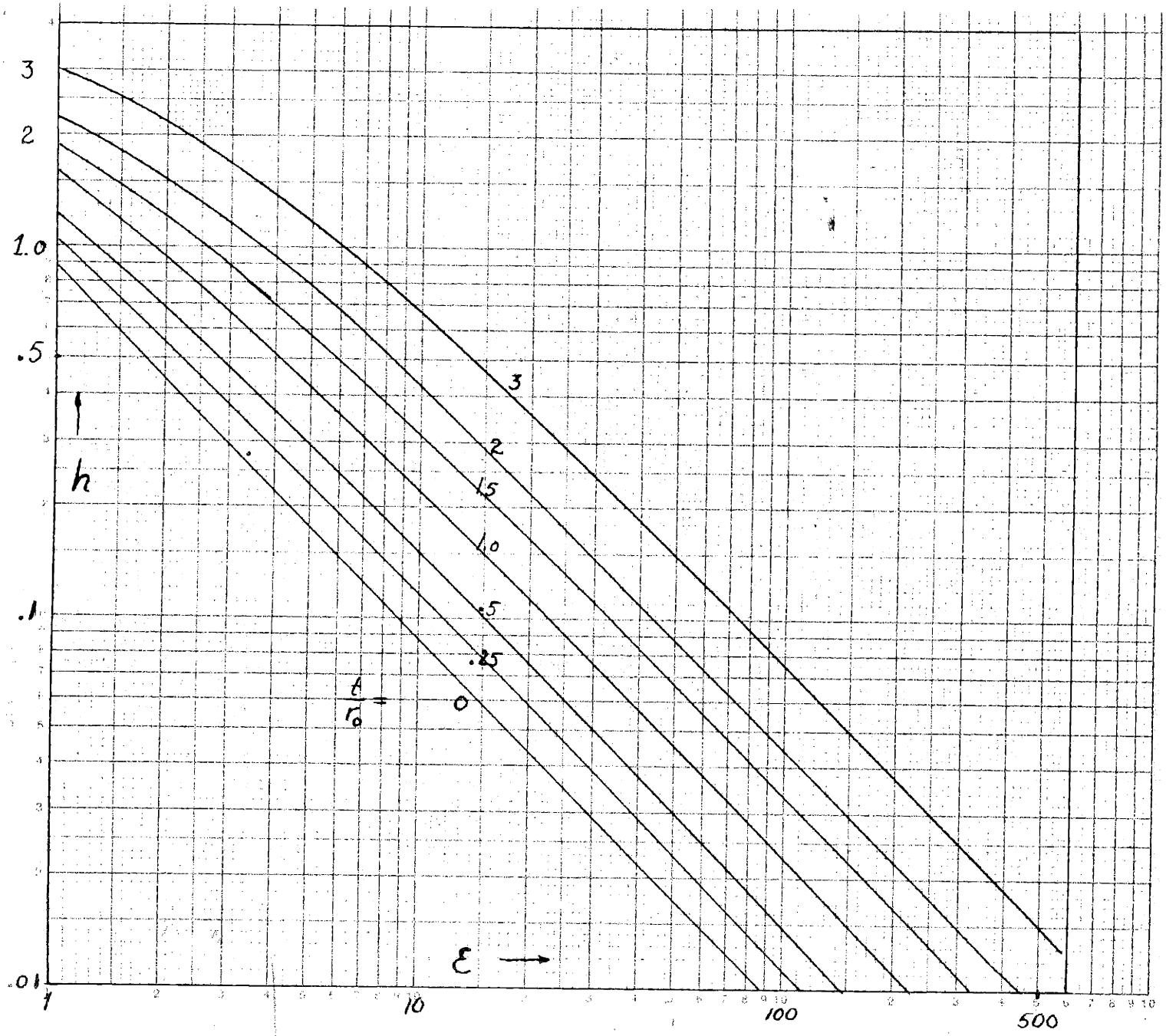

Figure 51

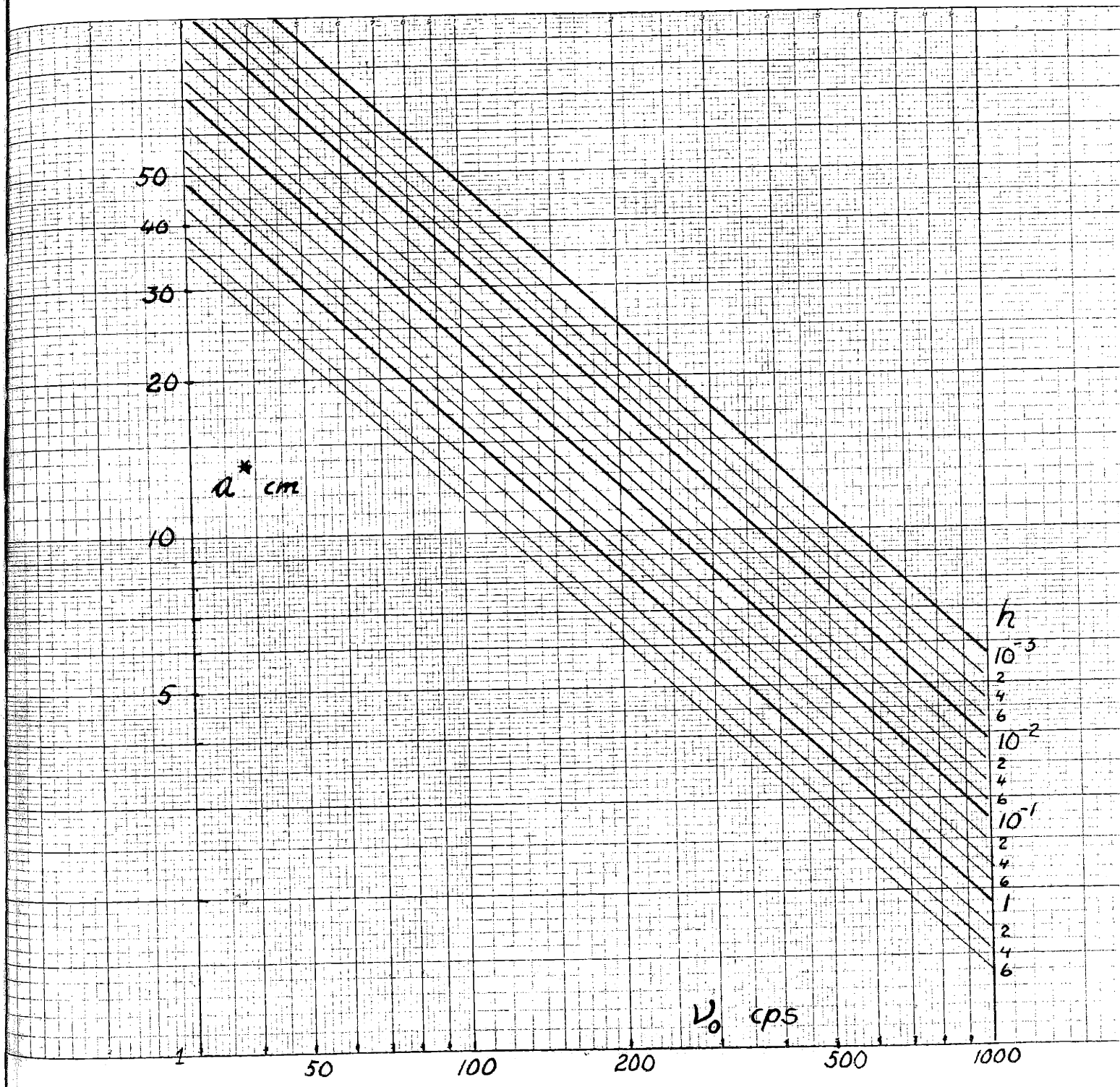

Figure 52

NO. 3123. LOGARITHMIC; 2¾ BY 2 3¾-INCH CYCLES.

CODEX BOOK COMPANY, INC. NORWOOD, MASSACHUSETTS
PRINTED IN U.S.A.

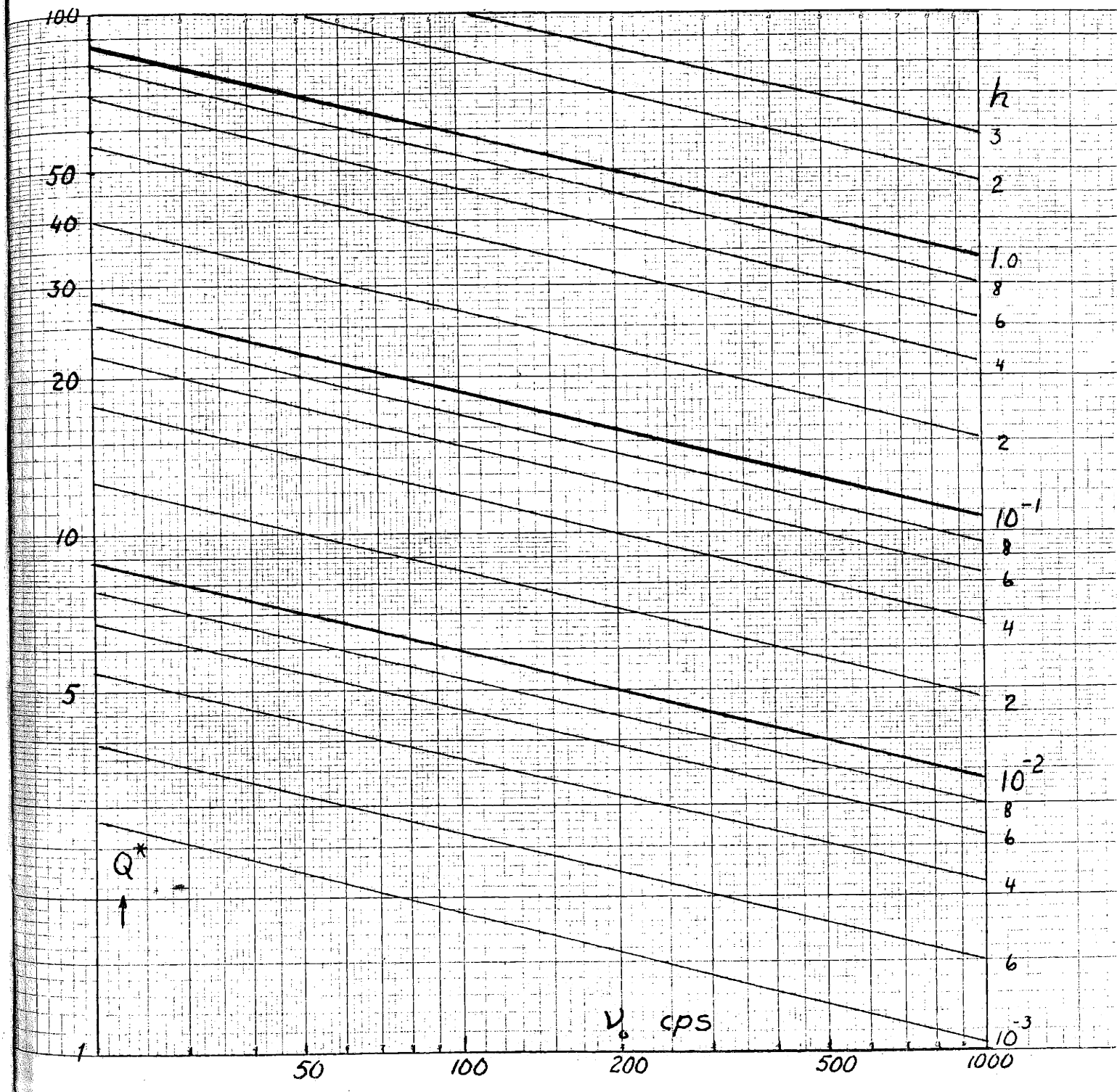

Figure 53

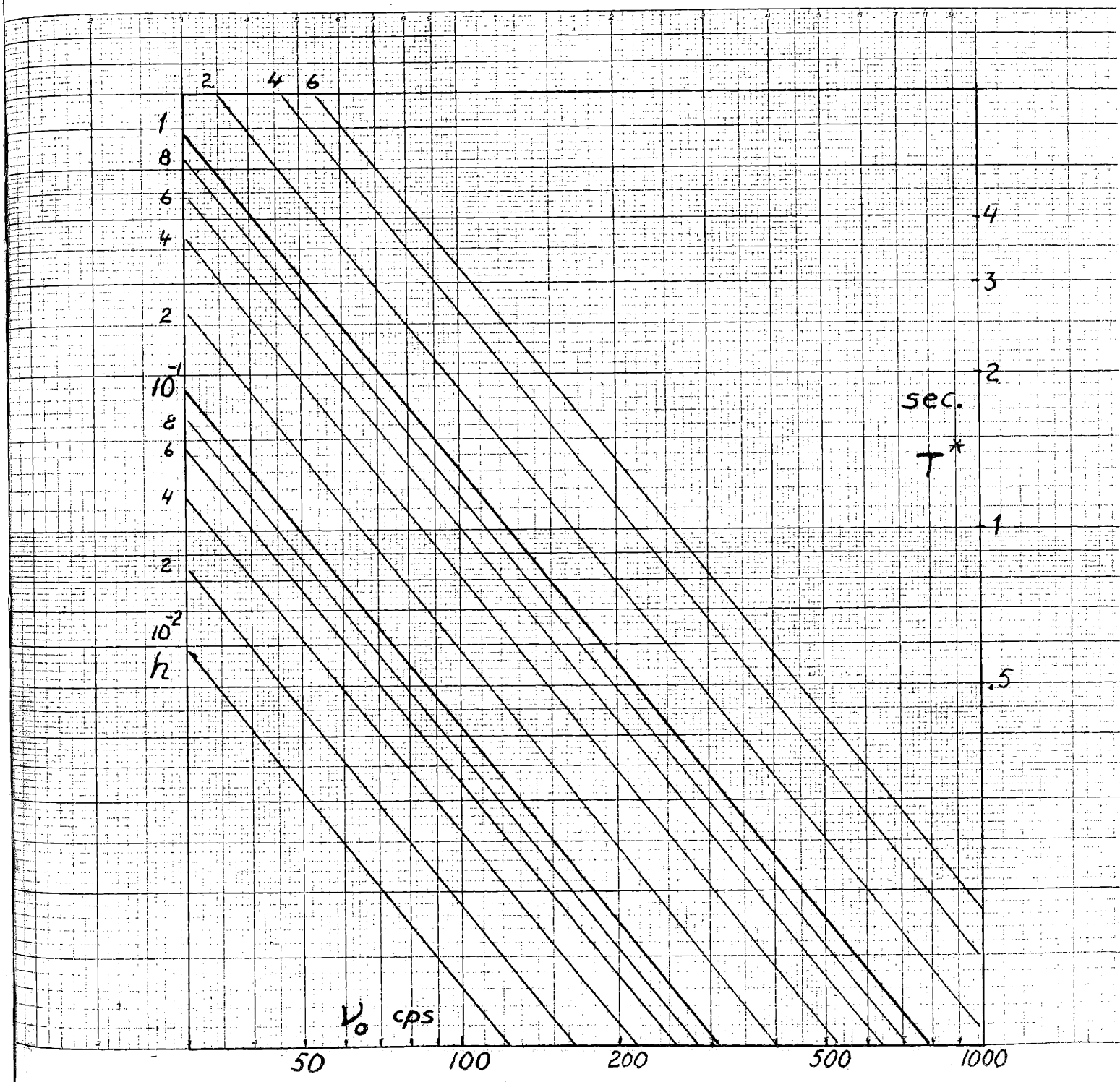

Figure 54

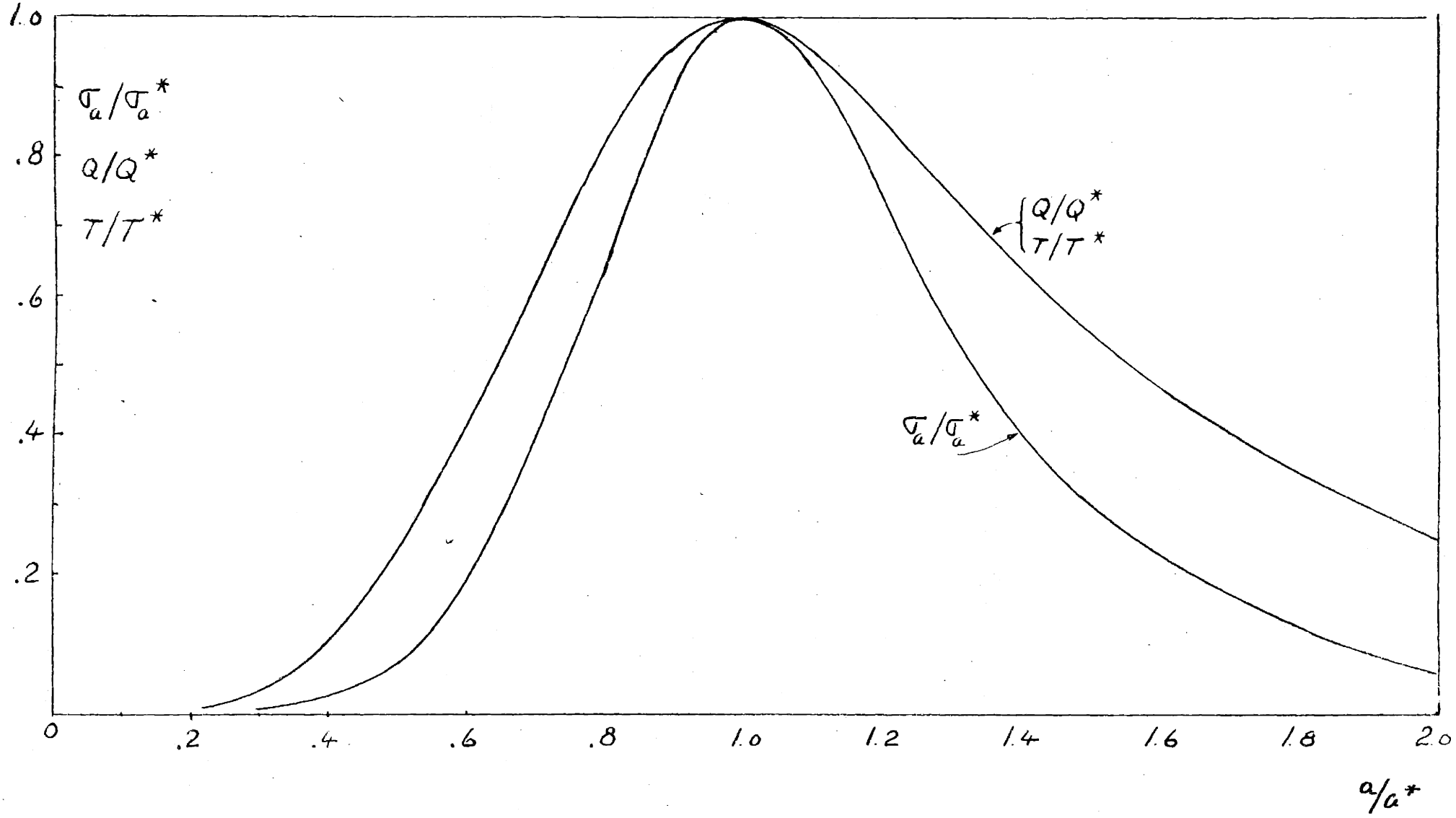
1.0
.8
.6
.4
.2
0
.2
.4
.6
.8
1.0
1.2
1.4
1.6
1.8
2.0
σ_a/σ_a^*
Q/Q^*
T/T^*
Q/Q^*
T/T^*
σ_a/σ_a^*
a/a^*

Figure 55

$r_o = 0.185 \cdot 8,4 = 1.55$ cm. The maximum absorption cross section is then $\sigma_a^* = (\lambda_o^2/4\pi)F \simeq 1.2\ {}^2_o/4\pi$, or expressed in terms of the cross section of the sphere, $\sigma_a^* = 13.3\ \pi a^2$, The corresponding Q and reverberation time T are obtained directly from figures 53 and 54, $Q^* = 50$; $T^* = 0.56$ sec.

If we in addition to the maximum requirements on σ_a had, for example, the restriction $Q < 25$, then we must have a hole parameter equal to 0.25 (figure 53) and an additional resistance in the hole equal to $\Theta_e \varrho c = (3.5-1)\ 2R_w \simeq 0.085$ (figure 51). The optimum radius is then increased to $a^* = 10.5$ cm (figure 52). If we, however, instead of 10.5 cm, choose $a = 8.4$ cm, then $a/a^* = 0.8$ and $\sigma_a = 0.65\ \sigma_a^* \simeq 8.6\ \pi a^2$ and $Q = 0.83 \cdot Q^* = 20.7$ (figure 55).

Turbulence criterion.

The turbulence criterion described in (I. §3) can now be used to determine the pressure $(P_o)_c$ of the primary wave at which turbulence starts in a resonator in free field.

If we assume the resonator to have optimum dimensions in the sense described above, the total resistance is $\Theta = 4R_w(1 + \alpha t/r_o)$. The "displacement" and "velocity" criteria described (I.22) lead then to the following value of the critical pressure $(P_o)_c$.

$$(P_o)_{cd} = 4R_w\ \omega t \qquad \text{(II.46)}$$

and

$$(P_o)_{cv} = 4R_w(1 + 0.5\ t/r_o)\ U_c \qquad (II.47)$$

respectively.

With the numerical value of the surface resistance R_w used in (II.21a), and with $U_c \simeq 0.06\ \omega$ (see(I.22)), we obtain the critical sound pressure levels

$$20 \log \left[(P_o)_{cd}/P_{ref}\right] \simeq 43 + 20 \log(\nu_o^{3/2}\ t)\ \text{db}\ (t < 0.06) \qquad (II.46a)$$

$$20 \log \left[(P_o)_{cv}/P_{ref}\right] \simeq 43 + 20 \log(1 + 0.5\ t/r_o) + 20 \log(0.06\ \nu_o^{3/2})\ \text{db}\ (t > 0.06) \qquad (II.47a)$$

$$(P_{ref} = \sqrt{2}\ 0.0002\ \text{dynes/cm}^2)$$

In the case when the resonator is not designed for optimum conditions the radiation resistance may be negligible and the critical pressure levels are then 6 db lower than those given in (II.46a) and (II.47a).

As an example consider $\nu_o = 200$ and $t = 0.05$ cm. The criterion (II.46a) then gives a critical sound pressure level of 86 db. At 100 cps. the corresponding value is 77 db. In cases where the radiation resistance can be neglected these levels are reduced by 6 db.

It must be realized that the non-linearity in the resistance is noticeable at a considerably lower level, presumably 10 - 15 db lower than indicated by the turbulence criterion, because of the steady circulation effects which precede the turbulence, as was shown in (I.§3). The reactance, however, remains independent of level until turbulence is reached, where it starts decreasing.

The analysis of the cirtical levels above refer naturally to the resonance frequency of the resonator at which the hole impedance is simply $\Theta \rho c$. Since the Q is high, the non-linearity will presumably disappear at a frequency slightly outsice resonance. (It seems therefore possible that a double peak may occur in the curve representing σ_a as a function of frequency). However, it is the properties of the resonator at resonance which are of major interest, and an acoustic resonator must therefore in general be considered as a non-linear device even at "ordinary" sound levels.

§ 4. Measurement of resonance frequency and Q-value.

Some measurements were made on a spherical resonator to investigate especially the existence of an "optimum" design. For that purpose a resonator with $a = 9$ cm was used and the hole diameter was varied from 1.6 cm up to 4.9 cm. The wall thickness at the hole was $t = 0.1$ cm. The measurements were performed under free field conditions in the anechoic chamber

at the Acoustics Laboratory. The resonator was placed in an approximately plane wave and by measuring the pressure inside the cavity as a function of frequency keeping the primary pressure constant, the Q and the resonance frequency can be determined. The frequency could be measured by means of a stroboscope within a tenth of a cycle and the resonance frequency was determined with an accuracy better than 0.3 %.

In table 6 measured and calculated resonance frequencies are listed for resonators with six different hole diameters.

The measured frequencies are higher than those calculated from a uniform velocity distribution, as expected, but not so high as to favour the non-uniform distribution (II.15), the average deviation being +2 % and -5.8 % respectively. Although the non-uniform velocity distribution is theoretically the more correct, we see that the measured values are in better agreement with the uniform distribution. This may be explained by the effect of viscosity which prevents the velocity to rise to infinity at the edges of the hole, which is assumed in the non-uniform distribution. One can therefore expect, that the true distribution is going to lie somewhere between the two distributions discussed, which also is indicated by the experimental results, as seen in table 6.

Table 6.

Resonance frequencies of a spherical resonator. a = 9 cm, t = 0.1 cm.

Hole diameter d - cm	Measured resonance frequency ν_o	Calculated resonance frequency. Uniform distribution ν_o	deviation %	Non-uniform distribution see(IL15) ν_o	deviation %
1.6	120	117	-2.5	123	+2.5
2.05	135	134	-0.75	142	+5.2
3.1	168	168	0	180	+7.8
3.7	190	185.5	-2.27	202	+6.3
3.82	195	189	-3	206	+5.65
4.9	224	216	-3.57	242	+7.4

The presence of an "optimum" design of a resonator is apparent from figure 56 where the measured Q-values are plotted as a function of hole diameter. The calculated curve, shown in the same figure, is obtained from (II.35a) in which $R_w = 2R_s$ has been used when calculating Q^*. That means, in order to obtain a fair agreement with measurements, we have to use about twice the classical surface resistance in the expression for the resistance end correction. However, this point, which was discussed in (I. §2), is of minor interest to us now. The major thing is to see that there exists an optimum value for the hole diameter, at which Q is a maximum.

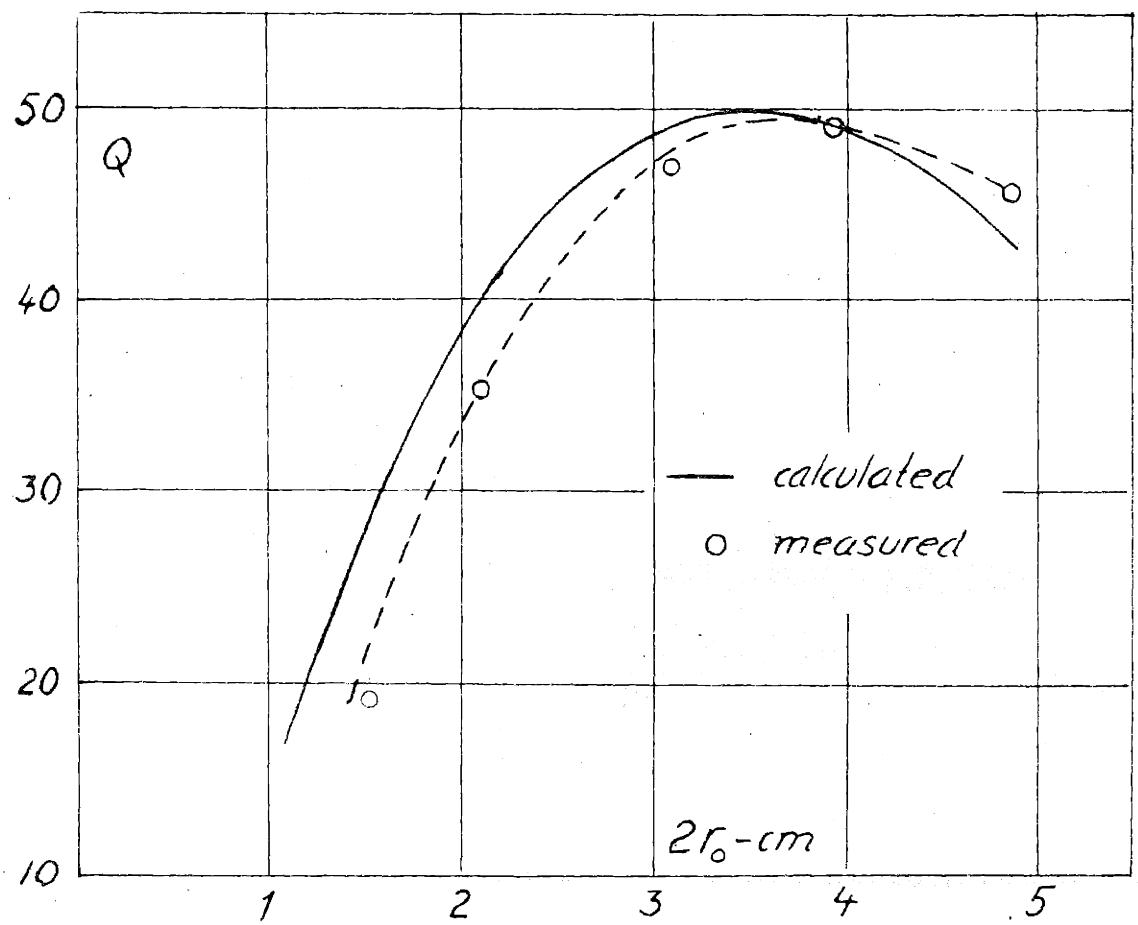

Figure 56

5. Pressure distribution around a spherical resonator.

The total pressure around the resonator can be considered made up of the primary plane wave p_p, the scattered wave from the hole p_{s1} and the scattered wave p_{s2} from the rigid spherical shell with the hole blocked.

$$p_p = P_o e^{ikr\cos\vartheta} \tag{II.48}$$

$$p_s = p_{s1} + p_{s2} = \sum_{m=o} (A_{1m} + A_{2m}) P_m(\cos\vartheta) h_m(kr) \tag{II.49}$$

A_{1m} and A_{2m} are expressed in (II.25) and in the low frequency limit they become

$$A_{1m} = \frac{cU_o}{2}\left[P_{m-1}(\cos\vartheta_o) - P_{m+1}\cos\vartheta_o)\right](-1)^m \frac{(ka)^{m+2}}{1\cdot 3\cdot 5(2m-1)(m+1)} (m>0)$$

(II.50)

$$A_{10} = (1-\cos\vartheta_o)(ka)^2 \frac{\rho cU}{2}$$

$$A_{2m} = P_o \frac{m(ka)^{2m+1}}{1^2\ 3^2\ 5^2(2m-1)^2\ (m+1)}\ i^{m+1} \quad (m>0) \tag{II.51}$$

$$A_{20} = -P_o i(k_o a)^3/3$$

Using (II.10) for the average "blocked" pressure, the velocity U is, according to (II.7)

$$U = -\frac{P_o}{\rho c \zeta}\left[1 - i\,\frac{3}{4}(ka)(1+\cos\vartheta_o)\right] \tag{II.52}$$

The predominant part of the scattered pressure is p_{s1}, which

can be written, using (II.49,50,52)

$$p_{s1} = - P_o \frac{1 - \frac{3}{4} i\, ka(1+\cos\vartheta_o)}{2} F(\vartheta, r)$$

where $F(\vartheta, r) = \frac{2}{\varsigma cU} \sum A_{1m} P_m(\cos\vartheta)\, h_m(kr)$

The phase angle of $F(\vartheta, r)$ is almost $-\pi/2$ in the vicinity of the hole. Roughly speaking, the scattered pressure can therefore be said to be in phase with the primary wave when $\nu < \nu_o$ ($\zeta \sim i\chi$), 90° out of phase when $\nu = \nu_o$ ($\zeta \sim \theta$), and 180° out of phase when $\nu > \nu_o$ ($\zeta \sim -i\chi$). The destructive interference with thus occurs at frequencies above resonance gives rise to rather interesting pressure distribution, with "node circles" appearing in the vicinity of the hole.

At resonance the scattered pressure p_{s1} may exceed P_o by more than 30 db near the hole. Although p_{s2} is then much smaller than p_{s1} it may not be neglected, because p_{s1} and p_p almost cancel each other under certain conditions.

The pressure distribution was measured and calculated for a resonator with radius $a = 9$ cm, hole diameter $2r_o = 3.82$ cm, wall thickness $t = 0.1$ cm and a resonance frequency 195 cps. (see table 6). The impedance ζ is then

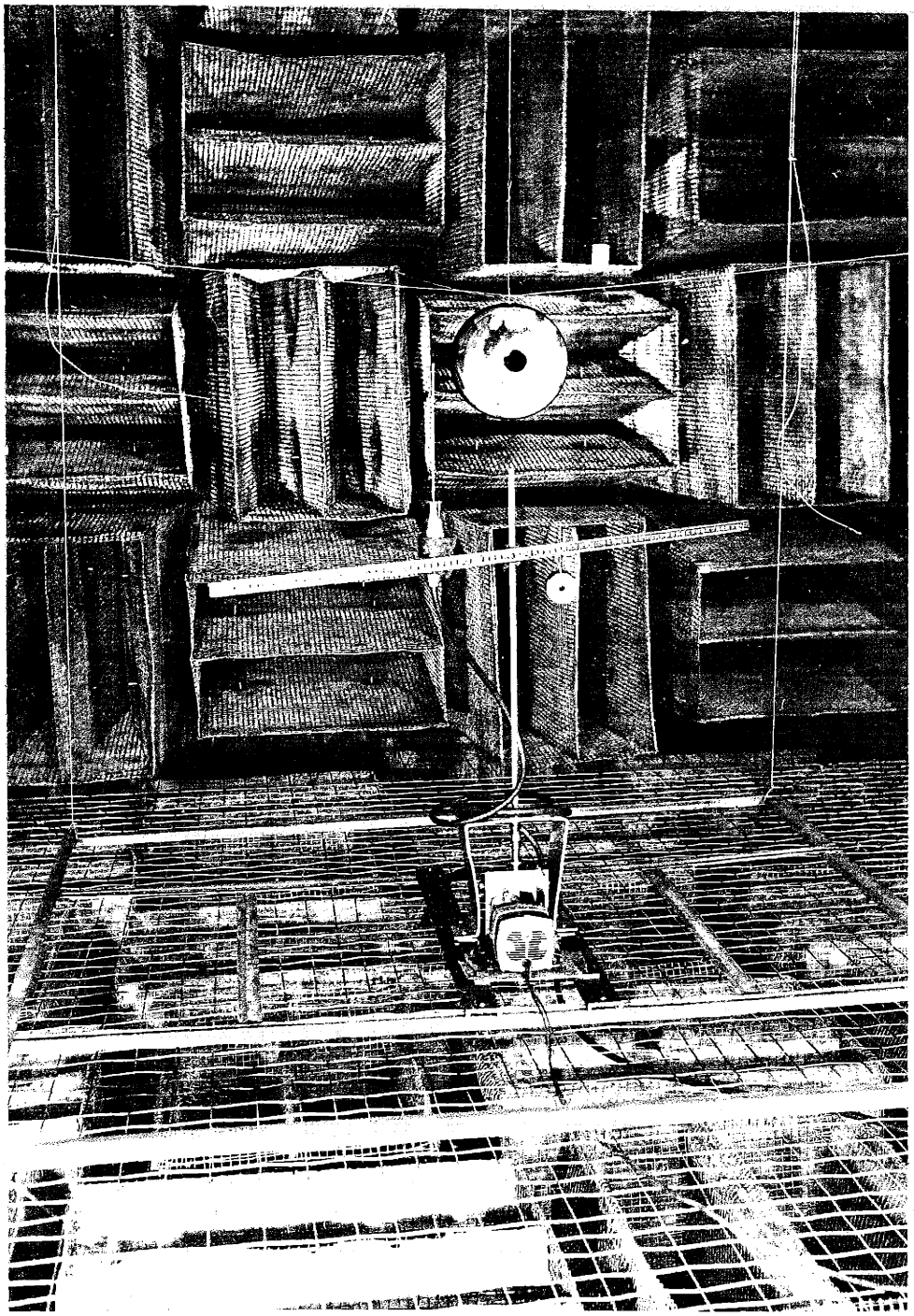

Figure 57

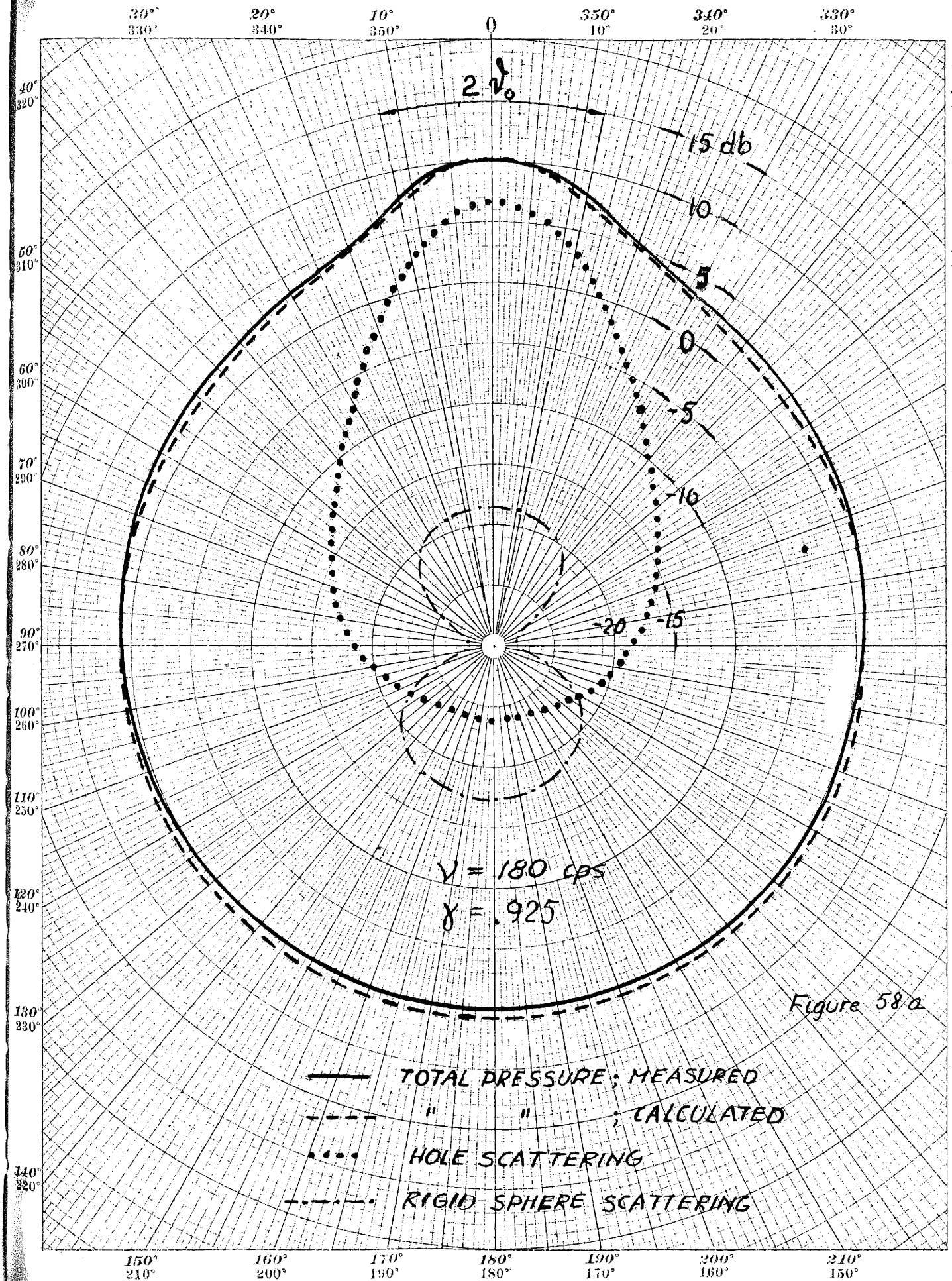
2 r₀
15 db
10
5
0
-5
-10
-15
-20
ν = 180 cps
γ = .925
TOTAL PRESSURE; MEASURED
" " ; CALCULATED
HOLE SCATTERING
RIGID SPHERE SCATTERING

Figure 58a

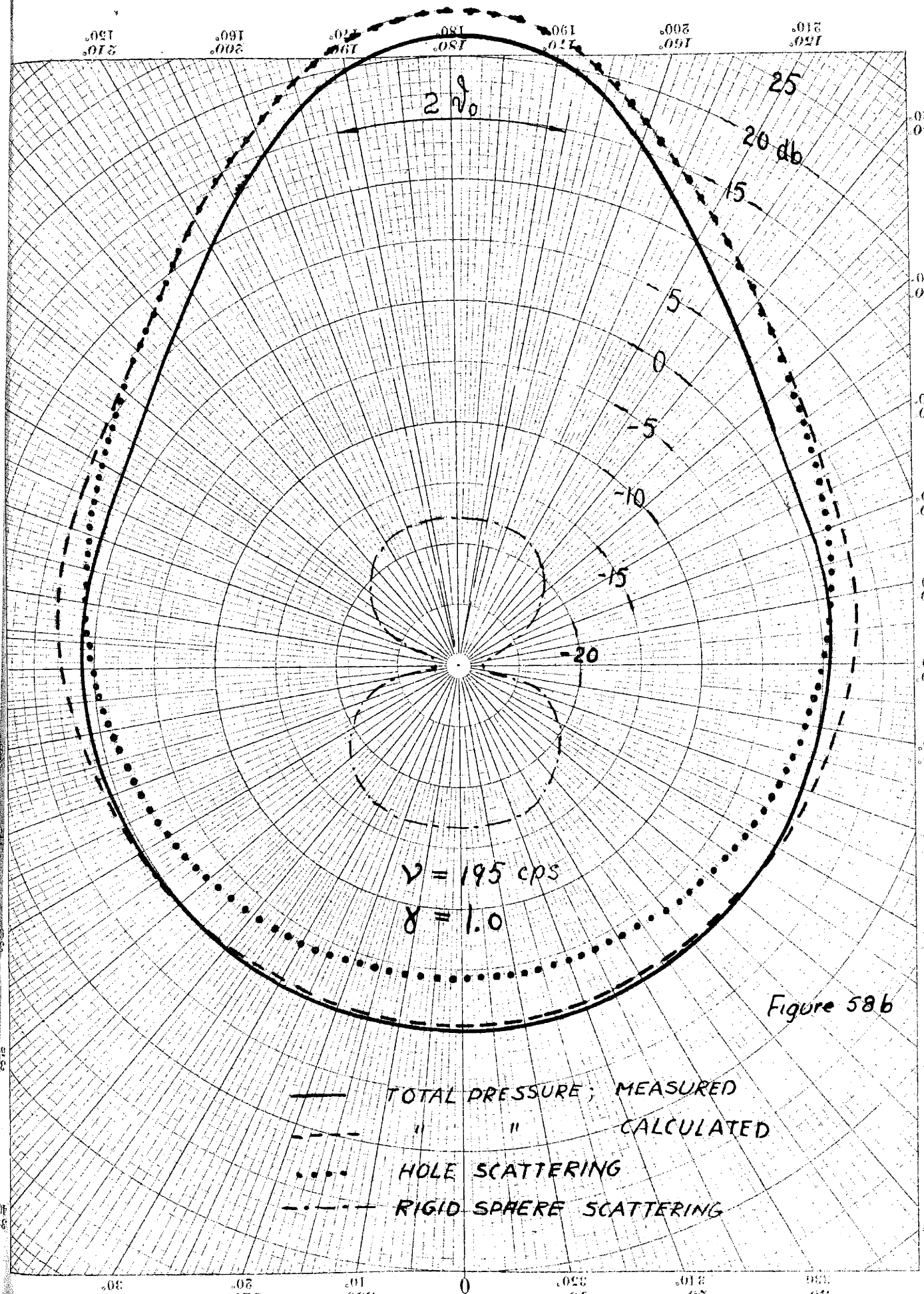

Figure 58b

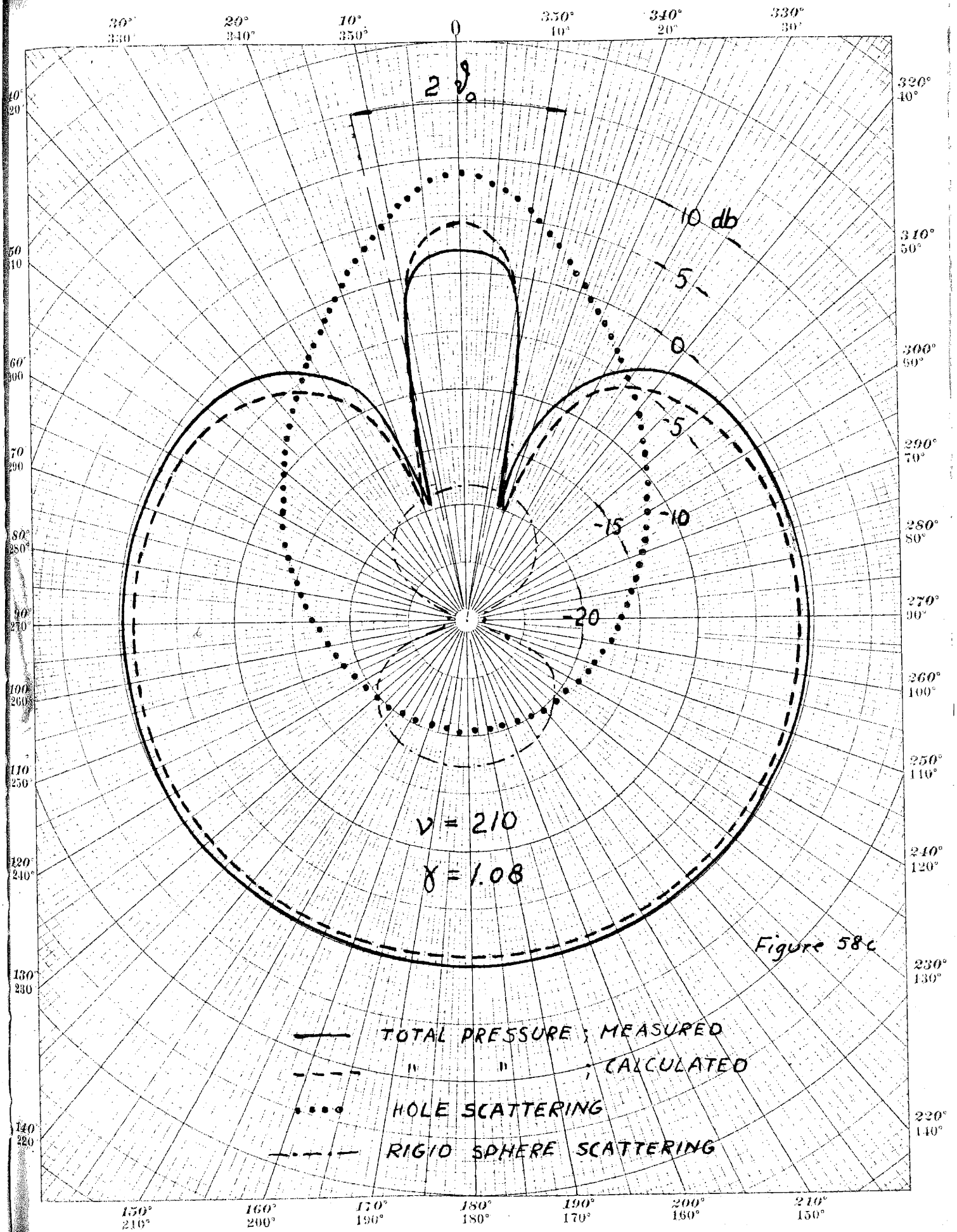
2 ϑ₀
10 db
5
0
-5
-10
-15
-20
ν = 210
γ = 1.08
TOTAL PRESSURE ; MEASURED
" " ; CALCULATED
HOLE SCATTERING
RIGID SPHERE SCATTERING

Figure 58c

$$\rho c \zeta = 22.9\ 10^{-4}\left[(11.1\ \gamma^{1/2} + 11.8\ \gamma^{2})/22\ 9 - i\ 48(\gamma - 1/\gamma)\right]$$

in which the resistance was obtained from (II.21a), (II.27) and the mass end correction corresponds to the uniform velocity distribution.

Calculations were made only for three frequencies and an example of the results is shown together with the corresponding measured pressure distribution in figure 58. The agreement is evidently satisfactory. For the sake of comparison the magnitude of the different pressure components is also shown in figure 58.

The measurements were made under free field conditions in the anechoic chamber at the Acoustics Laboratory. The resonator was placed in an approximately plane wave and the pressure was measured with a probe tube as illustrated in figure 57, and recorded continously as a function of angle. A mapping of the field up to a distance of one sphere radius from the surface was thus obtained.

§ 6. Notes on the propagation of sound through arrays of resonators.

The single layer sound screen.

We have seen in §2 that a single resonator in free field has a maximum absorption cross section approximately equal to $\lambda^2/4\pi$. The following question now suggests itself:

if a screen of a single layer of resonators is put up in an array with a cell area equal to $\lambda^2/4\pi$, do we then get 100 % absorption and no transmission through the screen ? To answer that question we consider a plane wave of normal incidence on the screen. Due to symmetry this is analogous to the case of a resonator in a square tube with cross section equal to $\lambda^2/4\pi$. The characteristic acoustic impedance of the tube is $Z_o = \rho c/A_1$ and $R_i = \rho c \Theta_i/A_o$ is the acoustic resistance of the resonator. (A_1 = area of the tube, A_o = = area of the hole of the resonator.) The equivalent circuit for the arrangement is then a line of characteristic impedance Z_o, terminated by the resonator impedance in parallel with Z_o. The inductance corresponding to the constriction between the tube and the resonator, is generally small and may be neglected in the following calculations. (This inductance can be determined in the case of a rectangular cavity cross section from an analysis similar to that carried through in chapter I for the square aperture in a square tube.)

If we put $x = R_i/Z_o$ the power absorbed by the resonator is

$$W_a = 4 \frac{x}{(1+2x)^2} I_o A_1 \qquad \text{(II.53)}$$

And the power transmitted is

$$W_t = 4 \frac{x^2}{(1+2x)^2} I_o A_1 \qquad \text{(II.54)}$$

where I_o is the intensity ofthe incoming primary wave. To compare this case with the single resonator in free field we determine the conditions under which the resonator absorbes a maximum amount of energy. According to equation (II.53) this occurs when $x = 1/2$, and the maximum absorbed energy is $I_o A_1/2$, corresponding to an absorption cross section $A_1/2$. The transmitted part is then $I_o A_1/4$, and the remaining $I_o A_1/4$ is reflected. Since under optimum conditions $R_i = \rho c/2A_1$, we see that absorption cross section of the resonator is the same as for the single resonator in free field, namely $A_2/4\pi_i$. The analogy is complete also with respect to scattered power since we can consider an amount $A_2/4\pi_i$ scattered forwards and an equal amount backwards, so that the total scattered power equals the absorbed.

Since the transmitted power is $I_o A_1/4$ we get only a transmission loss of 6 db under three conditions.

A higher transmission loss can obviously be obtained by making R_i/Z_o smaller than 1/2, which can be cone by moving the resonators closer together. But the absorption per resonator is the highest possible when the conditions above are fulfilled although the transmission loss is not a maximum.

The same reasoning holds naturally for a resonator placed in

the side wall of a tube.

Note on the propagation of sound in a lattice of resonators. From the expression (II.26) for the resonance frequency of the spherical resonator it follows that the value of $k_o a$ hardly can exceed about 0.4. In order to get a first indication about the propagation of sound in a lattice, we can therefore use a low frequency approximation, in which we assume that the dimensions of the resonator are small compared to a wave length. For a plane wave of sound, propagating in a direction normal to a plane of the lattice, we get by a repitition of the equivalent circuit for the single layer of resonators a periodically loaded line, which represents the lattice in this simple one-dimensioned case. The analysis is greatly simplified if we make the assumption that the spacing between the resonators is small compared to the wave length, so that line element between the resonators is represented by a capacitance in parallel with the resonator impedance. In such a case we may say, that the medium has a compressibility obtained from the sum of the admittance of the resonator and this parallel capacitance. If we let the resonator volume be v and the cell volume in the lattice be V, the compressibility of the volume V can be written

(compressibility) =

$$= \frac{-i\omega V}{\rho c^2}\left\{1 - f \frac{1}{\gamma\left[1-iQ\gamma(1-1/\gamma^2)\right]}\right\} = \frac{-i\omega V}{\rho c^2} n^2 \quad \text{(II.55)}$$

$\gamma = (\omega/\omega_o)$; ω_o = resonance frequency of resonators.

Q = Q - value.

$f = v/V$ = percentage filling of the medium.

This compressibility corresponds to a propagation constant $k_1 = nk$, where n is the index of refraction, given by (II.55). The real and imaginary parts of n which determine the phase velocity and attenuation are:

$$n_1 = \mathrm{Re}(n) = \frac{\sqrt{1-f}}{\sqrt{2}} \left[\sqrt{1+\alpha} + (1-\beta)\right]^{1/2}$$

$$n_2 = \mathrm{Im}(n) = \frac{\sqrt{1-f}}{\sqrt{2}} \left[\sqrt{1+\alpha} - (1-\beta)\right]^{1/2}$$

where $$\alpha = \frac{Q^2 f_1}{1+Q^2(\gamma-1/\gamma)^2}\left[(2+f_1)\frac{1}{\gamma^2} - 2\right]$$

$$\beta = Q^2 \frac{(1-1/\gamma^2)}{1+Q^2(1-1/\gamma)^2} f_1; \quad \left(f_1 = \frac{f}{1-f}\right)$$

In the low frequency limit $\gamma \to 0$, n_1 goes to unity whereas at high frequencies it approaches $\sqrt{1-f}$. The attenuation constant n_2 goes in both these cases to zero. The absorption peak occurs at a slightly higher frequency than the resonance frequency, as shown in a special example in figure 59. In this case Q has been chosen equal to 20. The extreme values of the phase velocity are in this case about 0.56 c and 1.40 c, which are remarkably different from the free field velocity. The attenuation at the peak is very large, corresponding to an attenuation of about 40 db per wave length.

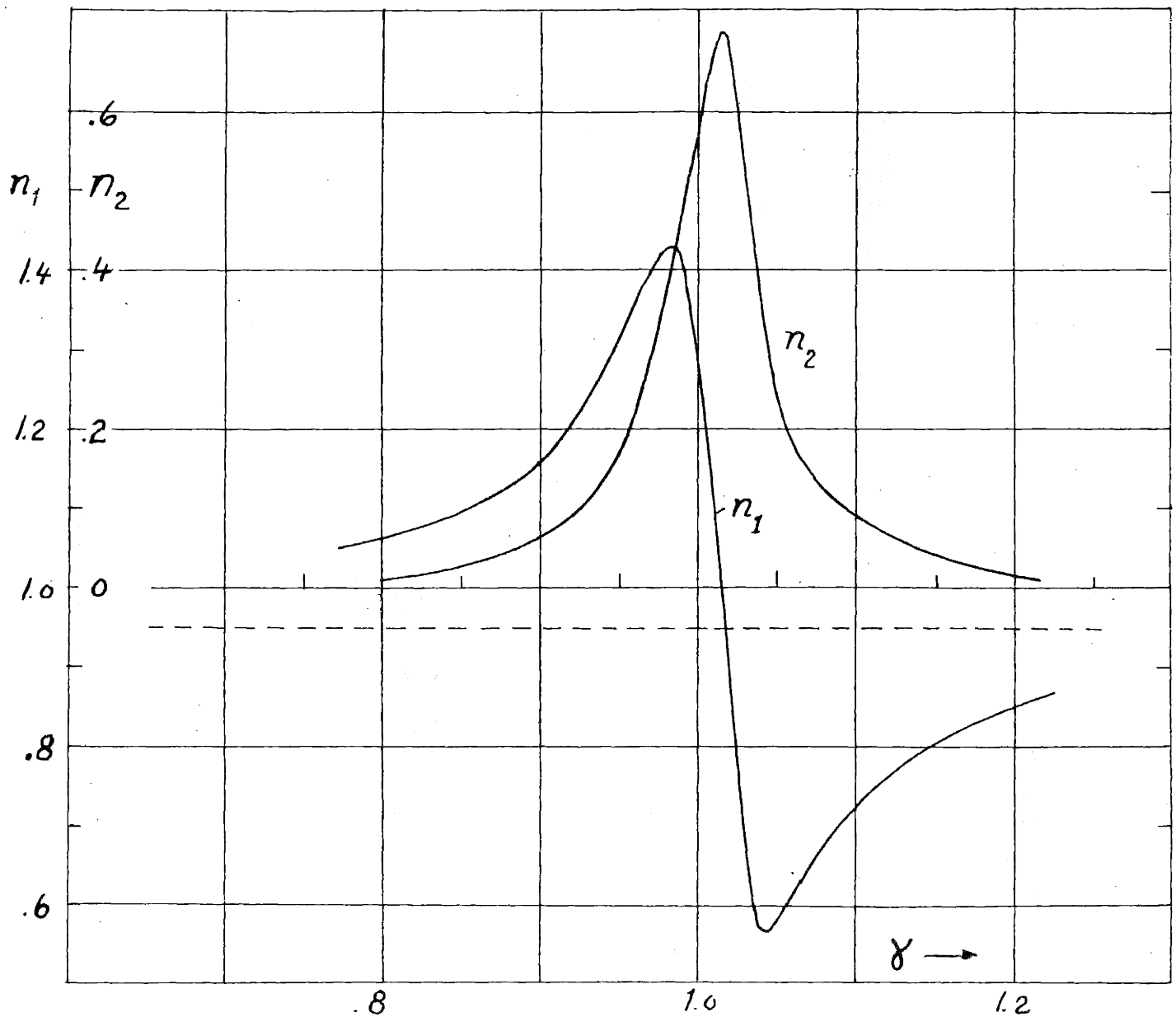

Figure 59

A thorough experimental study of the field inside a lattice of this kind is a problem of general interest in other branches of physics, dealing with periodic structures.

In such an experimental study resonators are preferably chosen as scattering centra, because their scattering and absorption cross section can be varied continously and with controllable amount by means of a flow resistance in the hole, as illustrated in the previous analysis. At low and medium frequencies single hole resonators could then be used, and perforated spheres or similar arrangements at higher frequencies.

III. Resonators in walls.

There are two cases concerning (Helmholtz) resonators in walls, that permit a simple analysis. The first corresponds to an arrangement where the resonators can be considered independent of each other, and the second case represents a uniformly covered wall of resonators, so close together as to render a practically uniform surface impedance. As an example of the first case we can consider a wall with resonators of different resonance frequencies which do not overlap considerably, and in the second case we have the perforated facing as a typical example.

Although these two extreme types of wall resonators have been studied in some detail [42] - [48], they still contain problems of some interest, which require further investigation. One of these concerns the angular dependence of the normal impedance and absorption coefficient of perforated facings. It is the main purpose of the present section to describe an experimental study of this problem.

A short discussion of the single wall resonator is also given applying the analysis made for the free field resonator in (II.§2). The optimum dimensions of a single wall resonator are determined and its usefulness as a sound absorber is dis-

cussed and compared with a resonator in an array.

§ 1. A single resonator in a wall.

The analysis of a single resonator in a wall is very closely related to that of the resonator in free field. The only differences are that the "blocked" pressure at the hole is now equal to $2P_o$ and independent of frequency and the radiation resistance of the hole is twice that of the resonator in free field. An analysis of the conditions for optimum design leads therefore to practically the same results as those already obtained in (II. 2); only minor numerical differences occur. In the list of optimum design values for the free field resonator in (II.32 - 45) we have also presented the corresponding results for the wall resonator. To distinguish the two cases the values valid for the wall resonator are written within paranthesis. These results follow from the original equations (II.29-31) if C in the denominator is replaced by $2C$ and the C in the numerator is left unchanged.

In the case when the frequency is kept constant and the resonator volume is varied we see that the following relations hold between the optimum values for the wall- and free field resonator

$$(\sigma_a^*)_w = 2(\sigma_a^*)_f; \quad Q_w^* = 1/\sqrt{2}\, Q_f^*; \quad T_w^* = (1/\sqrt{2})\, T_f^*; \quad a_w^* = (1/2)^{1/6} a_f^*$$

The "design charts" in figures 50-55 can therefore be used also for the wall resonator if the following changes are considered.

1) Replace the maximum absorption cross section $\sigma_a = (\lambda_o^2/4\pi)\, F$ by $\lambda_o^2/2\pi$.

2) Multiply T^* and Q^* by $1/\sqrt{2} = 0.707$.

3) Multiply a^* by $(1/2)^{1/6} \approx 0.893$.

4) When applying the curves in figure 55 the optimum values a^*, Q^* and T^* have to be replaced by the corrected ones.

Application to architectural acoustics.

A single resonator in a wall evidently contributes a relatively large absorption at resonance under optimum conditions. However, the Q-value is then necessarily high for the undampened resonator, which limits its usefulness as a sound absorber. To lower the Q-value an extra resistance has to be introduced in the hole, but in order to keep optimum absorption, the resonator volume has to be increased; this often leads to impractical dimensions.

Let us, as an example, consider a resonator for 100 cps. We assume $t/r_o = 1$ and start with no extra resistance in the hole, i.e. $\varepsilon = 1$. The hole parameter $\underline{h}$ is then 1.5 and from figure 52 we get the optimum equivalent sphere radius $a = 15 \cdot 0.893 \approx 13.4$ cm, which corresponds to maximum absorption cross section $\lambda^2/2\pi$. The corresponding Q-value obtained from figure 53 is $Q = 51$. Although this resonator has a

maximum peak absorption it has evidently no practical value as an absorber because of its high Q. A reduction of the Q-value to 10 requires a hole parameter $h = 0.06$ and hence an extra hole resistance $\Theta_e \varrho c = 1.4$ rayls ($\xi \approx 36$). In order to maintain maximum peak absorption we must increase a^* to 22.4 , that is, the volume must be taken about 4.7 times larger. If we decide not to change the volume, the new Q-value and absorption cross section are obtained from figure 55 where we have $a/a^* = 0.6$ and hence $\sigma_a = 0.19(\lambda_o^2/2\pi) \approx 0.35$ m^2 and $Q = 0.4 \cdot 10 = 4$.

This example shows that undampened resonators under optimum conditions have such a high Q that they can in general be considered of little value as sound absorbers, unless a very narrow frequency band is considered. If dampened properly, however, resonators can be useful as absorbers in cases where controllable amounts of low frequency absorption is required.

Since information about the flow resistance of screens and other material suitable for use in resonators evidently is of importance in the design, there is need for a simple way of measuring small resistances of this kind. Such a method employing a resonator as an acoustic Q-meter is discussed in an appendix.

If a single resonator in a wall has been found to offer an

absorption cross section σ_a, one may expect that resonators forming a uniform array with a cell area equal to σ_a should yield 100 % absorption for a plane wave of normal incidence. This is not the case, however. An absorption of 100 % is obtained only if the cell area is chosen to be the sum of the scattering and absorption area of the single resonator. In other words, the maximum absorption area for a resonator which is a member of an array is twice the maximum absorption area for the corresponding single wall resonator.

In practical applications of resonators it is therefore important to know whether an array can be considered as a uniform boundary or as a group of independent resonators. It seems to be preferable, that in cases where there is some doubt as to the classification of the system, the resonators should be treated as independent of each other, and designed according to the rules for the single resonator. The total absorption thus obtained is then going to be somewhat larger than estimated. This is a better situation, however, than the opposite one, obtained by treating the resonator array as an uniform boundary.

§ 2. Perforated facings.

If the spacing between the partitions behind a standard perforated facing is made small enough, we get a resonator array which practically can be considered as a uniform

boundary. In the following discussion throughout this section we assume that the normal specific impedance of the surface at resonance is matched to ρc. Such a matching can always be performed by a proper selection of an additional resistance $\Theta_e \rho c$ in the holes, so that $\Theta = \Theta_i + \Theta_e = A_o/A_1$ where A_o = hole area, A_1 = cell area and Θ_i the resistance of the facing itself.

The average normal impedance of the surface is then

$$\zeta = 1 - i(\gamma \cot k_o L - \cot \gamma k_o L) \qquad \text{(III.1)}$$

where $\gamma = \omega/\omega_o$

L = depth of the air space

The resonance frequency is obtained from

$$\frac{(t + \delta)}{(A_o/A_1)L} = \frac{\cot k_o L}{k_o L} \qquad \text{(III.2)}$$

where, strictly speaking, the end correction δ is that for a circular hole in a square tube, which was treated in (I.§1)

$$(t + \delta) = 1.7\, r_o\left(1 - 0.426\, \frac{r_o}{a} + 0.59\, t/r_o\right)$$

(a = distance between two holes in the facing, r_o = hole radius, t = wall thickness.)

If $k_o L \ll 1$ the resonators behave as lumped circuits with

a Q-value given simply by

$$Q = \frac{1}{k_o L} \qquad \text{(III.3)}$$

The largest possible value of $k_o L$ which can give a fundamental resonance is of course $\pi/2$ and the lowest possible Q is therefore $Q = 0.64$. Generally $k_o L$ is around 0.7 - 0.8 with corresponding Q-values 1.4 - 1.25.

The normal absorption coefficient is

$$\alpha = \left\{1 + \frac{1}{4}\left[\gamma \cot(k_o L) - \cot(\gamma k_o L)\right]^2\right\}^{-1} \qquad \text{(III.4)}$$

The statistical average of the absorption coefficient is obtained from well-known relations [49] as long as the normal impedance is independent of angle of incidence.

(Acoustic materials of the Celotex C4- type may be considered as perforated facings with close partitions. In most materials of that kind the matching is not complete, and can probably be considerably improved,)

If the partitions in the perforated facing array are removed, the normal impedance of the air layer behind the facing is going to be dependent on angle of incidence φ and equals then $\varrho c (\cos\varphi)^{-1} \cot(k_o L \cos\varphi)$, [48]. The impedance contribution from the perforated panel itself remains unchanged and the total normal surface impedance

is

$$\zeta' = 1 - i\left[\gamma \cot kL - \frac{\cot(k_o L \gamma \cos\varphi)}{\cos\varphi}\right] \qquad \text{(III.5)}$$

the reactance of which is plotted ina special case in figure 60.

From this expression we see that the perforated facing can be thought of as having a resonance frequency depending on the angle of incidence according to the relation

$$\nu_{res} = \nu_o/\cos\varphi$$

By resonance frequency we mean then the frequency at which the reactance of the normal impedance is zero. For frequencies higher than ν_o there is always an angle of incidence at which resonance occurs. The absorption coefficient at this particular angle reaches then a large value. The expression for α is

$$\alpha = \frac{4\cos}{(1+\cos\varphi)^2 + \chi^2\cos^2\varphi} = \qquad \text{(III.6)}$$

$$= \frac{4\cos}{(1+\cos\varphi)^2 + \left[\gamma\cos\varphi\cot(k_o L) - \cot(\gamma k_o L\cos\varphi)\right]^2}$$

and the behaviour of α as a function of φ is shown in a special case, $k_o L = 0.80$, in figure 72b, which clearly indicates how the high frequency absorption is emphasized.

The statistical average, $\alpha_{stat} = 8\theta \int_0^{\pi} \alpha(\varphi)\cos\varphi\sin\varphi d\varphi$ of

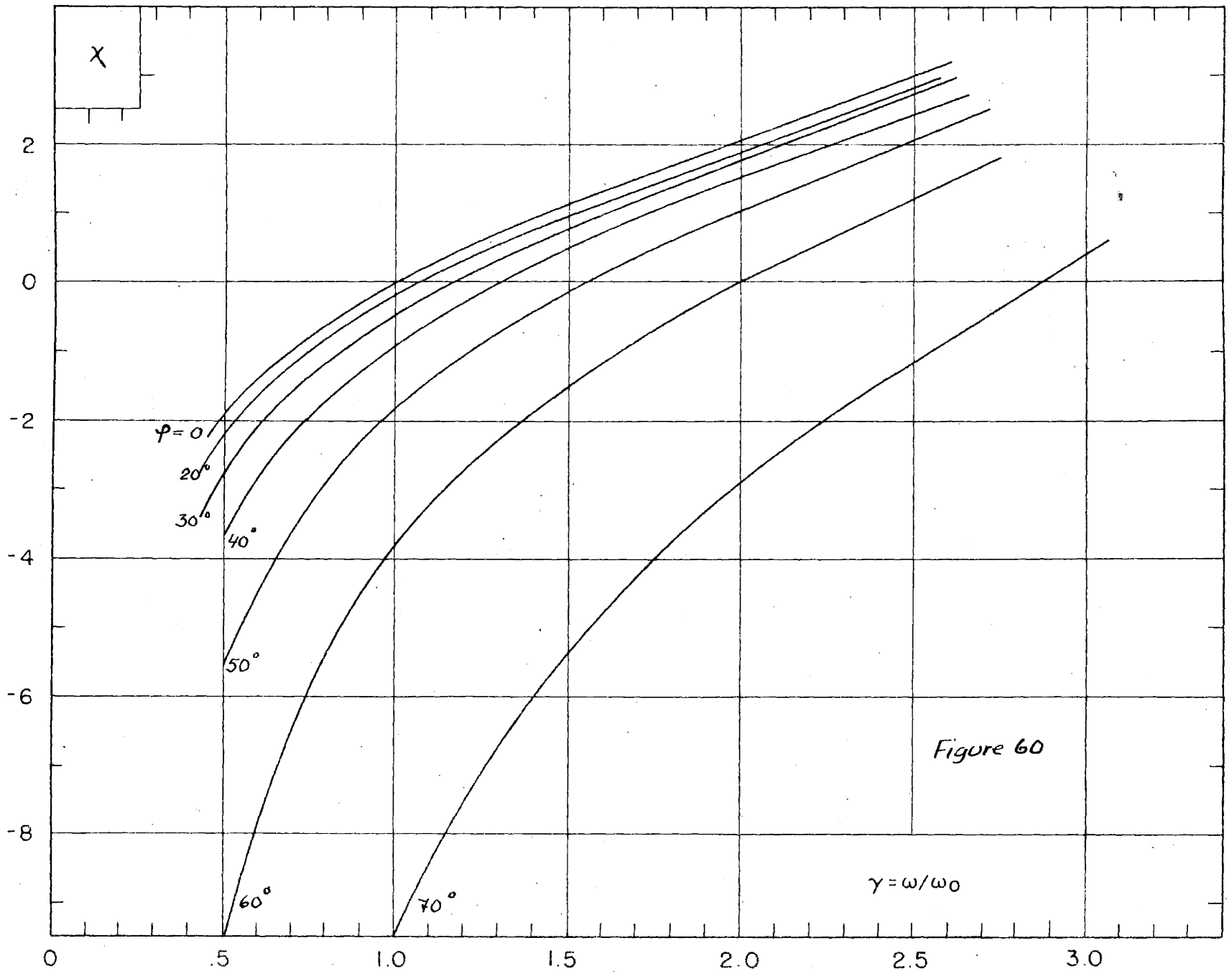

Figure 60

the absorption coefficient (III.6) had to be determined by numerical integration and the result in the special case concerned is shown in figure 73. The maximum value occurs at a frequency higher than ν_o as expected, in this case at $\nu \approx 1.3\,\nu_o$. This displacement of the maximum can be shown to be even more pronounced if the resistance increases with frequency rather than being constant and the curve is then going to be more asymmetrical with higher absorption on the high frequency side.

For comparison, the corresponding curves of $\alpha(\varphi)$ and α_{stat} for a perforated facing with partitions is shown in figures 77b and 73. Here the absorption curves for frequencies on both sides of the resonance frequency are about the same and the maximum value of the statistical average occurs approximately at $\nu = \nu_o$.

The peak value of α_{stat} for the facing with partitions in the case considered is about 92 % whereas for the facing without partition the corresponding value is only about 74 %.

In practical applications of perforated facings the partitions are never so close together as to secure an impedance which is independent of angle of incidence, and the statistical average of the absorption coefficient lies presumably somewhere between the two extreme cases discussed.

Other features of the two different types of perforated facings are discussed in more detail in § 3, where the expressions for the normal impedance and absorption as a function of angle of incidence are verified experimentally.

§ 3. Measurement of the normal impedance and the absorption coefficient of perforated facings for sound of oblique incidence.

The acoustic properties of perforated facings, mentioned in the previous paragraph, will now be studied experimentally, employing a new method of measuring the normal impedance and the absorption coefficient of a surface as a function of angle of incidence. This method may be applied for studies of other materials also and is described in some detail. A discussion of previously reported methods of measuring the angular dependance of the impedance is outside the scope of the present section. Some methods are discussed in [50] and [51] where also a number of references are given.

The surface pressure method.

The basic idea of the method described is to measure the magnitude and the phase of the pressure $p_2 = P_2 \exp(i\Psi_2)$ at the surface of the material under test in free field when the corresponding quantities of an incoming plane wave are known. We assume a surface large enough so that we can

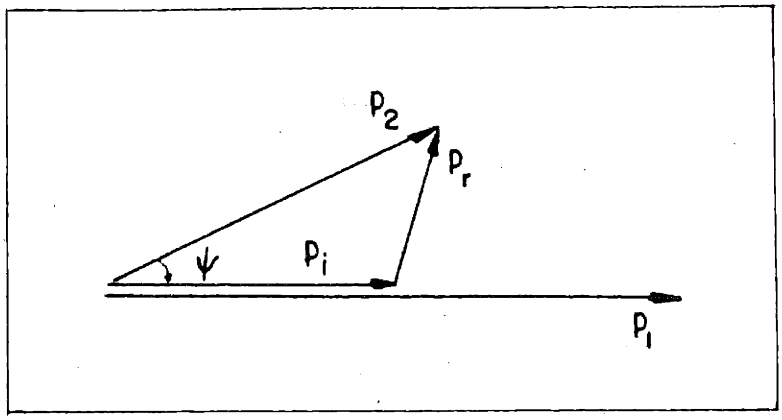

Figure 61

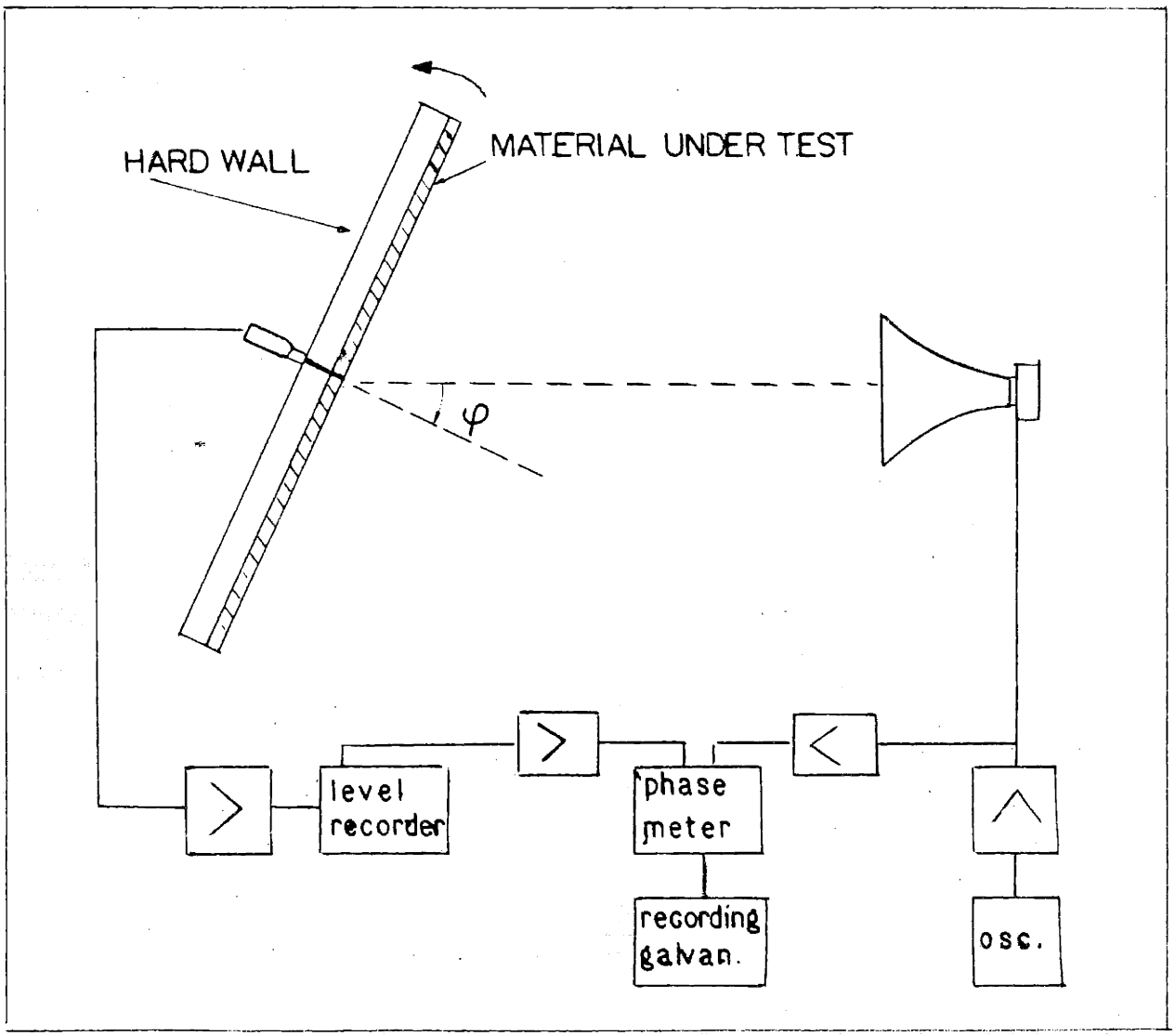

Figure 62

use the standard analysis of reflection at a plane boundary.

The pressure magnitude and phase of the primary wave at the surface, $p_i = P_i \exp(i\Psi_i)$ are determined indirectly by measuring the pressure magnitude and phase of the pressure $p_1 = (2p_i) = P_1 \exp(i\Psi_1)$ at a hard wall replacing the material. The pressure of the reflected wave at the wall, $p_r = P_r \exp(i\Psi_r)$ is then uniquely determined, and the absorption coefficient and the normal impedance can then be calculated. The relation between the quantities mentioned are visualized in figure 61.

The absorption coefficient $\alpha = 1 - (P_r/P_i)^2$ expressed in terms of the measured quantities P_1, P_2 and $\Psi = \Psi_1 - \Psi_2$ is

$$\alpha = \cos^2\Psi - 4 \left(\frac{P_1}{P_2} - \frac{1}{2}\cos\Psi \right)^2 \qquad \text{(III.7)}$$

which is plotted in figure 63 as a function of P_1/P_2 with Ψ as parameter.

The normal impedance $z = \varrho c \zeta$ of the wall, can be expressed in terms of $w = p_2/p_1 = (P_2/P_1)\exp(i\Psi)$, by employing the boundary conditions at the surface. If φ is the angle of incidence, we obtain $p_r/p_i = (\zeta\cos\varphi - 1)/(\zeta\cos\varphi + 1)$, which together with $p_2/p_1 = (1/2)(1 + p_r/p_i)$ yields

$$\zeta\cos\varphi = (\Theta - i\chi)\cos\varphi = \frac{w}{1-w} \qquad \text{(III.8)}$$

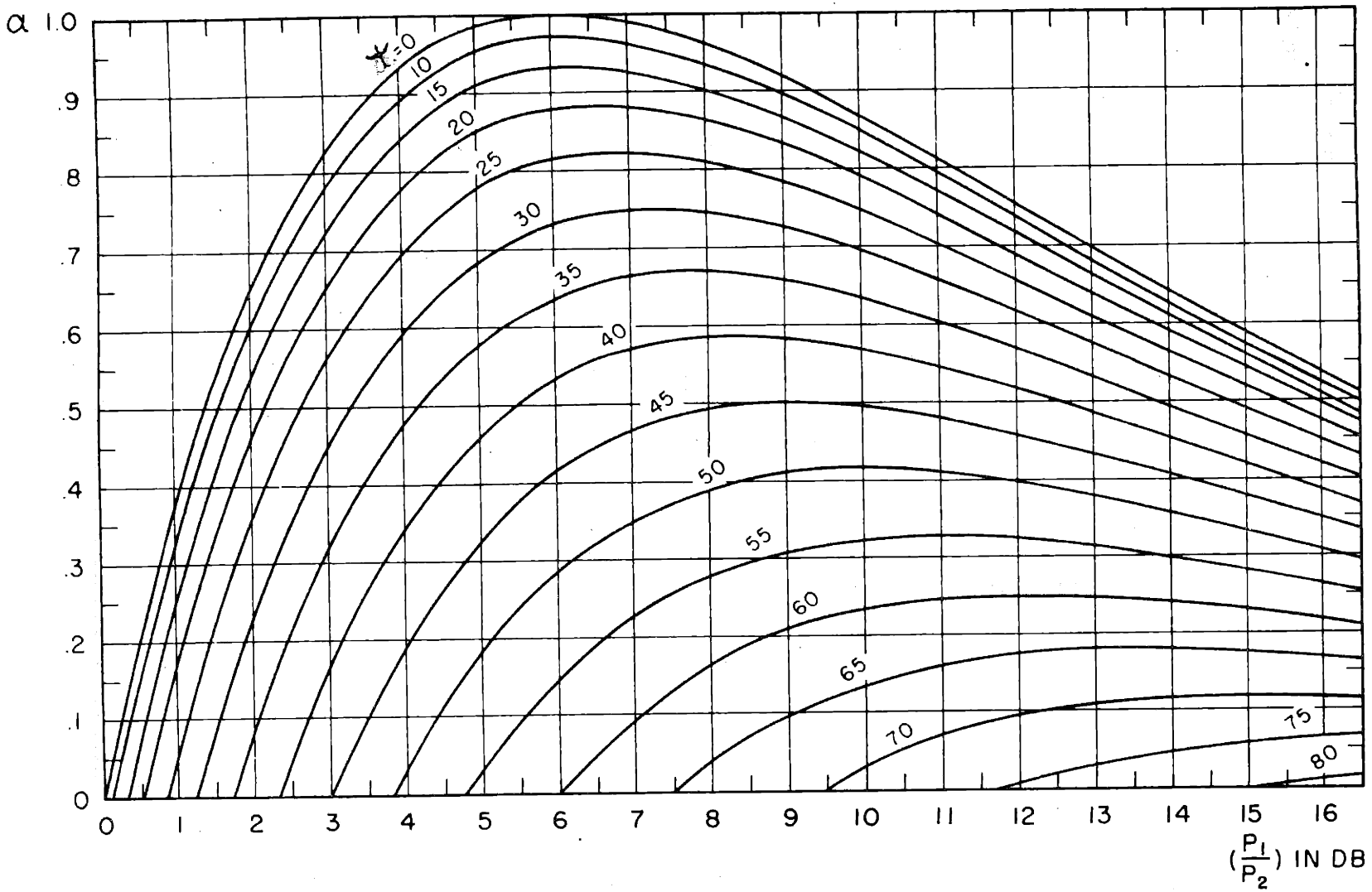
α 1.0
.9
.8
.7
.6
.5
.4
.3
.2
.1
0
0 1 2 3 4 5 6 7 8 9 10 11 12 13 14 15 16
(P1/P2) IN DB
ϕ=0
10
15
20
25
30
35
40
45
50
55
60
65
70
75
80

Figure 63

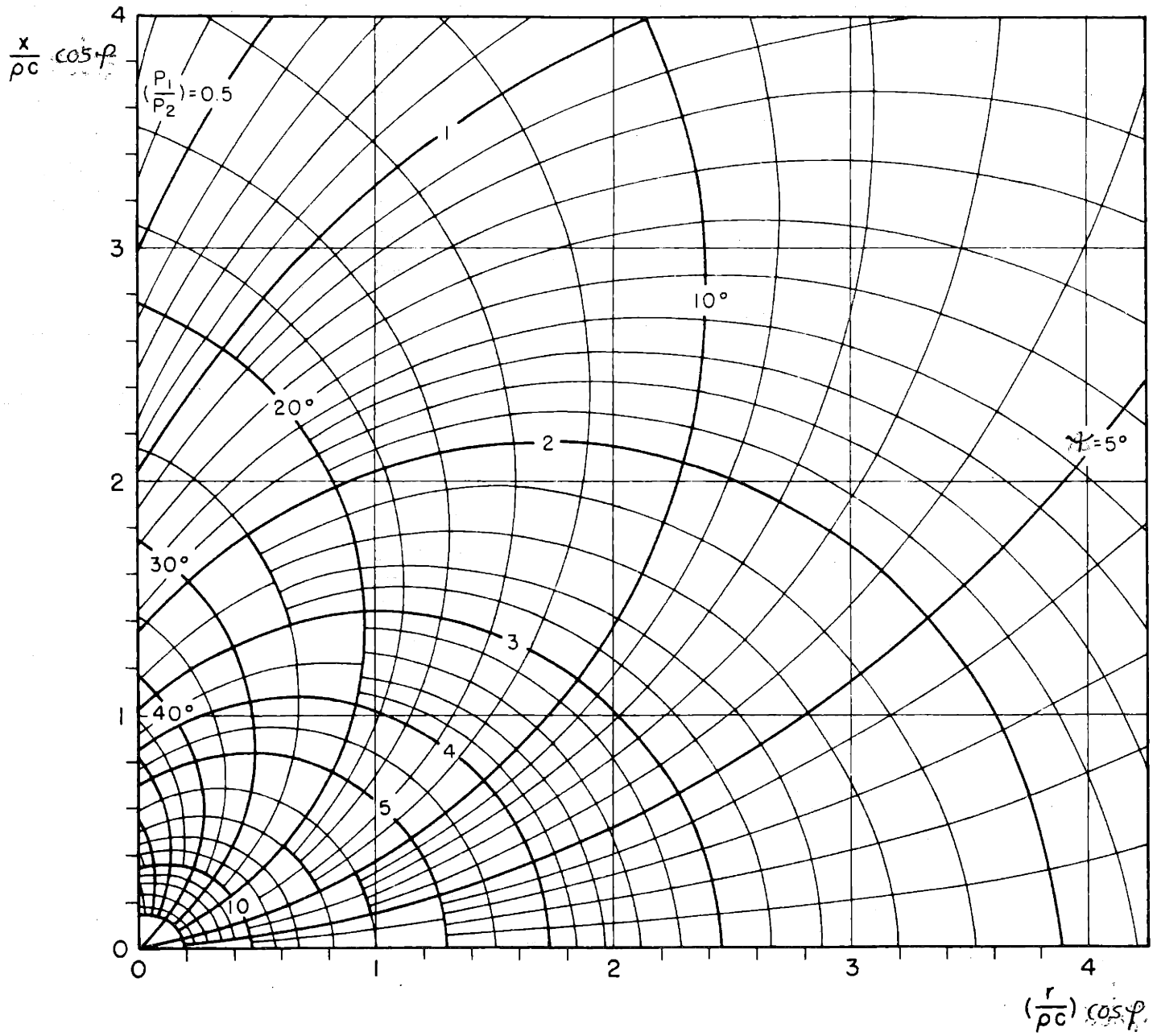
$\frac{x}{\rho c}\cos\varphi$
$(\frac{P_1}{P_2})=0.5$
1
2
3
4
5
10
10°
20°
30°
40°
$\psi=5°$
0
1
2
3
4
$(\frac{r}{\rho c})\cos\varphi$

Figure 64

This transformation from w to $\zeta\cos\varphi$ is represented by the two sets of circles

$$\left(\theta - \frac{1}{|w|^2 - 1}\right)^2 + \chi^2 = \left(\frac{|w|}{1 - |w|^2}\right)^2$$

$$\left(\chi + \frac{1}{2}\cot\Psi\right)^2 + \left(\theta + \frac{1}{2}\right)^2 = \left(\frac{1}{2\sin\Psi}\right)^2 \qquad \text{(III.9)}$$

The expression (III.2) can be simplified if expressed in terms of $w_1 = w^{-1}$ and $\eta = \zeta^{-1}$. We then get

$$\eta(\cos\varphi)^{-1} = (\kappa - i\sigma)(\cos\varphi)^{-1} = w_1 - 1$$

The sets of circles in (III.9) make up the impedance chart shown in figure 64, from which ζ is obtained as a function of the measured quantities P_1/P_2 (in db) and Ψ. Only the upper half, the first quadrant of the diagram, is given since the lower half, corresponding to negative χ, is symmetrical. When using the chart in its present form one has to remember that positive Ψ corresponds to positive χ, negative Ψ corresponds to negative χ.

Experimental arrangement.

The experimental arrangement is illustrated schematically in figure 62. The material under test is mounted on a panel, the back of which is used as the hard wall mentioned above. The panel is mounted in an anechoic chamber and rotated about a vertical axis (with a speed of about 1/2 revolution per minute) in the presence of a fixed horizontal beam of

approximately plane waves, obtained from a large horn placed about 15 feet from the panel. The pressure at the surface of the material is measured by means of a thin probe tube connected to a 640 AA condensor microphone as indicated in thefigure. The phase is determined relative the input voltage of the loudspeaker and is, like the pressure, recorded continuosly as a function of angle of incidence with the microphone first in the hard wall surface then in the soft wall surface. From the curves thus obtained P_2/P_1 in db and $\Psi = \Psi_1 - \Psi_2$ can be read off directly.

The electronic equipment used is shown in figure 65. For determining the phase a standard phase meter is used coupled together with a recording galvanometer. A special frequency meter may not be necessary in general but in the special application discussed below it is of great value.

A couple of details of practical interest may be worth mentioning. We have to realize that if the end of the probe tube does not lie on the axis of rotation of the panel, it is going to describe a circle when the panel rotates and the phase of the incoming wave at the probe tube is going to vary with the angle of incidence. However, the same variation for both sides of the panel is obtained by proper centration. Otherwise a phase correction has to be introduced.

The phase meter in use requires an input voltage on both

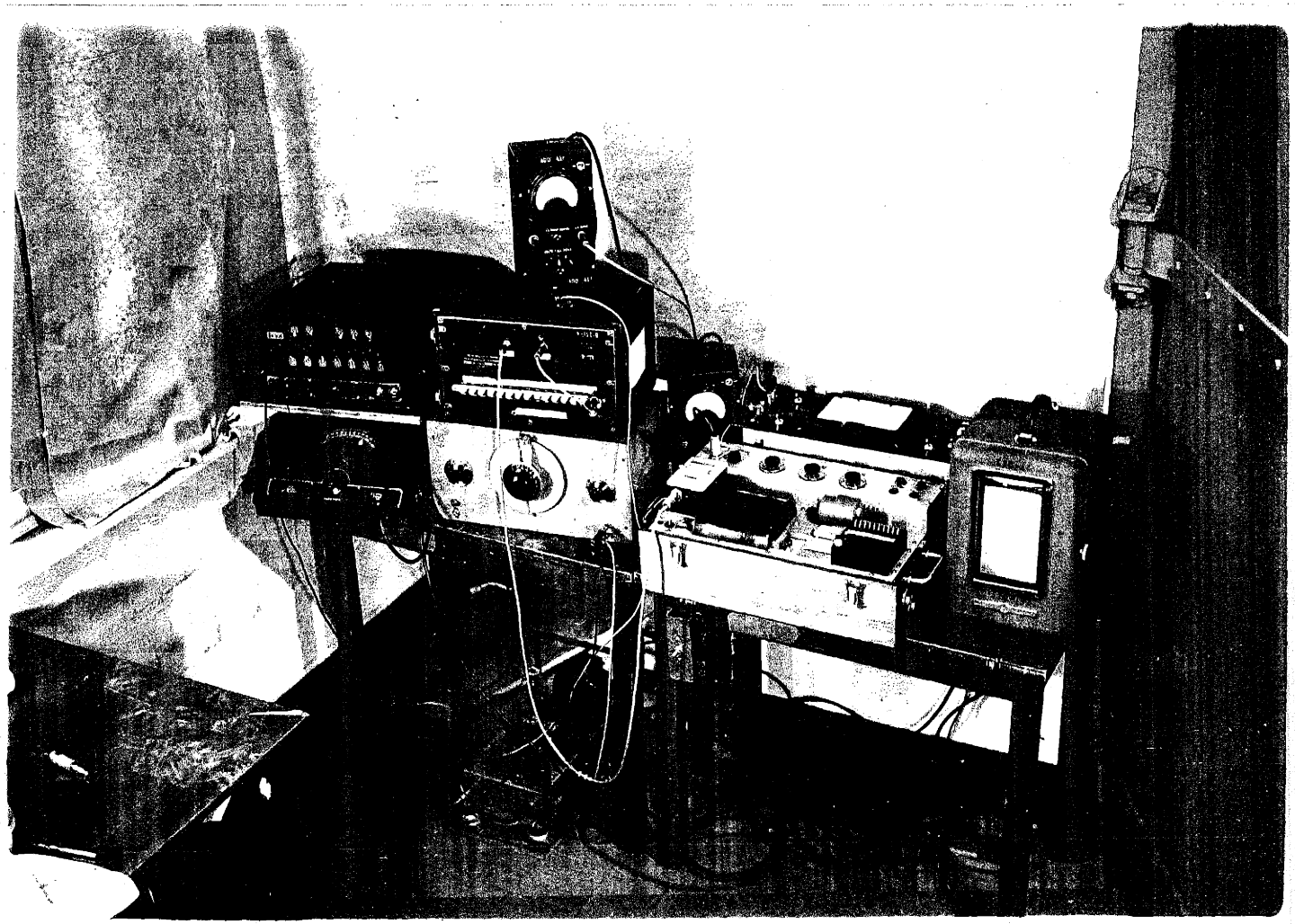

Figure 65

channels larger than 2 volts. In order to secure fulfillment of this requirement independent of the variations in the microphone voltage it is preferable to have this voltage regulated to a constant value before it is amplified and put on the phase meter. This is conveniently obtained by using the input voltage to the amplifier of the level-recorder, which voltage is regulated by the recorder potentiometer.

Measurements on perforated facings.

The perforated facing which is chosen for the experiments described here has the following dimensions: hole diameter $d = 0.42$ cm, thickness $t = 0.38$ cm and spacing between the holes $a = 1.22$ cm. The depth L of the air space between the panel and the hard backwall is chosen 6.5 cm.

We calculate first the resonance frequency of the system, which is the same as for a resonator with square cross section $a \times a$ and a circular hole with a diameter d. The mass end correction of the hole, obtained from (III.15) or figure 2 is $0.58 \sqrt{\pi r_o^2} = 1.03\, r_o = 0.216$. With $\ell_m = t + \delta = 0.596$ and the percentage open area $A_o/A_1 = 8.5\ \%$ introduced in equation (III.2) we get $k_o L = 0.84$ and hence the resonance frequency 687 cps. This is in good agreement with the measured resonance frequency obtained from tube measurements of the normal impedance. As seen in figure 70 the reactance is zero for $\nu = 700$ cps. The reactance curve fol-

lows well the calculated, as expected. However, the measured resistance 0.085 ρc at resonance, is larger than the viscous resistance calculated from (III.6), which gives a resistance at resonance equal to 0.048 ρc, and a maximum absorption coefficient of 19 %, instead of the measured 29 %. This can be understood from the fact that the holes in the perforated facing are not clean, many of them have fibers crossing the hole which increases the resistance.

In this mismatched condition the facing is not suitable for the intended free field experiments, since we require a system with high absorption. However, by adding a matching resistance the normal absorption at resonance can of course be brought up to 100 %. Theoretically the required additional resistance is $(A_o/A_1)\,\rho c$ minus the viscous resistance of the facing itself. It was found that "Indian head cloth" (manufacturer's name), put over the surface of the facing, gives an almost perfect matching as can be seen from the measured impedance curve, shown in figure 70. The cloth does not represent an absolutely pure resistance, however, but contains a small inductance, which lowers the resonance frequency down to 660. (The inductance is probably mainly caused by the vibrations of the cloth, but a small part comes from the additional constriction of the air flow when passing through the cloth).

The calculated impedance, obtained from equation (III.1)

in which we have put $k_oL = 0.80$, is also plotted in figure 70. The measured and calculated reactance agree perfectly as expected. The frequency dependence of the resistance cannot simply be assumed to be $\omega^{1/2}$, expected from pure surface boundary layer dissipation. The resistance is nearly constant in the frequency range considered here, 400 - 1500 cps, and in the expression for the impedance, $\zeta = \theta - i\left[\gamma\cot(k_oL) - \cot(\gamma k_oL)\right]$, we may use $\theta = 1$ as a good approximation.

Perforated facing without partitions.

It was shown in (III.§2) that the behaviour of a surface of resonators made up of perforated facings is strongly dependent on whether they are separated by partitions or not. We are now particularly interested in a facing without partitions. One reason is, that little is known about its behaviour and we want to check the results given in (III.§2) and particularly the angular dependence of the "resonance frequency", which is the most characteristic feature. Another reason, not less important, is that a surface without partitions simulating the idealized case of infinite extension assumed in the analysis, is relatively simple to make.

An arrangement made to represent the ideal case is shown in figure 66. The facing is mounted on an 8' x 8' wooden panel with horizontal stuts. The cloth matching resistance

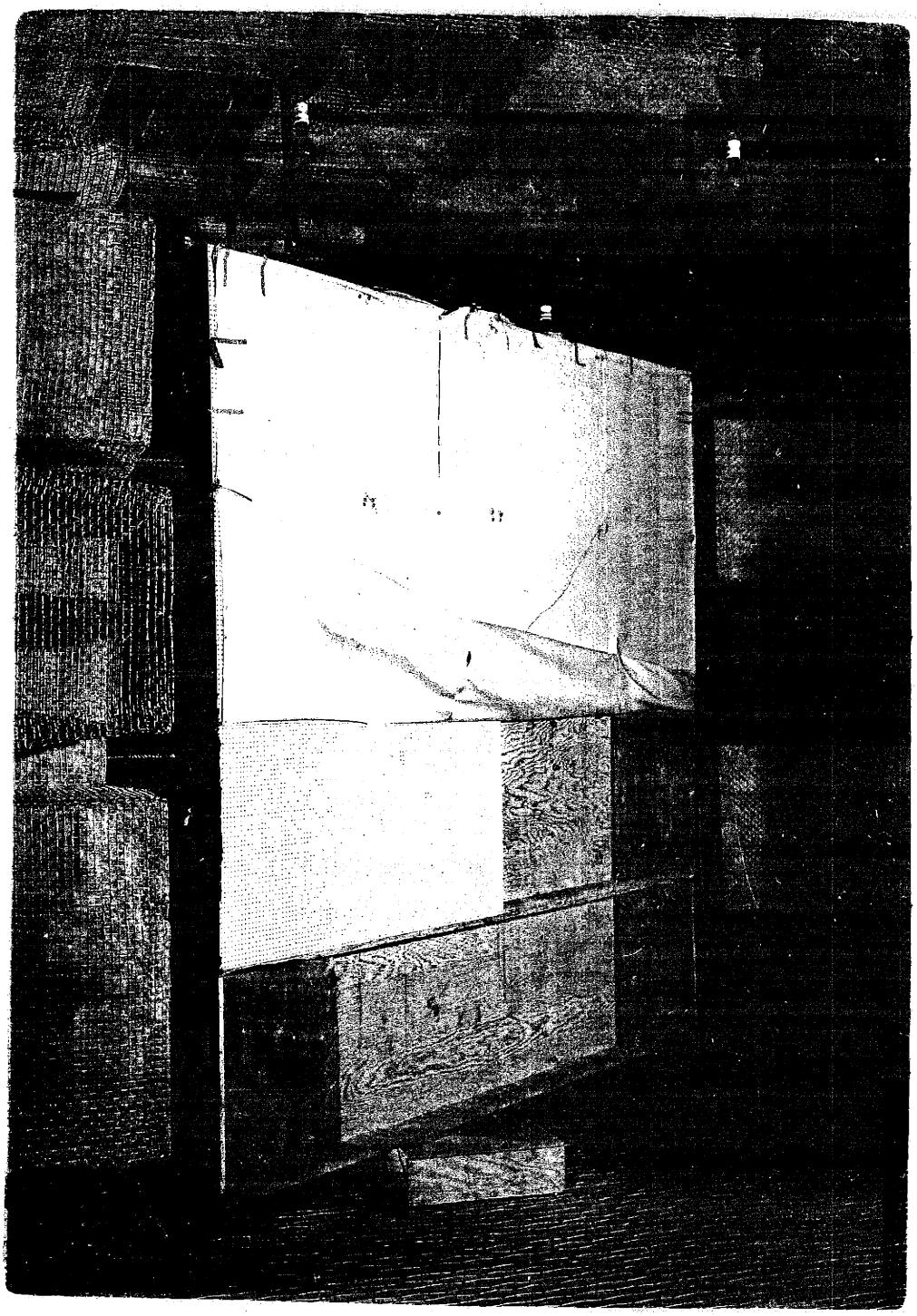

Figure 66

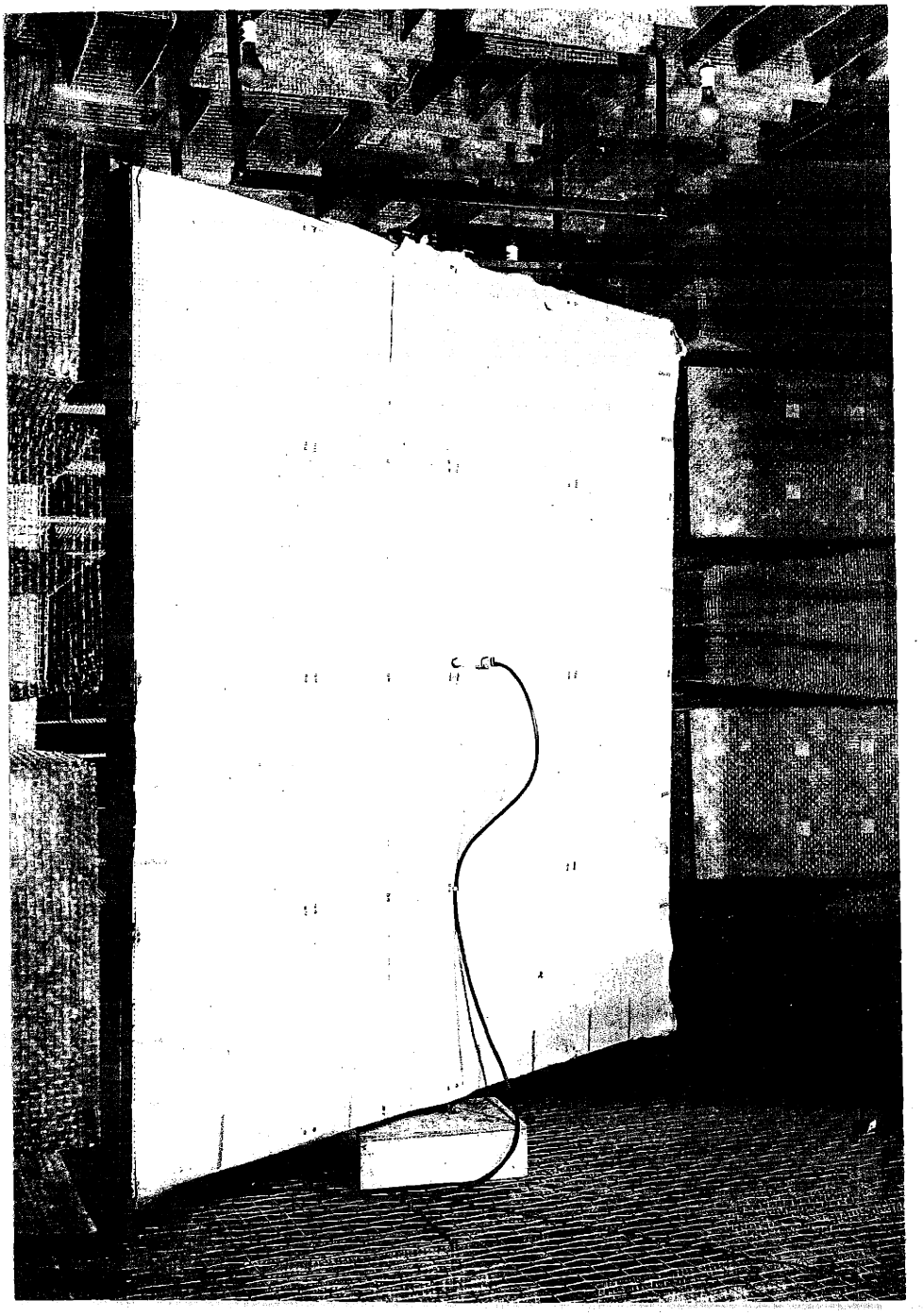

Figure 67

is put on the outside of and in contact with the perforated facing. In order to simulate the infinite extension, absorbing wedges (glass woll, 45 cm deep) were set up at the edges of the panel as can be seen in figure 66. (Wedges of this kind were expected to have an absorption coefficient of almost 100 % for frequencies higher than about 300 cps.) The openings between the back wall and the facing at the edges of the panel were blocked with wood plates, in the same time serving as supports for the absorbing wedges. All joints were carefully sealed with plasticin. The finished construction is shown in figure 67.

The "surface pressure method" is now used to determine the normal impedance and the absorption coefficient of the surface. We are then naturally limited to a certain angular range because of diffraction. Without having analyzed this problem theoretically one is left to find the magnitude of this range from the results of the measurements. At first sight one may think that the behaviour of the "hard" wall pressure should give information about the importance of the diffraction effect. This is not necessarily thus, however. To illustrate this we consider the pressure curves shown in figure 68. We see that the "hard wall pressure" p_1 stays constant up to a certain angle where it begins to drop. At 300 cps. this critical angle is about 60° and at 1000 cps. about 720, increasing slowly with frequency. A first guess is naturally that this effect is caused by diffraction and

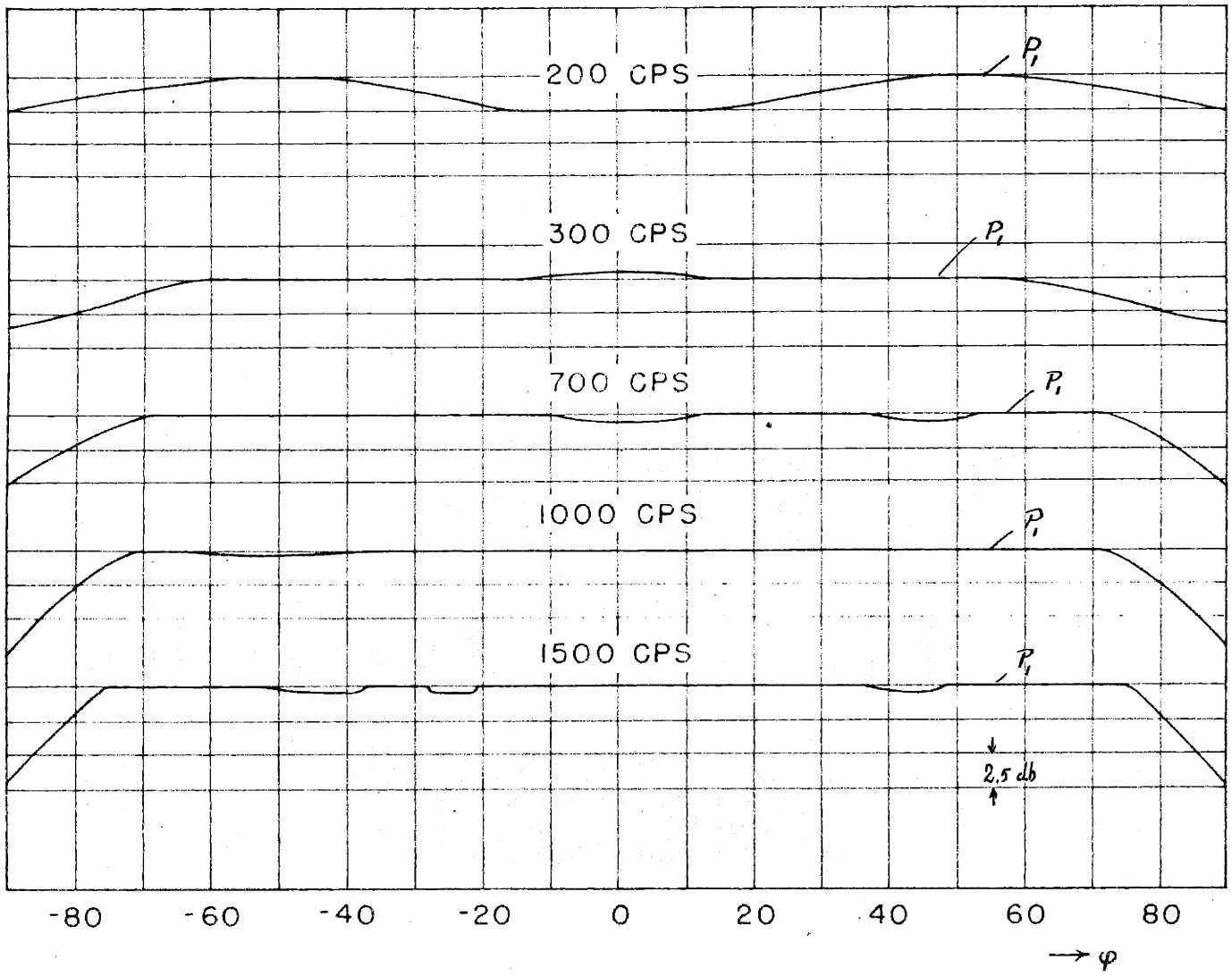
200 CPS
300 CPS
700 CPS
1000 CPS
1500 CPS
P_1
2,5 db
-80
-60
-40
-20
0
20
40
60
80
→ φ

Figure 68

that we from the critical angles thus found have our angular region defined. This may be partly true in some cases, but under the present conditions it seems to be incorrect, because the drop in the hard wall pressure is probably not caused by diffraction, but by the fact that the "hard" wall impedance is finite. It must namely be recognized that the pressure at the surface of a wall with an arbitrary finite normal impedance independent of angle of incidence approaches zero when the angle of incidence approaches 90 degrees. This follows directly from equation (III.8) which may be written $p_2/p_1 = \zeta\cos\varphi/(\zeta\cos\varphi + 1)$. Since we never can produce an infinite impedance, a pressure drop at the "hard" wall, of the same kind as that we have observed, must necessarily occur even if diffraction were not present. The critical angle φ_c at which the drop should start can easily be estimated. If we assume that the recording system can detect a change in pressure of y %, we obtain for the critical angle $\varphi_c = \pi/2 - 100(y\,|\zeta|)^{-1}$. If we as an example assume $|\zeta| = 200$ and $y = 2$ we get $\varphi_c \simeq 76^\circ$, a value of the same order of magnitude as that obtained in the present measurements.

(This suggests of course the possibility of reversing this relation to a method of measuring large wall impedances by determining φ_c. It seems also reasonable to assume that the idea of measuring surface pressure may be used to some extend in the study of vibrations of panels and especially

in detecting concidence effects and resonance, as will be shown below.)

In addition to the finite "hard" wall impedance there is another limitation in the present arrangement namely the poor absorption of the glass woll wedges at low frequencies. A systematic study of these limitations as a function of frequency and panel size is a comprehensive one and is not taken up here.

Results of pressure and phase measurements are shown in figure 71. The resonances discussed in (III.7) are clearly found to be present. The phase difference goes through zero at certain angles of incidence with a corresponding peak in the pressure difference P_1/P_2. The resonances should occur at angles given by $\cos \varphi_r = \nu_o/\nu_r$ and the validity of this relation is shown by the measured value of φ_r and ν_r listed in table 7, where $\nu_o = \nu_r \cos \varphi_r$ is calculated. The product $\nu_r \cos \varphi_r$ is constant within a variation of 3 % and is in good agreement with the normal resonance frequency $\nu_o = 660$ cps. determined from the tube measurements.

The absorption coefficient, obtained from equation (III.7) or from the chart in figure 63, are shown in figure 72 together with the calculated curves obtained from equation (III.6), in which the value of Θ found in the tube impe-

Table 7.

Experimental verification of $\cos \varphi_r = \nu_o / \nu_r$.
Perforated facin without partitions with normal resonance frequency $\nu_o = 660$ cps.

Measured oblique incidence resonance frequency ν_r	Corresponding angle of incidence φ_r	$\nu_o = \nu_r \cos \varphi_r$
1500	64	662
1200	56	655
1000	48	670
900	42	675
700	29	662

dance measurements has been used. This value of Θ differs very little from unity as seen in figure 70. There is evidently a good agreement between calculated and measured absorption coefficient except at frequencies near grazing where our method of measurement does not work any longer. When determining the statistical average of the absorption coefficient, plotted in figure 73, the extrapolated values, shown by the dashed lines in figure 72, has been used for angles near 90°.

The reactance obtained from the measurements, shown in figure 74, are generally in good agreement with the calculated

although there seems to be a tendency of obtaining too high reactance for $\varphi < \varphi_r$ and too low for $\varphi > \varphi_r$.

The resistance shows some fluctuations as seen in figure 75, which at least partly may be explained by the error in the measurements of the phase angle, on which θ depends strongly.

Perforated facings with partitions.

It is clear that in order to simulate the other extreme case which was discussed in (III. 2) we must have a wall with a large number of partitions well constructed in order to prevent any intercommunication between the resonator cells. To build such a wall is rather an elaborate task if it is supposed to simulate the ideal case over a large frequency range. Before going into any work of that kind a wall only with vertical and relatively few partitions was made as shown in figure 69. The spacing between the partitions is about 15 cm, which becomes half a wavelength at a frequency 1140 cps., and the facing cannot be expected to simulate the ideal case for frequencies much above this limit.

Some results of pressure and phase measurements are shown in figure 76. It is interesting to compare these curves with those obtained for perforated facings without partitions. In the first case the pressure ratio $P_1/P_2 \rightarrow \infty$ when $\varphi \rightarrow 90^\circ$, which is true for any material with a normal

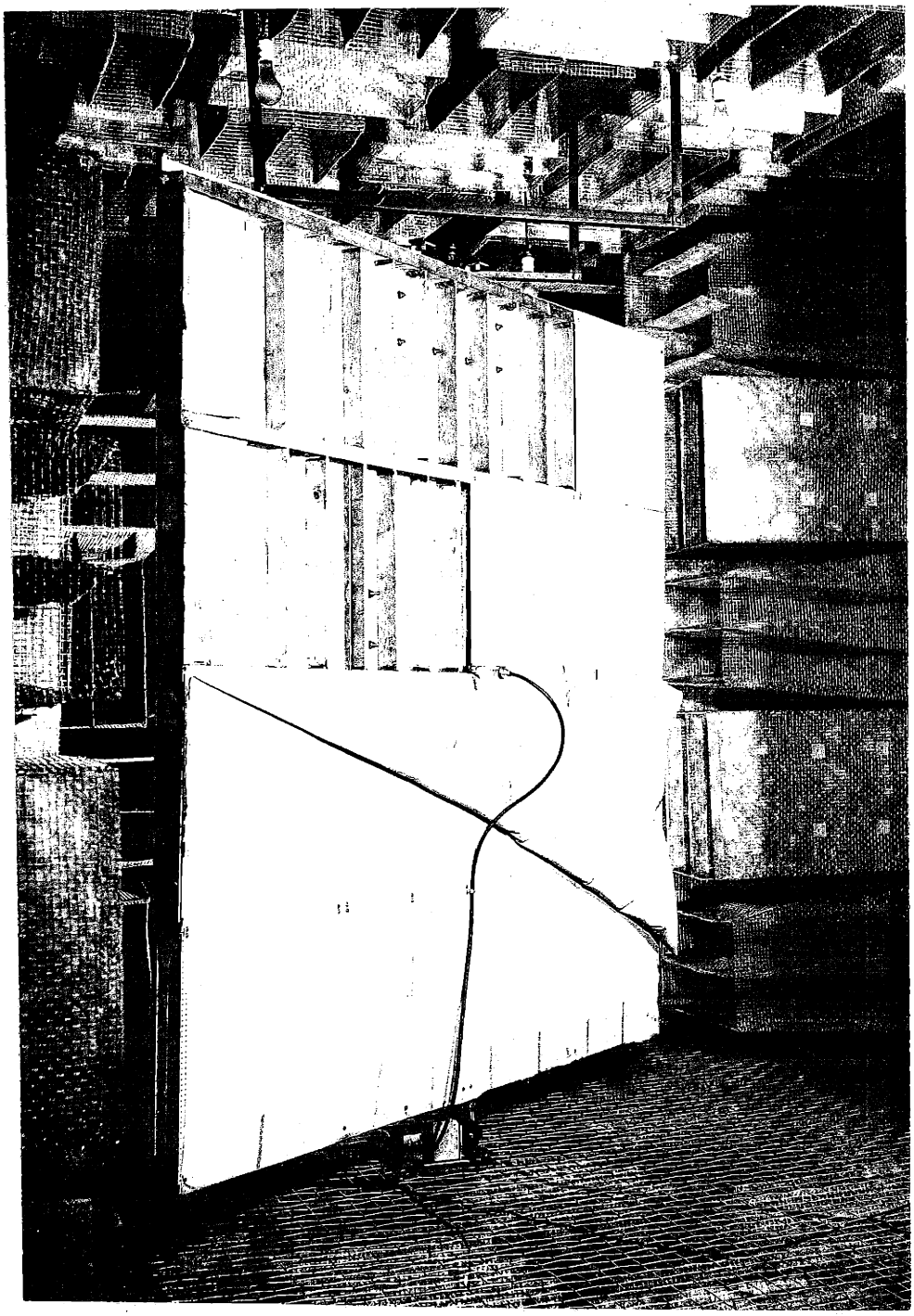

Figure 69

impedance of angle of incidence. In the second case the angular dependence of the normal impedance is such that $\zeta \cos\varphi \to \infty$ when $\varphi \to 90^\circ$ and hence $P_1/P_2 \to 1$ when $\varphi \to 90^\circ$, which follows from equation (III.8). The results of the pressure measurements are certainly consistent with this behaviour.

The angular dependence of the absorption coefficients obtained from the measurements are in very good agreement with the calculated, as shown in figure 77 and the same is true for the statistical average as can be seen in figure 73.

The normal impedance obtained from the measurements shown in figure 78 is found to be practically independent of angle of incidence and in good agreement with normal impedance, found in tube measurements, except at 1200 cps. However, this frequency is just on the upper limit, at which the spacing between the partitions is equal to half a wave length.

Above 1200 cps. and also at some other discrete frequencies, mainly below 700 cps., pressure curves were obtained, characterized by considerable dips at certain angles of incidence, but otherwise consistent with the results shown in figure 76. In all cases such anomalies were found at frequencies below 600, the product $\nu^* \cos\varphi^*$ was practically constant, φ^* being the angle of incidence where dip occurred and ν^* the corresponding frequency. The anomaly seems to represent a "Bragg

reflection", obtained when $\lambda^*/\cos\varphi^*$ is an even multiple of the structure periodicity. A strong absorption peak should then occur at the critical angles.

In order to obtain better understanding of these phenomena the wall was stopped at such an angle φ^* and the pressure distribution over the surface of the wall was measured. A strong standing wave was found consisting of a "fundamental" wave with a superimposed fluctuation corresponding to the structure periodicity. The wall then acts as a periodic boundary rather than a continous one and leads us into the field of periodic structure. However, a further analysis of the problem should require special studies, which are far beyond the scope of the present investigation.

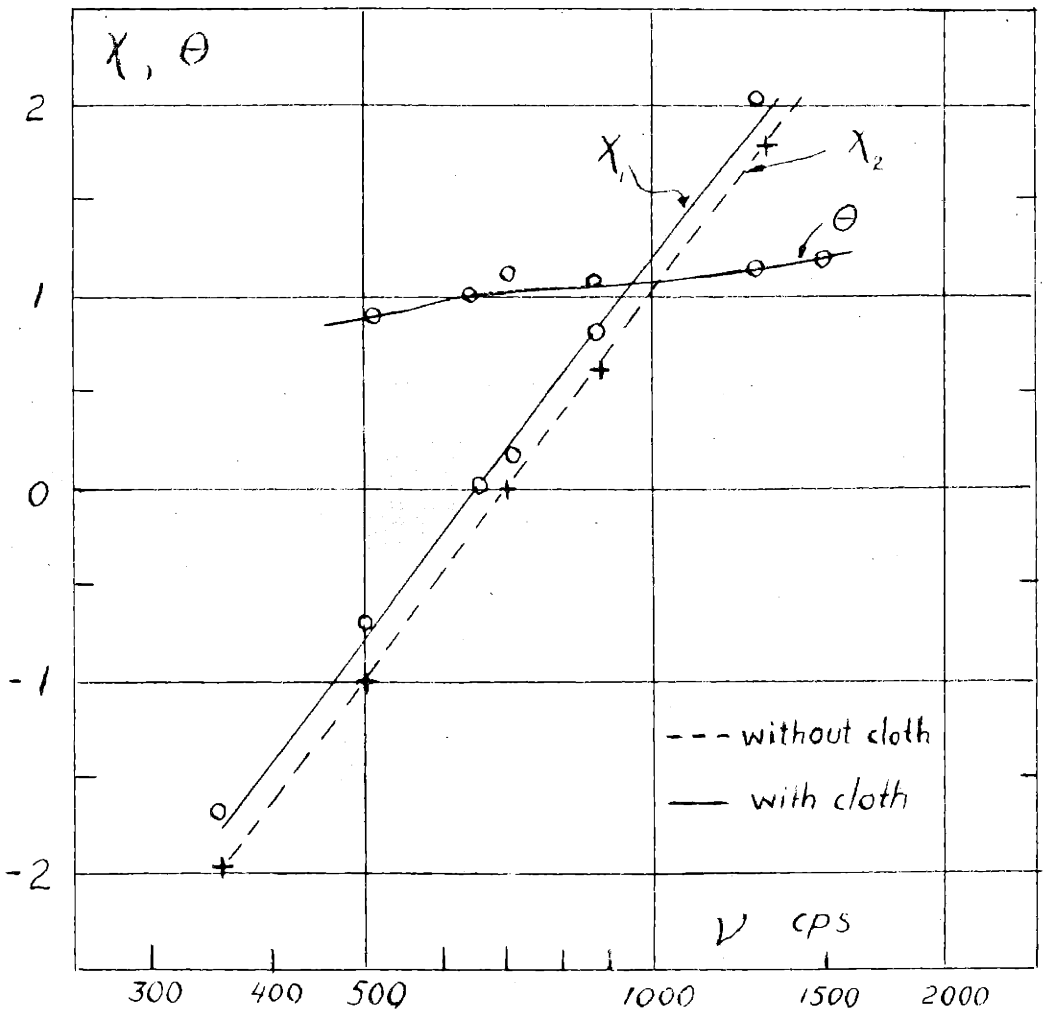
χ, θ
2
1
0
-1
-2
χ1
χ2
θ
--- without cloth
—— with cloth
ν cps
300
400
500
1000
1500
2000

Figure 70

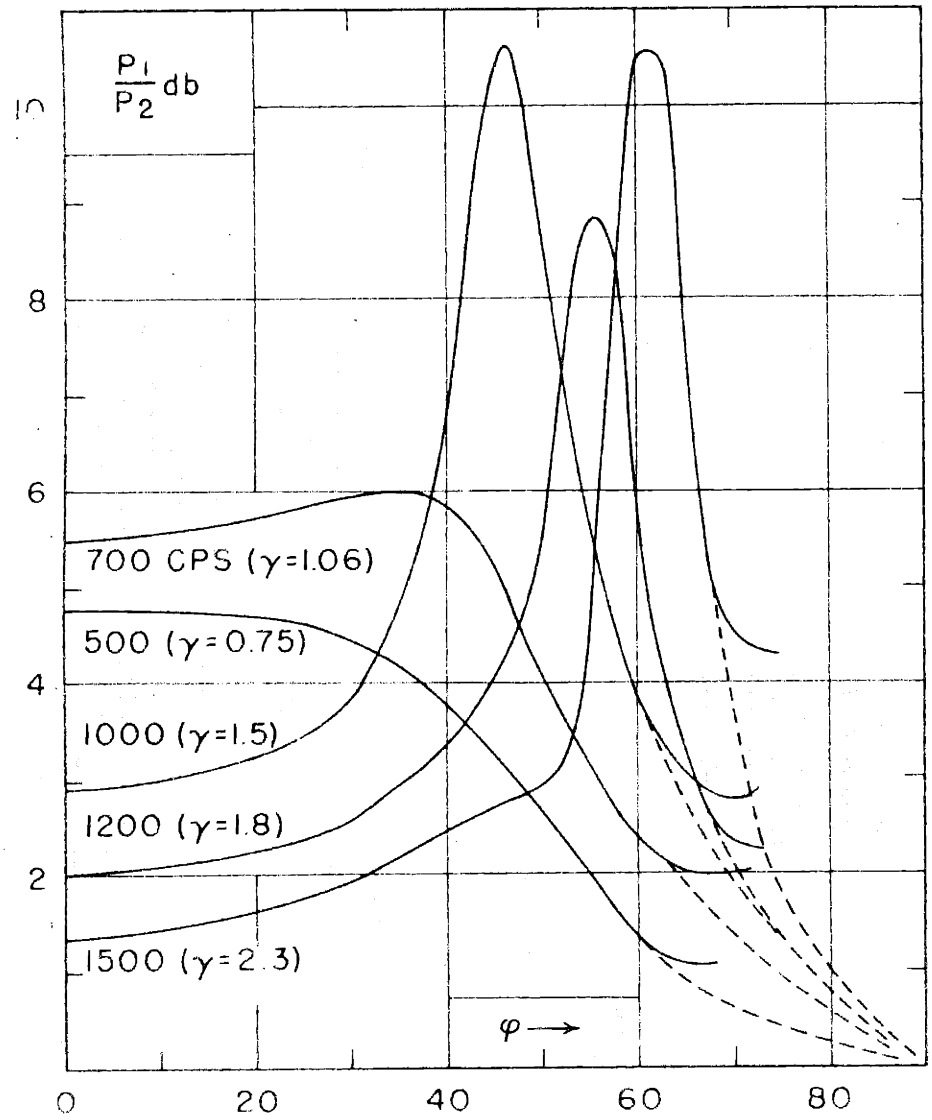
$\frac{P_1}{P_2}$ db
10
8
6
4
2
700 CPS (γ=1.06)
500 (γ=0.75)
1000 (γ=1.5)
1200 (γ=1.8)
1500 (γ=2.3)
φ →
0
20
40
60
80

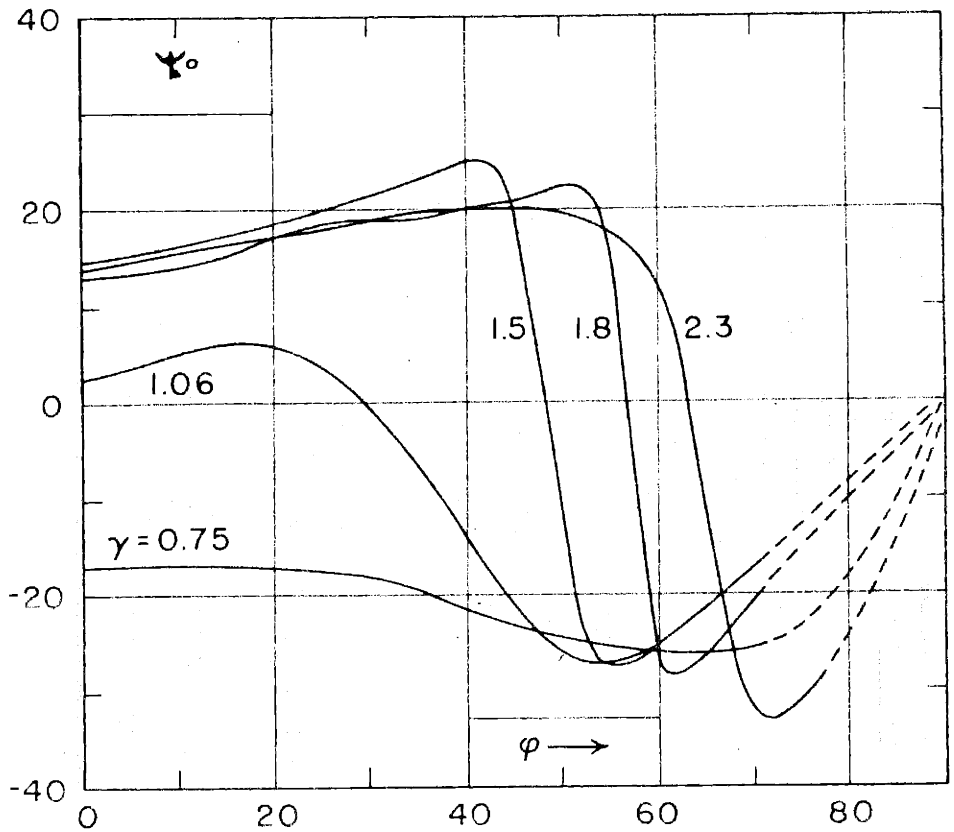
40
20
0
-20
-40
1.5
1.8
2.3
1.06
γ=0.75
φ →
0
20
40
60
80

Figure 71

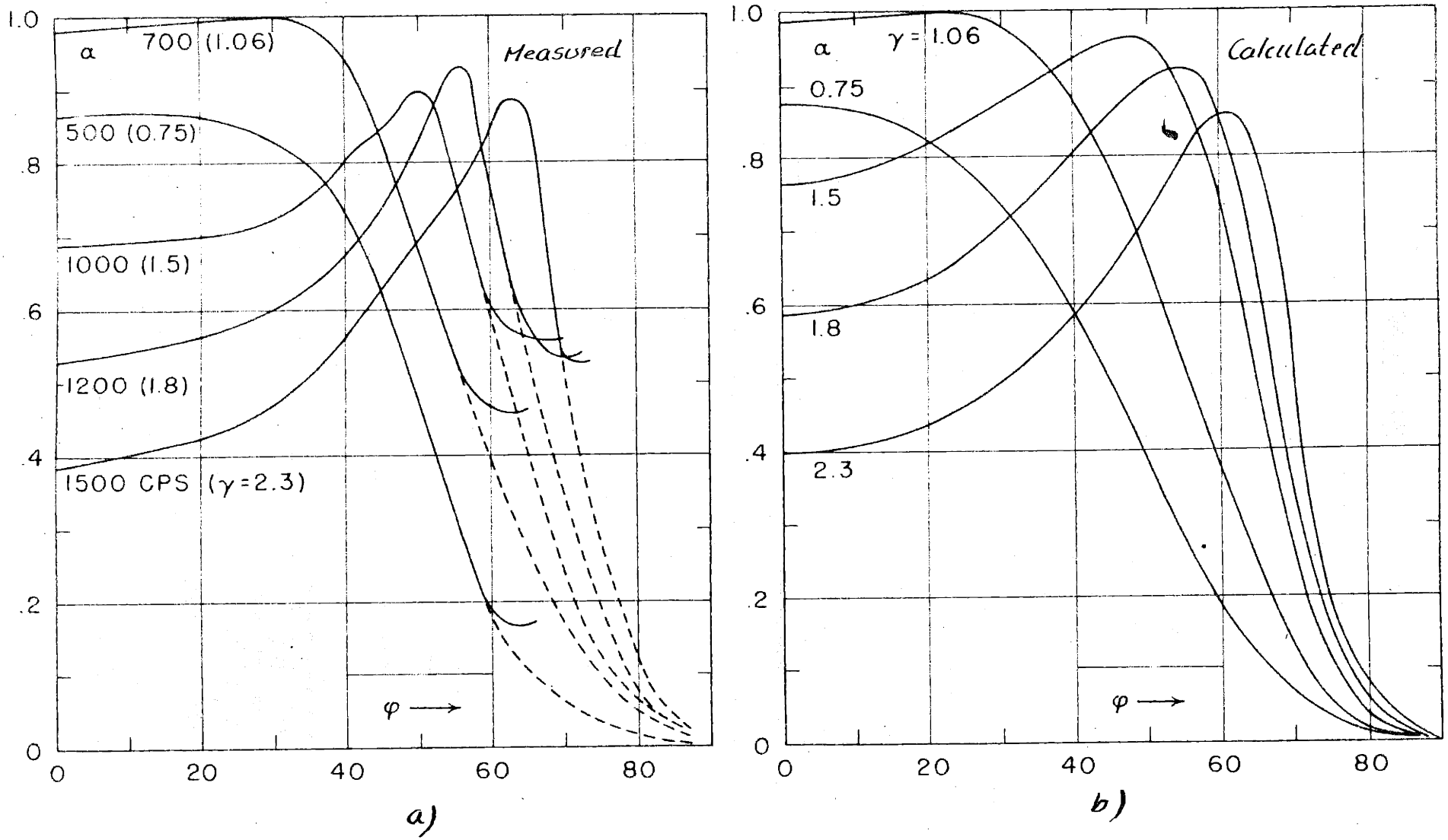
1.0
.8
.6
.4
.2
0
0
20
40
60
80
α
700 (1.06)
500 (0.75)
1000 (1.5)
1200 (1.8)
1500 CPS (γ=2.3)
Measured
φ →
a)
γ = 1.06
0.75
1.5
1.8
2.3
Calculated
b)

Figure 72

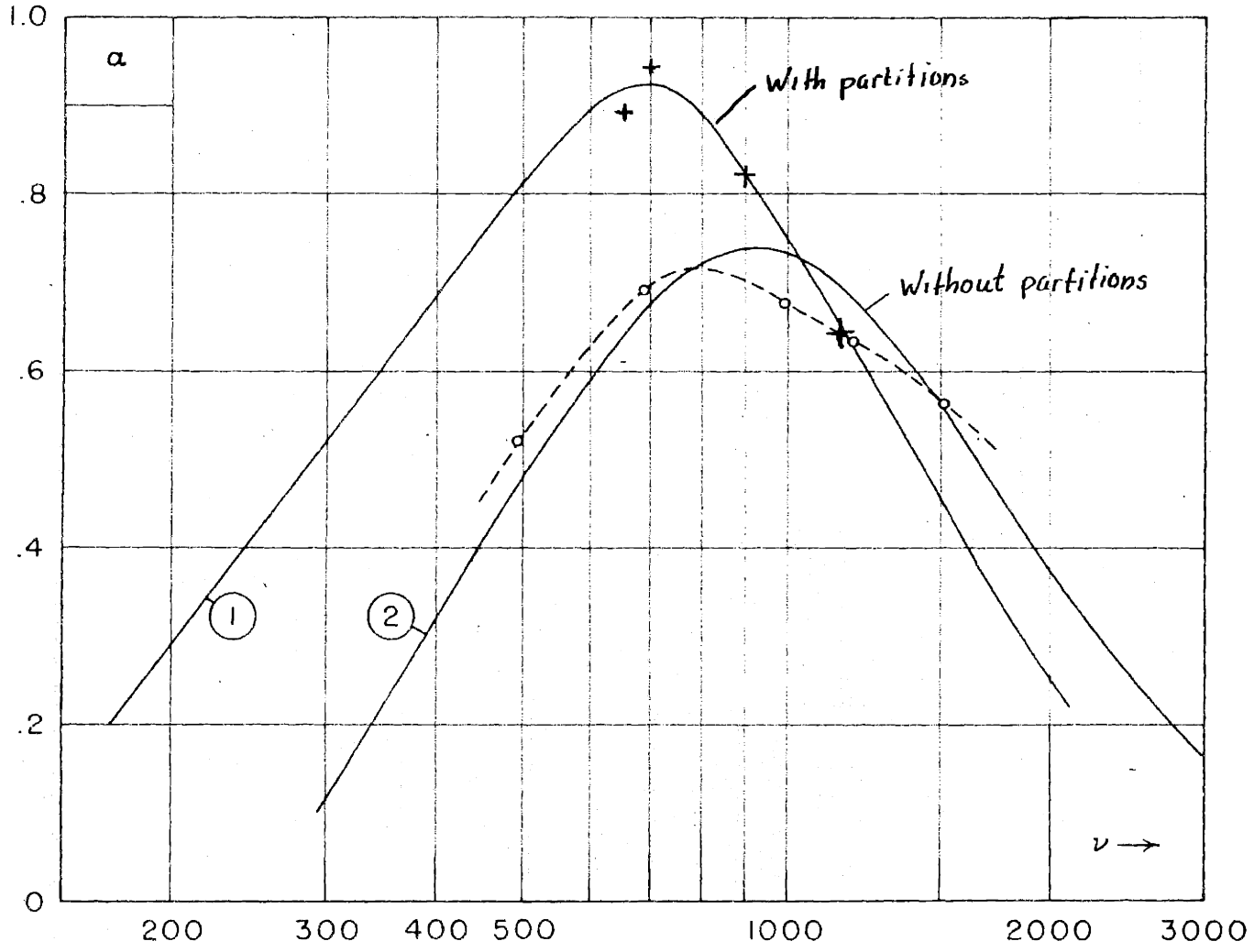
1.0
.8
.6
.4
.2
0
a
With partitions
Without partitions
1
2
ν →
200
300
400
500
1000
2000
3000

Figure 73

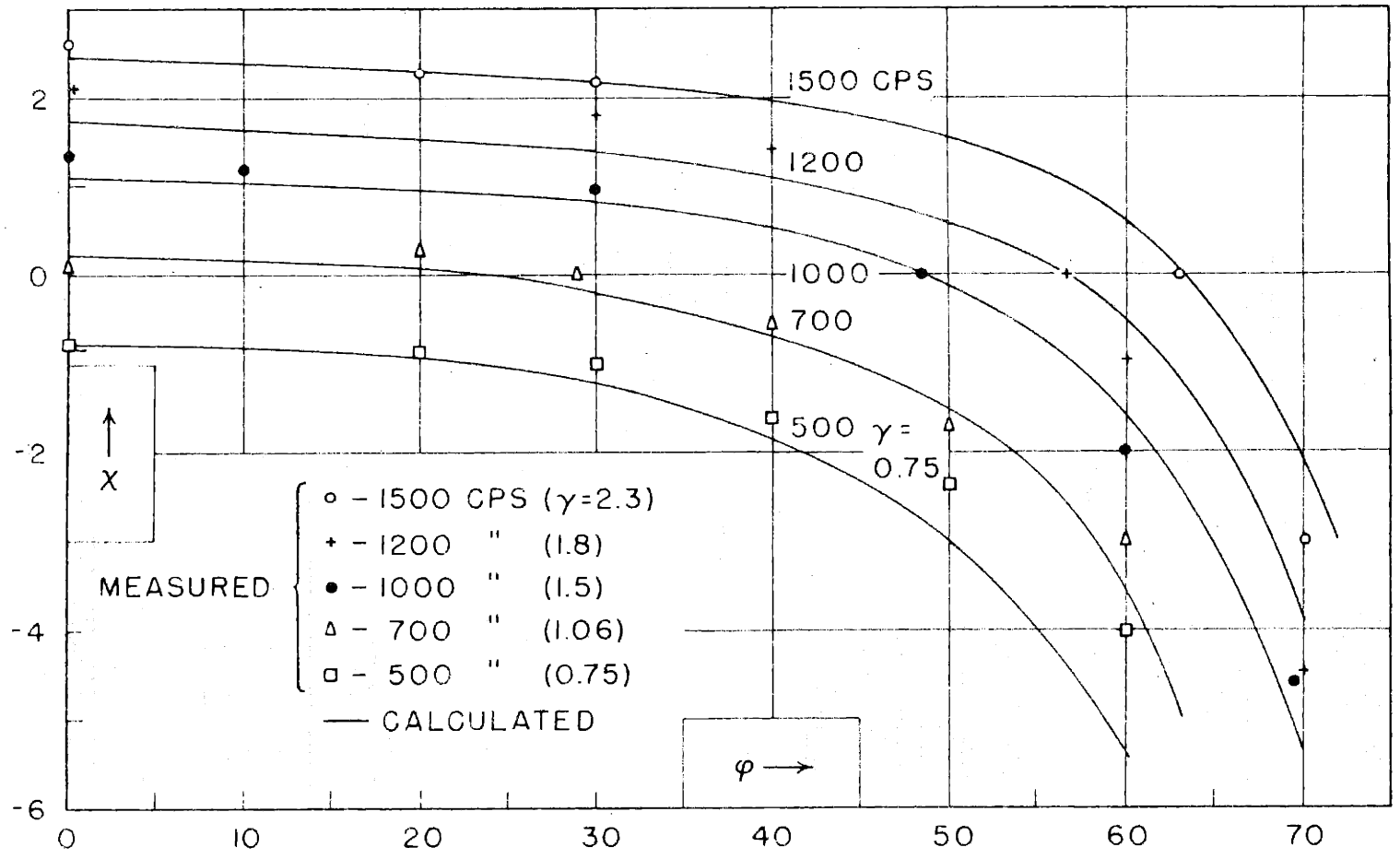
1500 CPS
1200
1000
700
500 γ = 0.75
2
0
-2
-4
-6
0
10
20
30
40
50
60
70
χ
φ →
MEASURED
○ - 1500 CPS (γ=2.3)
+ - 1200 " (1.8)
● - 1000 " (1.5)
△ - 700 " (1.06)
□ - 500 " (0.75)
— CALCULATED

Figure 74

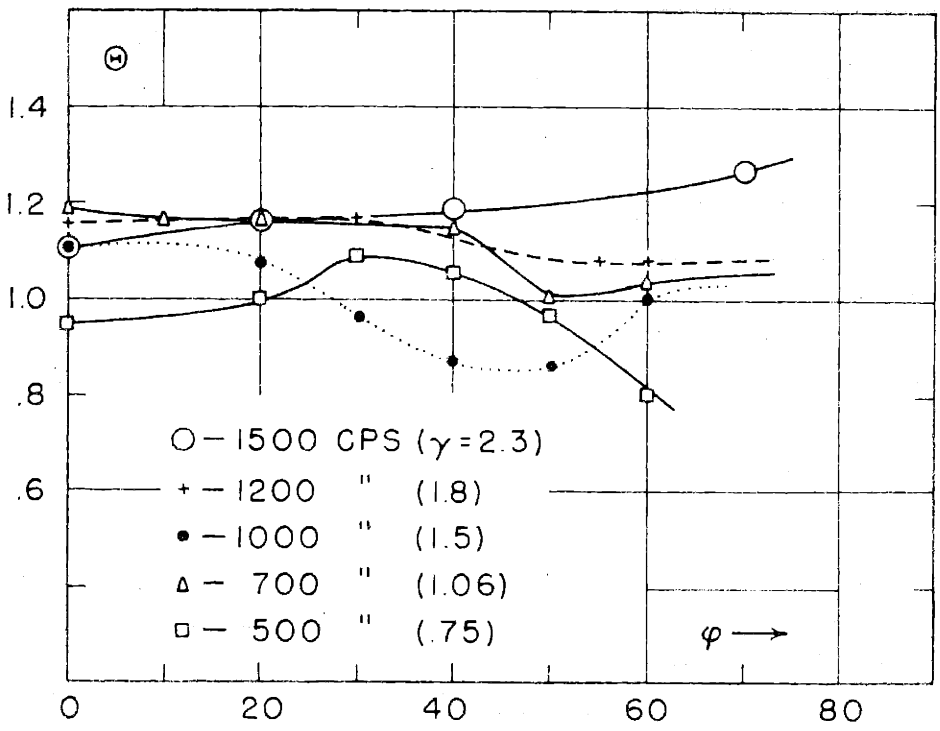
H
1.4
1.2
1.0
.8
.6
O — 1500 CPS (γ = 2.3)
+ — 1200 " (1.8)
• — 1000 " (1.5)
Δ — 700 " (1.06)
□ — 500 " (.75)
φ →
0
20
40
60
80

Figure 75

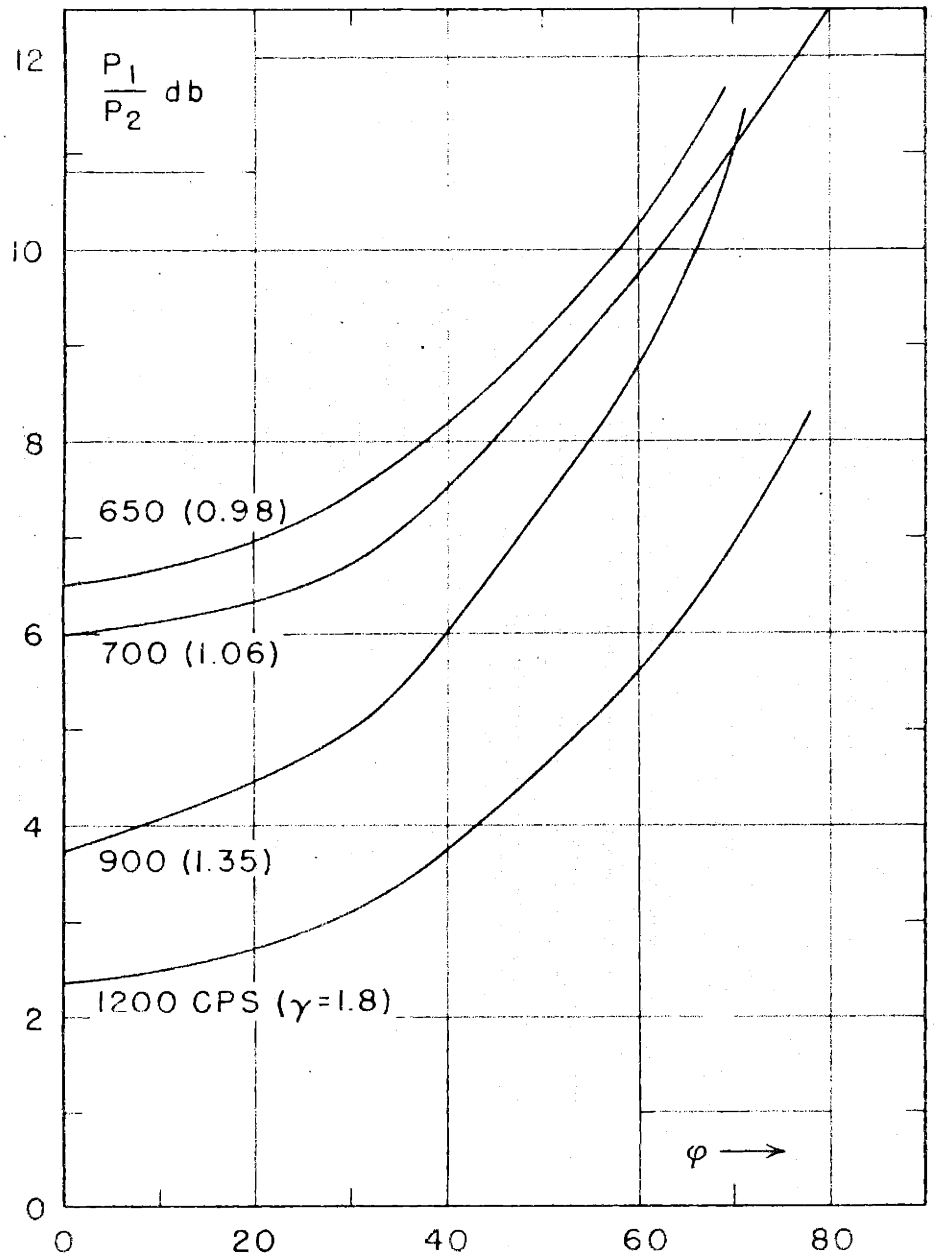
$\frac{P_1}{P_2}$ db
12
10
8
6
4
2
0
650 (0.98)
700 (1.06)
900 (1.35)
1200 CPS (γ=1.8)
$\varphi \rightarrow$
0
20
40
60
80

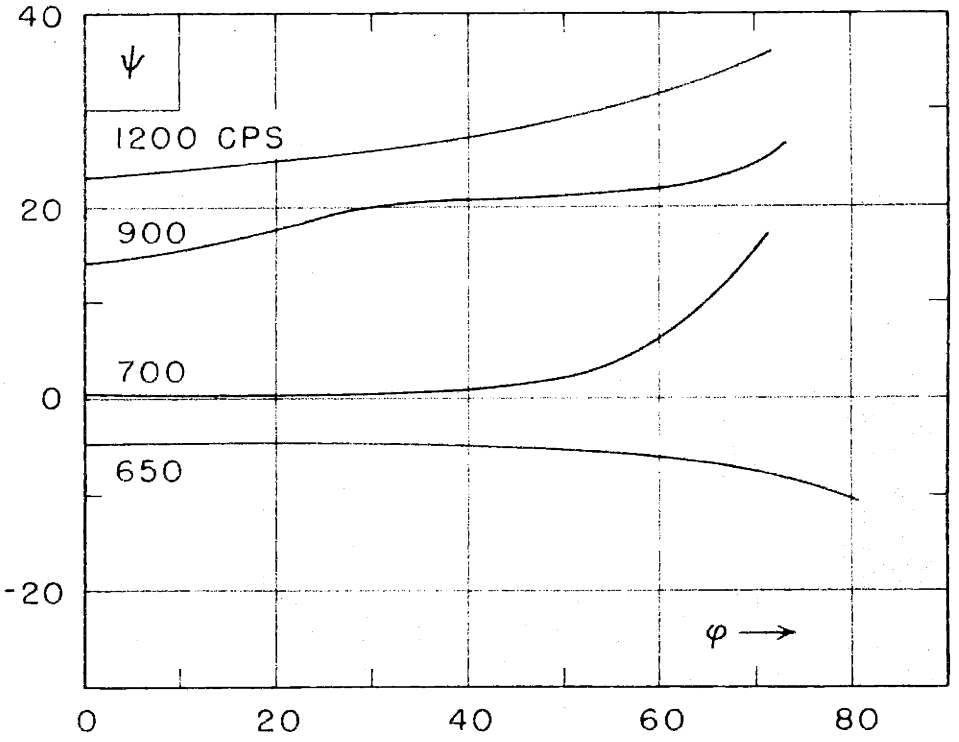
40
20
0
-20
ψ
1200 CPS
900
700
650
$\varphi \rightarrow$
0
20
40
60
80

Figure 76

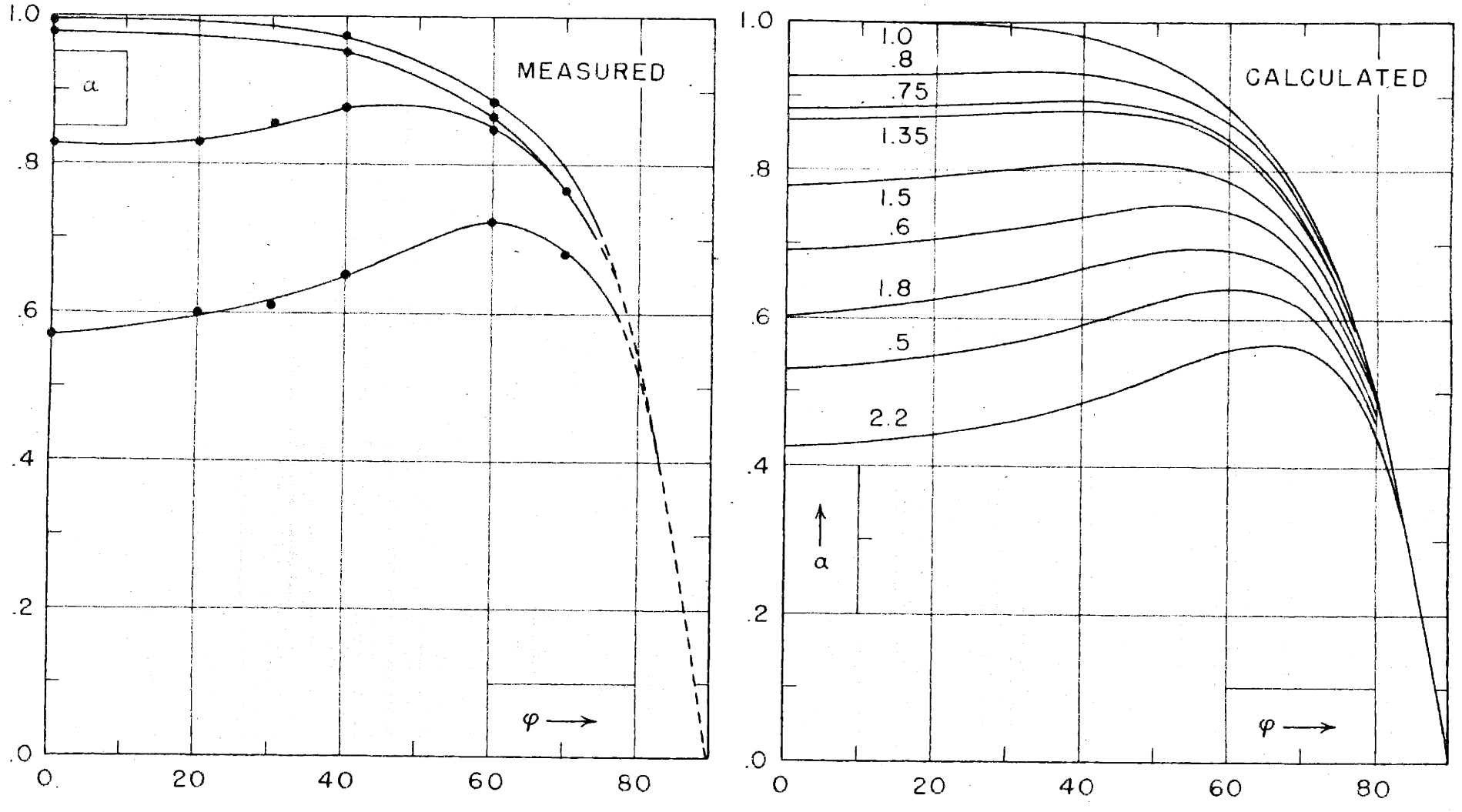

Figure 77

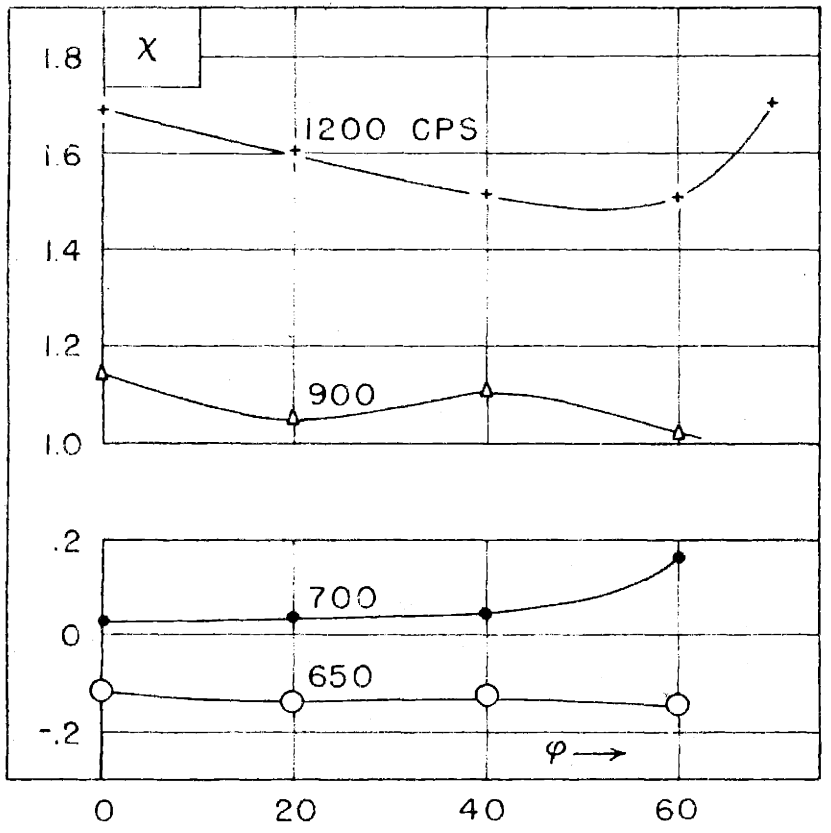
χ
1.8
1.6
1.4
1.2
1.0
1200 CPS
900
.2
0
-.2
700
650
φ →
0
20
40
60

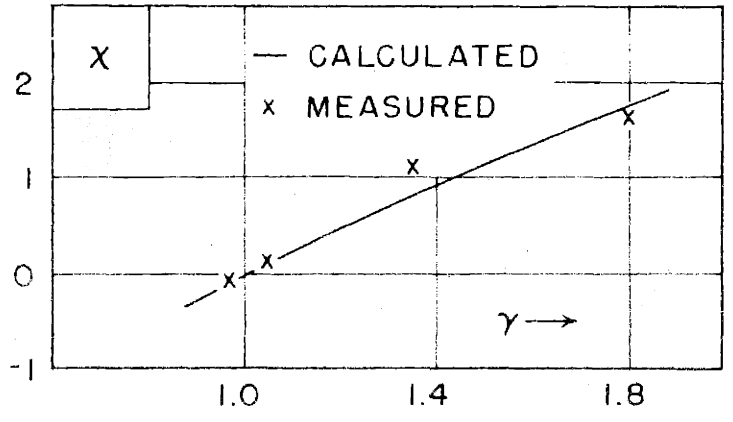
χ
— CALCULATED
x MEASURED
2
1
0
-1
γ →
1.0
1.4
1.8

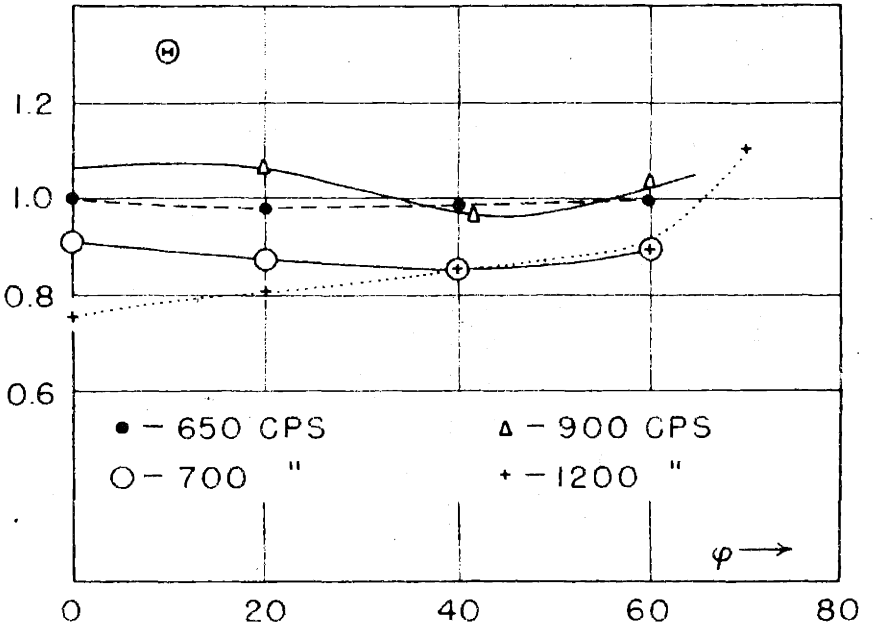
Θ
1.2
1.0
0.8
0.6
● – 650 CPS
Δ – 900 CPS
○ – 700 "
+ – 1200 "
φ →
0
20
40
60
80

Figure 78

Appendix.

Measurement of small flow resistances by means of an acoustic "Q-meter".

We have seen in chapter III, in connection with the design of acoustic resonators, that the impedance matching and the control of the Q of the resonators are of great importance. The additional resistances required are in many cases quite small, and can be obtained by putting a screen or porous cloth over the mouth of the resonator.

It is the purpose of this appendix to point out the possibility of using a resonator as a Q-meter for measurement of the acoustic impedance of thin layers of material and the complex compressibility of porous material. We are here mainly interested in the first of these two kinds of measurements.

A similar, but more elaborate method, for determining the acoustic impedance of very porous screens has been described by Harris [52], in which the dampening caused by a screen on a fundamental mode in a closed tube is studied. The method is restricted to very porous screens so that the pertubation introduced can be considered small.

The acoustic resonant circuit used in the measurements was a circular cylindrical cavity with a diameter $d = 10$ cm and a depth $L = 15$ cm. The side wall containing the hole was removable and made of two steel plates, between which the sample under test was placed thus covering the hole. The Q and the resonance frequency of the resonator is determined with and without the sample present. The impedance of the sample can be described by a resistance $\varrho c\theta$ and a mass m in series, the values of which are determined by

$$\varrho c\theta = \varrho c \frac{Ac}{2\pi V} \left(\frac{1}{\nu_1 Q_1} - \frac{1}{\nu_o Q_o} \right)$$

$$m = \varrho c \frac{Ac}{(2\pi)^2 V} \left(\frac{1}{\nu_1^2} - \frac{1}{\nu_o^2} \right)$$

A = area of hole = area of the sample

V = volume of the resonator cavity

ν_o = resonance frequency without sample

ν_1 = resonance frequency with sample

The resonator can be placed at the end of a tube or the measurements can be performed in free field. The sound pressure P_i inside the cavity is measured and the Q and the resonance frequency are determined as described in (II. 4)

It is worth emphasizing that special attention has to be paid to non-linearity. Since we are working with a resonant circuit considerable particle velocity may be obtained in the

orifice even at relatively low pressures of the primary wave.

Measurements on a number of different materials, paper, metal foils, cloth and metal screens have been made.

The resistance of four metal screens were measured also as a function of the particle velocity in the orifice, and non-linearity of the screen resistance was found as expected.

The impedance of screens of cloth is not simply a resistance and mass in series, although it may be reduced to such a circuit. There is one mass m_c due to the constriction, which the screen causes, and one mass m_v corresponding to the motion of the screen itself. In addition there may be a resistance in series with m_v because of internal losses in the material. The equivalent circuit for the impedance consists of parallel branches, one with r_s and m_s in series, the other with r_v and m_v in series. If r_v and m_s are assumed small then we have the equivalent serie mass $m = r_s^2/\omega^2 m_v$, from which m_v can be determined. Or, more general, m_s can be calculated, and if r_v is small, then m_v can be determined from the experiment.

A systematic study of the impedance of thin layers using the technique described may lead to a separation of the two masses m_c and m_v, which is an approach to the understanding of the

structure factor introduced in the theory of porous material. Several layers of the screen like material may be used and the resistance and reactance may be studied as a function of thickness.

Furthermore measurements on thin metal foils may lead to informations about their internal dissipation.

Finally it is suggested that the Q-meter may be used for measuring the complex compressibility of porous material. In this case the porous sample has to be introduced into the cavity, well out of the region of the near field of the aperture. The pure capacitance of the cavity is then partly replaced by the compressibility of the material introduced. If a cavity of sufficiently high Q is used it seems quite possible that measurements of this kind can be performed.

Bibliography.

1 . Rayleigh: "Theory of sound", (Mac Millan and Co., London 1940), Vol.II, p.170.

2 . J.R. Whinnery and H.W. Jamieson: "Equivalent circuits for discontinuities in transmission lines", Proc. Inst. Radio Eng. 32 , p. 98,(1944).

3 . J.R. Whinnery, H.W. Jamieson and T.E. Robbins: "Co-axial-line discontinuities", Proc.Inst.Radio Eng. 32 , p.695, (1944).

4 . J. Schwinger: Notes on lectures by Julian Schwinger "Discontinuities in wave-guides" by David S. Saxon.

5 . J.W. Miles: "The analysis of plane discontinuities in cylindrical tubes", Part I. J.Acous.Soc.Am. 17 , p.259, (1946).

6 . J.W.Miles: "The analysis of plane discontinuities in cylindrical tubes", Part II. J.Acous. Soc. Am. 17 , p.272, (1946).

7 . J.W. Miles: "The reflection of sound due to a change in cross section of a circular tube", J.Acous.Soc.Am. 16 , p.14, (1944).

8 . U. Ingard: "On the radiation of sound into a circular

tube with an application to resonators", J.Acous.Soc. Am. 20, p.665, (1948).

9 . A.K. Nielsen: "Acoustic resonators of circular cross-section and with axial symmetry", Trans. Dan.Acad. Techn. Sci. No 10,(1949).

10 . R.H. Bolt, S. Labate, U. Ingard: "The acoustic reactance of small circular orifices", J.Acous.Soc.Am. 21, p.94,(1949).

11 . P.M. Morse: "Vibration and Sound", (Mc Graw - Hill Book Company, Inc., New York, 1948.) p.238.

12 . G.N. Watson: "Theory of Bessel Functions", (Cambridge, University Press, 1944), p.360.

13 . L.L. Beranek: "Precision measurement of acoustic impedance", J.Acous. Soc. Am. 12 , p.3,1940.

14 . Rayleigh: loc.cit. Vol.II. p.318.

15 . G.W. Stewart: "Acoustic transmission with a Helmholtz resonator or an orifice as a branch line", Phys.Rev. 27 , p.487,(1926).

16 . E.G. Richardson: "The amplitude of sound waves in resonators", Proc.Phys.Soc. 40, p.206,(1928).

17 . A. Gigli: "Sound absorption and Transmission Measurements", J.Acous.Soc.Am. 20 , p.839,(1948).

18 . A.E. Bate: "The acoustical conductance of orifices",

Phil.Mag.10 , p.624, (1930).

19 . S. Labate: "Sound absorption by the use of acoustic resonators", Masters Thesis 1948, El. Eng. Dep. M.I.T.

20 . Rayleigh: loc.cit., Vol.II, p.217.

21 . C. Eckart: "Vortices and streams caused by sound waves", Phys.Rev., 73 , p.68,(1948).

22 . L.N. Liebermann: "The second viscosity of liquids", Phys.Rev. 75, p.1415, (1949).

23 . Rayleigh: loc.cit., Vol.II, p.340.

24 . E.N. Andrade: "On the circulations caused by the vibrations of air in a tube", Proc.Royal Soc. of London Series A, 134, (1931).

25 . Bouasse: "Tourbillons", Paris, 1932.

26 . L.J. Sivian: "Acoustic impedance of small orifices", J.Acous.Soc.Am. 7, p.94,(1935).

27 . S. Labate: loc.cit. p.23.

28 . P.M. Morse: loc.cit., p.354.

29 . Rayleigh: loc.cit., Vol II, p.272.

30 . H. Stenzel: " Über die von einen starren Kugel hervorgerufene Störung des Schall feldes", Elektr.Nachr.-Techn. 15 , p. 71, (1938).

31 . L. Schwarz: "Zur Theorie der Beugung einer ebenen Schallwelle an der Kugel", Akustische Zeitschrift, Heft 3, p.91,(1943).

32 . J.C. Slater: "Microwave Transmission", (Mc Graw-Hill Book Company, Inc., New York,1942), p.245.

33 . P.M. Morse: loc.cit., p.356. See equation (29.12).

34 . " " p.357 " (29.13).

35 . " " p.324 " (27.20).

36 . E.T. Copson: "Theory of functions of a complex variable", (Oxford,University Press,1935) p.285.

37 . G.N. Watson: loc.cit., p.403. See equation (2).

38 . P.M. Morse: Unpublished analysis of the spherical resonator.

39 . P.E. Sabine: "On the acoustic properties of small cavities", J. Acous. Soc.Am. 13, p.74, (1942).

40 . E.W. Hobson: "Spherical and ellipsoidal harmonics", (Cambridge, University Press, 1931), See Ex.12, p.74,

41 . P.M. Morse: loc. cit., p.355. See equation (29.11).

42 . P.O. Pedersen: "Lydtekniske Undersøkelser, Ingeniørvidenskabelige skrifter nr. 5, Kobenhavn 1940.

43 . V.L. Jordan: "The application of Helmholtz resonators to sound absorbing structures", J. Acous.Soc.Am. 19 , 972, 1947.

44 . P.V. Brűel: "Lydisolation og rumakustik", Goteborg, 1946.

45 . R.H. Bolt: "On the design of perforated facings for acoustic material", J. Acous.Soc.Am. 19 , p.917 (1947).

46 . W. Willms: " Über die Schallschluckung mit Hilfe von gedämpften Resonatoren", Akust.Zeitschrift, Heft 1, p.29, (1939).

47 . Kosten and Zwikker: "Sound Absorbing Materials", Elsevier publishing company, inc., New York, 1949.

48 . J. Brillouin: "Théorie de l'absorption du son par les structures á panneaux perforés", Cahiers du centre scientifique et technique du bátiement, 31, 1949.

49 . Morse and Bolt: "Sound waves in rooms", Rev. Mod. Phys. 16 , p.141, (1944).

50 . Morse and Bolt: loc.cit., p. 140.

51 . Kosten and Zwikker: loc.cit., p. 164.

52 . C. Harris: "Measurement of the acoustic impedance of very porous screens", J. Acous. Soc. Am. 20 , p.440,1948.

Biographical note.

Karl Uno Ingard was born in Gothenburg, Sweden, on February 24, 1921, of parents Karl Oscar Ingard and Anna Elisabeth Ingard. He graduated from the Technical Gymnasium in Gothenburg 1940, entered Chalmers Institure of Technology 1940 and graduated as Electrical Engineer 1944, receiving the John Ericson medal. During the period 1940-1942 he was part time employed in an electrical consulting firm in Gothenburg and was during 1942-1943 a teaching fellow in Experimental Physics at Chalmers Institute of Technology. He tought Electrical Engineering at the Technical Gymnasium in Gothenburg 1943-1945, worked in the research laboratory of electronics at the Institute during the period 1944-1945, and in the Electrical Laboratory in Stockholm during 1945-1946. He returned to Chalmers Institute of Technology 1946 to work in the Acoustics Laboratory and teach Architectural Acoustics and became director of the Acoustics Laboratory 1947. He received the Licentiate degree from Chalmers Institute of Technology 1948. From 1948 to date he has been pursuing a course of graduate study at the Massachusetts Institute of Technology leading to a Ph.D. He is a member of Sigma-Xi.

He was married to Doris Karlsson in 1948.

Publications of author.

"Från quasistationära svängningskretsar till vågledare och hålrumsresonatorer" ("From quasi-stationary circuits to wave-guides and cavity resonators"), Populär Radio, Häfte 8 p. 170,1946; häfte 9,p.194, 1946; häfte 10, p.259, 1946 ; häfte 12, p.282, 1946; häfte 1,p.8, 1947.

"Hurtige Nivea-skriver.", Ingenøren, 50 E,p.153 (1946). (Co-author)

"On the radiation of sound into a circular tube with an application to resonator", J.Acous.Soc.Am. 20 , p.665, (1948)

"A new high speed level recorder", J.Acous.Soc.Am. 21 , 80,(1949) (Co-author)

"The acoustic reactance of small orifices", J.Acous.Soc.Am. 21 p.94,(1949) (Co-author)

"Acoustic circulations and the non-linear impedance of orifices", J.Acous.Soc.Am. 22 , p. (1950) (Co-author)